# The Design and Optimization of a Condition Monitoring Device using Data Reduction Techniques to Estimate Leakage of a Load Sensing Axial Piston Pump

A Thesis Submitted to the
College of Graduate and Postdoctoral Studies
In Partial Fulfillment of the Requirements
For the Degree of Master of Science
In the Department of Mechanical Engineering
University of Saskatchewan
Saskatoon

By

Jonathan Neil Fernandes

# Permission to Use

In presenting this thesis/dissertation in partial fulfillment of the requirements for a Postgraduate degree from the University of Saskatchewan, I agree that the Libraries of this University may make it freely available for inspection. I further agree that permission for copying of this thesis/dissertation in any manner, in whole or in part, for scholarly purposes may be granted by the professor or professors who supervised my thesis/dissertation work or, in their absence, by the Head of the Department of Mechanical Engineering of the Dean of the College in which my thesis work was done. It is understood that any copying or publication or use of this thesis/dissertation or parts thereof for financial gain shall not be allowed without my written permission. It is also understood that due recognition shall be given to me and to the University of Saskatchewan in any scholarly use which may be made of any material in my thesis/dissertation.

Requests for permission to copy or to make other uses of materials in this thesis/dissertation in whole or part should be addressed to:

Head of the Department of Mechanical Engineering
University of Saskatchewan
57 Campus Drive
Saskatoon, Saskatchewan S7N 5A9 Canada

OR

Dean
College of Graduate and Postdoctoral Studies
University of Saskatchewan
116 Thorvaldson Building, 110 Science Place
Saskatoon, Saskatchewan S7N 5C9 Canada

# Abstract

Hydraulic systems are commonly used as solutions to industry challenges. Their excellent power-to-weight ratio can achieve specific design criteria that other power methods may not. In many hydraulic components, precision machining is present. This is to provide hydrodynamic lubrication between contacting components. By design, component life is greatly increased due to limited physical part interaction. Subsequently, any changes to the machined surfaces can result in accelerated and even catastrophic damage. Pressure compensated load sensing (PCLS) axial piston pumps are common in heavy duty hydraulic applications and provide flow in hydraulic systems. Typically, when a pump is exposed to common environmental contamination, internal machined surfaces can become damaged in the form of scoring. Depending on the degree of damage, this can result in increased leakage across lubricating boundaries or catastrophic failure due to adhesion. Component failure can then manifest in several ways. On a pump, slight wear can result in increased case drain leakage and the operator may not notice any performance issues, however, catastrophic failure may result in immediate system changes. A current method of evaluating the condition of an axial piston pump is by measuring the case drain leakage flow. This procedure involves installing a test flowmeter between the case drain leakage line and the reservoir and recording the flow at certain pressures. This can be an involved procedure and any time a closed hydraulic circuit is disassembled, the risk of introducing contamination is high. Additionally, robust, heavily used flowmeters can be inaccurate and unreliable due to wear and calibration errors. There is an obvious need to further develop the method of evaluating the health of a load sensing axial piston pump.

The research contained in this thesis provides a potential cost effective alternative to case drain flow monitoring of PCLS axial piston pumps through the analysis of dynamic pump data. A nonlinear dynamic model of a load sensing axial piston pump and circuit is developed and validated with experimental dynamic pressure and swash angle position signals. The dynamic response of the pump outlet pressure, control piston pressure, and swashplate angle of a load

sensing pump is shown to change with case drain leakage, both with the model and experimentally.

A statistical procedure, Principal Component Analysis, (PCA), is applied to a large training dataset developed by the dynamic model. PCA is a fundamental piece of the leakage prediction algorithm developed in this research. In a simulation study, the designed leakage prediction algorithm is able to predict leakage using clean training and test data with a root mean square (RMS) error of less than 1%.

Further algorithm development includes determining the best dynamic measurements to obtain, the amount of training data, a filter design for the raw experimental data, and training data manipulation. A simulation study shows that the signal combination that gives the best prediction performance is a combination of the pump pressure, control piston pressure, and the swashplate angle. This was confirmed by evaluating the leakage prediction performance with experimental pump response data. Having determined the optimal sensor data, the amount of training data is investigated. This was shown to improve from 100 samples and peak at 1000 samples. An optimization using experimental data was performed to determine the best filter to apply to the experimental response data. It was determined that a low pass filter with a cutoff frequency 10% below the piston pumping frequency gave the best leakage prediction results. This research includes a thorough investigation into the manipulation of the training data. The detailed optimal noise addition parameters give a predictive error of less than 20% using a signal combination of pump pressure, control piston pressure, and swashplate angle for experimental pump response data. Using just the pump and control piston pressure transients results in approximately 40% prediction error. Swashplate response data give conflicting results as the predictive error for the minimally worn pump is much different than the high wear pump (<10% for minimally worn pump and >20% for severely worn).

This research is an investigation into the feasibility of a load sensing axial piston pump condition monitoring device that measures case drain leakage via dynamic measurements. A comprehensive analysis is performed to optimize a leakage predictive algorithm and the design is tested in simulation as well as with experimental data and shows good potential.

# Acknowledgements

I'd like to thank all the good people that have helped me over the last two years. Thank you, Prof. Travis Wiens, for teaching me, your patience and advice will always be appreciated. A big thank you to my friend Douglas Bitner for your support both in and out of the lab, I couldn't have done this without you.

Thank you to The National Research Council, Wiltech Industries, and to The University of Saskatchewan Travel award for the funding provided.

I'd also like to thank my parents Steve and Eileen. Your support is truly endless and your love unconditional. Thank you to my sister Alison and my nephew Nick. Alison, you have always been there for me. Nick, you're there every day.

# Contents

# List of Tables

# List of Figures

# Nomenclature

| | | |
|---|---|---|
| $A_{bias}$ | Area of bias piston | $[m^2]$ |
| $A_{chrg}$ | Charging orifice effective area | $[m^2]$ |
| $A_{cp}$ | Area of control piston | $[m^2]$ |
| $A_{cpo}$ | Area of control piston damping orifice | $[m^2]$ |
| $A_{dchrg}$ | Discharging orifice effective area | $[m^2]$ |
| $A_{ls}$ | Area of load sense orifice | $[m^2]$ |
| $A_p$ | Area of pumping piston | $[m^2]$ |
| $A_{pls}$ | Area of orifice leading to control piston | $[m^2]$ |
| $A_{pso}$ | Area of orifice leading from control piston to tank | $[m^2]$ |
| $c$ | Control piston clearance | [m] |
| $C_c$ | Contraction coefficient | |
| $C_{cc}$ | Charging orifice correction constant | |
| $C_{cp}$ | Control piston leakage conductance constant | $[m^4 s^{-1}\ Pa^{-1}]$ |
| $C_d$ | Discharge coefficient | |
| $C_{dc}$ | Discharging orifice correction constant | |
| $C_1$ | Swashplate torque term | $[kg\ m^2 rad^2 s^{-2}]$ |
| $C_2$ | Swashplate torque term | $[m^3 rad]$ |
| $c_{ls}$ | Radial clearance of load sense spool | [m] |
| $cp_{guide}$ | Control piston guide diameter | $[m^2]$ |
| $D_{bias}$ | Diameter of bias piston | [m] |
| $D_{cp}$ | Diameter of control piston | [m] |
| $d_{cpo}$ | Diameter of control piston damping orifice | [m] |
| $dia_{ls}$ | Load sense spool diameter | [m] |
| $d_{ls}$ | Load sense spool damping | $[Nm^{-1}s^{-1}]$ |

| | | |
|---|---|---|
| $D_{piston}$ | Diameter of pumping piston | [m] |
| $d_{pls}$ | Diameter charging/discharging hole | [m] |
| $d_{pso}$ | Diameter of charging hole | [m] |
| $F_{bias}$ | Bias spring preload | [N] |
| $F_{chrg}$ | Charging flow force on load sense spool | [N] |
| $F_{dchrg}$ | Discharging flow force on load sense spool | [N] |
| $F_F$ | Total flow force acting on load sense spool | [N] |
| $f_{gain}$ | Flow gain of pump | $[\mathrm{m^3 s^{-1} rad^{-1}}]$ |
| $K$ | Number of folds for K-fold cross validation | |
| $K_{ag}$ | Swashplate assembly damping term | $[\mathrm{Nm^{-1} s^{-1}}]$ |
| $k_{bias}$ | Bias spring constant | $[\mathrm{Nm^{-1}}]$ |
| $K_{chrg}$ | Charging orifice constant | $[\mathrm{sm^{\frac{9}{2}} kg^{-\frac{1}{2}} Pa^{-\frac{1}{2}}}]$ |
| $K_{dchrg}$ | Discharge orifice constant | $[\mathrm{sm^{\frac{9}{2}} kg^{-\frac{1}{2}} Pa^{-\frac{1}{2}}}]$ |
| $K_{load}$ | Load orifice lumped parameter | $[\mathrm{m^2}]$ |
| $K_{ls}$ | Load sense orifice lumped parameter | $[\mathrm{m^2}]$ |
| $k_{ls}$ | Load sense spring constant | $[\mathrm{Nm^{-1}}]$ |
| $L$ | Moment arm of bias and control pistons | [m] |
| $LP_{max}$ | Maximum control piston leakage path length | [m] |
| $LP_{min}$ | Minimum control piston leakage path length | [m] |
| $LP_{slope}$ | Control piston leakage path gradient | |
| $max_{sw}$ | Maximum swashplate angle | [rad] |
| $m_{bias}$ | Mass of bias piston | [kg] |
| $m_{cp}$ | Mass of control piston | [kg] |
| $m_{ls}$ | Mass of load sense spool | [kg] |
| $m_p$ | Mass of single pumping piston | [kg] |
| $m_{swash}$ | Mass of swashplate | [kg] |
| $N$ | Number of pumping pistons | |
| $O.S.$ | Overshoot | [%] |

| | | |
|---|---|---|
| $O_l$ | Measured overlap of load sense spool | [m] |
| $O_s$ | Measured offset of load sense spool from end | [m] |
| $O_1$ | Load sense spool first charging variable orifice | $[m^2]$ |
| $O_2$ | Load sense spool 2nd charging variable orifice | $[m^2]$ |
| $O_3$ | Load sense spool fixed damping orifice | $[m^2]$ |
| $O_4$ | Load sense spool discharging variable orifice | $[m^2]$ |
| $P_{cp}$ | Control piston pressure | [Pa] |
| $P_{load}$ | Load pressure | [Pa] |
| $P_s$ | Pump discharge pressure | [Pa] |
| $Ps_{peak}$ | Peak pressure | [Pa] |
| $Ps_{SS1}$ | Pressure at steady state before step | [Pa] |
| $Ps_{SS2}$ | Pressure at steady state after step | [Pa] |
| $P_{tank}$ | Tank pressure | [Pa] |
| $P_s$ | Pump discharge pressure frequency content | [Pa] |
| $P_{cp}$ | Load pressure frequency content | [Pa] |
| $Q_{charge}$ | Load sense charging flow | $[m^3 s^{-1}]$ |
| $Q_{control}$ | Total flow into control piston | $[m^3 s^{-1}]$ |
| $Q_{cpleak}$ | Control piston leakage flow | $[m^3 s^{-1}]$ |
| $Q_{leak}$ | Pump leakage flow | $[m^3 s^{-1}]$ |
| $Q_{load}$ | Flow across load orifice | $[m^3 s^{-1}]$ |
| $Q_{ls}$ | Flow across load sense orifice | $[m^3 s^{-1}]$ |
| $Q_{pump}$ | Total theoretical pump flow | $[m^3 s^{-1}]$ |
| $r$ | Piston pitch radius | [m] |
| $r_{bias}$ | Bias piston radius | [m] |
| $r_{cpo}$ | Radius of control piston damping orifice | [m] |
| $r_{ls}$ | Radius of load sense spool | [m] |
| $r_{pls}$ | Radius of charging orifice hole | [m] |
| $r_{pso}$ | Radius of charging/discharging orifice hole | [m] |
| $R_{slope}$ | Pump leakage conductance term | $[m^3 s^{-1}\ Pa^{-1}]$ |

| | | |
|---|---|---|
| $S_{rOS}$ | Relative sensitivity of overshoot | |
| $S_{rtrise}$ | Relative sensitivity of rise time | |
| $T_{celc}$ | Temperature | [°C] |
| $t_{rise}$ | Rise time | [s] |
| $t_{10\%}$ | Time it takes for response to reach 10% of final value | [s] |
| $t_{90\%}$ | Time it takes for response to reach 10% of final value | [s] |
| $\boldsymbol{U}$ | Eigenvectors of training dataset | |
| $VB_{Pcp}$ | Control piston volume | [$m^3$] |
| $VB_{load}$ | Load volume | [$m^3$] |
| $VB_{pump}$ | Pump volume | [$m^3$] |
| $V_{cp}$ | Nominal control piston volume | [$m^3$] |
| $V_d$ | Pump theoretical displacement | [$m^3$rev] |
| $\boldsymbol{W}$ | Weights matrix from least squares solution | |
| $x_{cp}$ | Control piston position | [m] |
| $x_{ls}$ | Load sense spool position | [m] |
| $\boldsymbol{X}$ | Training dataset | |
| $\boldsymbol{X_{pc}}$ | Principal components | |
| $\boldsymbol{X_{reg}}$ | Reduced principal components matrix | |
| $y_{int}$ | Leakage flow intercept | [$m^3s^{-1}$] |
| $Y_{bcp}$ | Control piston volume bulk modulus factor | |
| $Y_{bl}$ | Load volume bulk modulus factor | |
| $Y_{bps}$ | Pump volume bulk modulus factor | |
| $Y_{max}$ | Maximum control piston travel | [m] |
| $Y_{reg}$ | Leakage factor of training data sample | |
| $\hat{Y}_{rslope}$ | Predicted leakage factor | |
| $Y_{rslope}$ | Measured leakage factor | |
| $\alpha$ | Jet angle for flow forces | [rad] |
| $\beta_{cp}$ | Control piston volume bulk modulus | [$m^3$] |

| | | |
|---|---|---|
| $\beta_l$ | Load volume bulk modulus | $[m^3]$ |
| $\beta_{ps}$ | Pump volume bulk modulus | $[m^3]$ |
| $\boldsymbol{\Sigma}$ | Covariance | |
| $\gamma$ | Pressure carryover angle | [rad] |
| $\mu$ | Dynamic viscosity of hydraulic fluid | $[kg\ m^{-1}s^{-1}]$ |
| $\mu_k$ | Kinematic viscosity of hydraulic fluid | $[m^2s^{-1}]$ |
| $\omega$ | Pump rotational speed | $[rads^{-1}]$ |
| $\varphi$ | Swashplate angle | [rad] |
| $\Phi$ | Swashplate angle frequency content | [rad] |
| $\rho$ | Density of hydraulic fluid | $[kg\ m^{-3}]$ |

# Chapter 1 Introduction to Condition Monitoring

The introduction to this research outlines the prevalence and value of condition monitoring in modern industry. Common failures of axial piston pumps are outlined with previous research efforts and current condition monitoring devices for hydraulic components are summarized. The value of dynamic modelling is discussed followed by the objectives of this research and a brief thesis overview.

## 1.1 Background of Condition Monitoring in Industry

Fluid power is characterized by large amounts of energy contained in a small package. Hydraulic systems have the potential to crush rocks, fell massive pine trees, and actuate aircraft control surfaces. Multibillion dollar industries utilize the good power-to-weight ratio that hydraulic systems can provide. In the mining industry machines are operated for extended periods of time with little to no maintenance. Unexpected equipment shutdowns are extremely costly but, through the implementation of engineering systems, can be avoided. Hydraulic failures can also put human lives at risk. Woch et al. (2019) show how hydraulic equipment failure in the aviation industry has caused loss of human life.

An important part of operating a fleet of equipment is maintenance. This can consist of regularly replacing machine fluids to scheduled service intervals in which the manufacturer recommends replacing components because, based on the number of cycles, the component is likely worn out. Watton (2007) categorizes maintenance schemes as breakdown maintenance, preventative maintenance, and condition-based maintenance. He highlights advantages and disadvantages of each and emphasizes how condition based monitoring can be the most effective but can also be the most costly due to instrumentation setup. Neale (1995) introduces condition monitoring as the selection of a measurement and monitoring at regular intervals to detect trends. He gives a high-level introduction to condition-based monitoring and its implementation as well as a review of current techniques from a tribology standpoint. He reviews damaged component repair techniques and design for wear resistance.

There exist numerous maintenance protocols currently in effect. Fluid sampling is a non-intrusive method in which the particles present in a machine's fluid are analyzed. The size, quantity, and type of particle can aid in predicting component failures. For example, an engine oil sample containing higher than normal bronze particles can indicate excessive wear in parts known to contain bronze. Hydraulic systems are viable options for condition monitoring since many hydraulic components can and do fail and the consequence of an unexpected shutdown is significant. A failure of the workhouse of the hydraulic system, the pump, requires extensive repair times. Depending on the nature of the failure, repairs can range from an hour or two changing a leaking fitting to days of completely flushing the hydraulic system of wear contaminants created by a catastrophic pump failure. Implementing condition-based maintenance in hydraulic systems has the potential to significantly reduce long term maintenance costs.

## 1.2 Operation and Failure of Axial Piston Pumps

Axial piston pumps are complex machines with many interacting components. A fully instrumented pump coupled to an electric motor is shown in Figure 1.1. Figure 1.2 provides a view of the sophisticated internal rotating assembly.

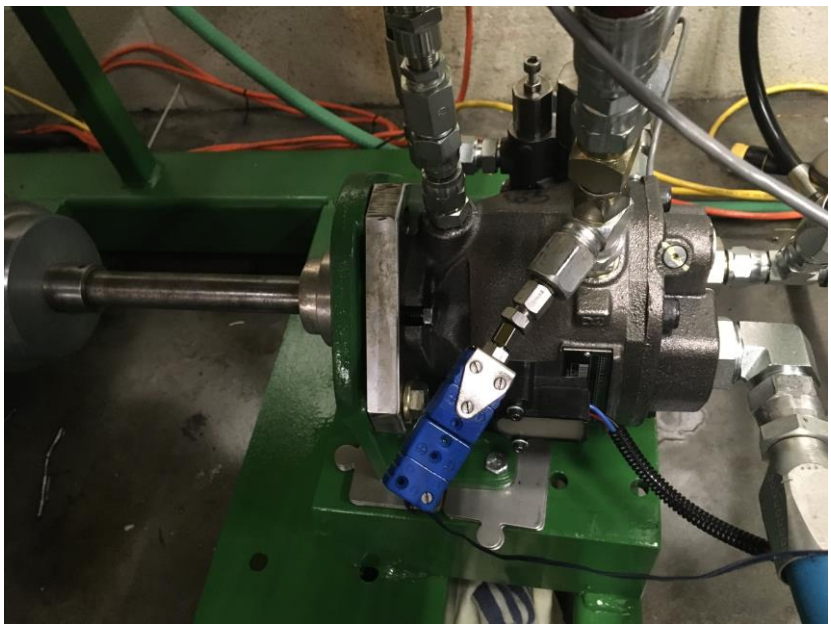

**Figure 1.1:** Load sensing axial piston pump, fully instrumented and coupled with electric motor

**Figure 1.2:** Load sensing axial piston pump internal rotating assembly

Figure 1.3 provides a cross sectional sketch of the internal rotating assembly of a load sensing axial piston pump. The sketch includes the bias and control pistons as well as the pumping pistons, barrel, valve plate, barrel spring, and retaining ring. The pump shaft is driven by a power source. The shaft and barrel are splined together so that when the shaft is driven, the barrel, pumping pistons, and retaining springs rotate as an assembly. The pumping pistons assemblies (piston and slipper) are pushed firmly against the swashplate by the pre-compression of the barrel spring against the retaining ring and the retaining ring against the slippers. With the rotation of the assembly, the pumping pistons follow the angled swashplate surface and translate axially. With axial translation, a low pressure volume at the inlet port of the pump is created in which fluid is supplied. The volume of fluid is trapped in the barrel chamber of each individual pumping piston and the barrel rotates 180 degrees, the volume becomes smaller and the fluid is expelled through the outlet port of the pump. This creates nine pumps of each piston chamber

volume for a single pump shaft rotation. The variation in swashplate angle (through pressurization of the control piston volume) changes the difference in volume from the inlet to outlet ports of the pump effectively changing the displacement of the pump. A no displacement condition can be created with a zero degree swashplate angle.

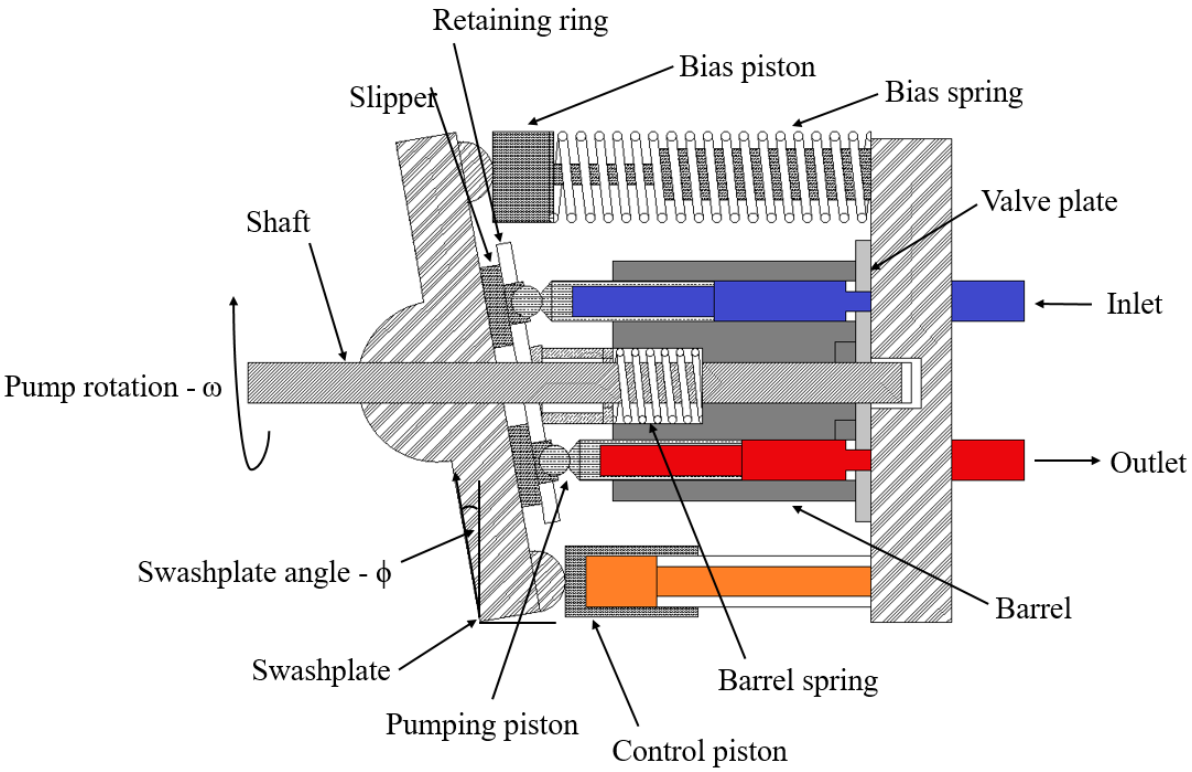


**Figure 1.3:** Cross sectional sketch of load sensing axial piston pump, not to scale

During operation, a load sensing axial piston pump has many interacting components. Failure of a pump can take many forms. Research areas include bearing failures in rotating equipment, contamination studies of hydraulic pumps, and frequency investigation of pump components.

How does an axial piston pump fail? Fey et al. (2001) provide a thorough summary of common failure modes in axial piston pumps summarizing pump failures into two general categories: failures as a result of hardware, and failures as a result of fluid condition. The authors outline how failures caused by fluid contamination comprise the majority of pump failures. The researchers inspect already failed pumps, mostly catastrophic. There is no investigation into how the failures initially manifest during pump operation. Eaton Corporation

(2002) claims that 90-95% of pump failures are a cause of the following: aeration, cavitation, contamination, excessive heat, over-pressurization, and improper fluid. Most of the causes listed can be avoided through careful system design, however, due to the necessity of maintenance and testing, and the lack of components' seals to be 100% effective, contamination to some degree is likely present in most hydraulic systems. Battat and Babcock (2006) further classify contamination failures as degradation, intermittent failures, and catastrophic failures. The authors estimate 75% of hydraulic system failures as a result of some form of contamination.

Atkinson (1979) performs a thorough axial piston pump wear test by introducing abrasive contamination into a simple hydraulic circuit in a precisely controlled environment. The main purpose of his research was to investigate the effects of solid contamination (air cleaner fine test dust) on an axial piston pump. Apart from obvious scoring of pump surfaces, Atkinson captured a significant decline in the volumetric efficiency (the ratio of pump outlet flow to pump inlet flow) of the pump due to degradation. This indicates increased leakage flow through the clearances designed into the pump and highlights the potential for case drain flow as an indicator of pump health. Other authors have performed tribology studies on axial piston pumps to further understand how pumps fail. Scuhler et al. (2017) perform an experimental analysis on axial piston pumps, focusing on three important interactions. These include the slipper and swashplate, the slipper and piston, and the slipper and retaining ring. The research concludes with a clear understanding of the cause and effect of the piston, retaining ring, and swashplate assembly. Wolfe (2018) further investigates the slipper and piston interaction. Wolfe takes a practical approach and shows how the frequency magnitude of the piston shoe socket vibration changes as the endplay increases due to wear.

## 1.3 Condition Monitoring Techniques

There has been a significant amount of research into the development of condition monitoring devices for axial piston pumps. In recent years there has been an increase in data processing capabilities and a significant development of automatic feature extraction algorithms. Research has attempted to apply machine learning techniques in an attempt efficiently capture value within large datasets.

Faults in rotating equipment can show up in many ways. Researchers have had success detecting faults by analyzing vibration and acoustic data. Mba and Rao (2006) summarize the

development of acoustic emission technology for various types of rotating equipment. They mention the limitations to the advancement of the technology as being issues with the attenuation of the signal and the practical issue of requiring the sensor to be in close proximity to the rotating component.

Hindman et al. (2002) give a thorough review of condition monitoring research specific to the fluid power industry. They break up past research into four categories: contamination control, parameter/state estimation, artificial neural networks and spectral analysis, and conclude that large amounts of data are required in the development of robust condition monitoring strategies.

As the internal components of an axial piston pump wear, particles can be created. Barraclough et al. (2018) outline the advantages and disadvantages of various particle detection technologies for the detection of ferrous particles in hydraulic fluid. They recommend a combination of particle detection devices to detect both small and large particles. To further this research suggestion, large amounts of particle and pump wear data may need to be obtained in order to design a reliable condition monitoring device.

Li (2005) performed simulated condition monitoring of an axial piston pump and compared simulation results to experimental data. To monitor one faulty pump piston requires extensive time to properly disassemble and machine a single piston to simulate wear. Li developed a fault simulation of an axial piston pump. Li's research only looked into excessive leakage in a single piston. Typically pistons will wear evenly and it is less common for a single piston to develop significant leakage relative to the others. Li suggested the research can go further in monitoring wear in more than one piston.

Latas and Stojek (2011) develop a complex dynamic model of an axial piston pump. They show that by modeling changes in parameters, measured vibrations at various points on the pump housing will change. This is because lubricating films disappear and all that is left is metal contact. No correlation to experimental data is made.

Shinn et al. (2015) applied an extended Kalman filter in an attempt to predict changes in state of a load sensing circuit. The filter was unable to detect excessive pump leakage.

## 1.4 Dynamic Modelling

There are many advantages to developing dynamic models that show correlation with physical systems. The analysis required for system improvement is computationally efficient and inexpensive with an accurate model.

Wu (2003) analyzed a load sensing and pressure compensated hydraulic system driving a motor. He investigated different operating conditions and commented on stability. The simulated dynamic model that he developed showed excellent correlation to experimental data. More recently, Manring and Mehta (2011) developed a comprehensive dynamic model of a pressure controlled axial piston pump. The model includes a hydro-mechanical servo valve. The complete model includes flow forces, inertia, and leakage. The model was used to determine pump parameters that would have the largest effect on the pump's bandwidth frequency. In another publication, Manring (2005) uses a similar pump model to develop equations that determine the dynamic response of a pressure controlled axial piston pump. By determining the characteristic equation of the dynamic model, Manring shows that leakage affects the pumps dynamic response and describes how leakage is a design tradeoff in that it reduces response times but decreases efficiency.

Wagner (2014) used a simplified load sensing pump model to investigate instabilities of the load sensing system. He developed a linearized model as well as a nonlinear model that was simulated using Simulink. He compared the Simulink model to experimental results. The results compared well in terms of the dynamics of the response. Wagner assessed the stability of the load sensing system and describes the accuracy of stability analysis methods.

## 1.5 System Dynamics and Condition

System dynamics is an area of intense research. Dynamics often relate to how fast something can be done and today there exists much research to improve actuation speeds of systems. Schoenau et al. (1990) derive a complex dynamic model of a variable displacement axial piston pump for potential controls optimization. Instead of investigating dynamics for control optimization, Hamad (2016), and Ding and Mei (2009) have shown that system dynamics can strongly correlate with condition.

Hamad (2016) discusses condition monitoring of a vehicle's suspension through the analysis of the systems dynamic response. He develops a complex dynamic model of a vehicle's

suspension system and verifies its accuracy. The vehicle's suspension system is a complex mechanical system including springs and dampers. He then shows how the response of the system will change when the suspension parameters of the system are altered. This simulates how worn out or damaged suspension components can be detected by analyzing changes in response.

The idea of using dynamics to indicate wear has been successfully applied to other vehicular systems. Ding and Mei (2009) uses a simple mathematical model to describe the interaction between system components of rail cars. Using cheap inertial sensors, the model was verified with experimental data. The authors highlight the potential for their research to be applied to other dynamic systems.

Many authors have investigated the dynamics of hydraulics components but there exists a research gap in the application of pump dynamics as a useful indicator of pump condition.

## 1.6 Objectives

The primary objective of this research is to investigate the feasibility of designing a condition monitoring device that can detect pump condition through dynamic pressure and swash angle measurements. In this research, pump condition is a measure of the pump's case drain leakage, a measure of volumetric efficiency, and does not encompass changes in mechanical efficiency (related to friction). To assess the potential of a condition monitoring device that detects changes in pump dynamics, other objectives will be fulfilled. A secondary objective is to develop a validated dynamic model of a load sensing axial piston pump. As previously mentioned, a valid dynamic model of the pump can aid in efficient system analysis. The validated dynamic model is used for multiple sub-studies throughout this research as well as developing the training data used by the leakage prediction algorithm. A framework for the design criteria of the device is laid out.

## 1.7 Thesis Overview

This section provides a short outline of this research. Previous literature has been summarized and an objective has been developed to fill a current gap in research. Chapter 2 provides a detailed description of model derivation using a variety of literature models and

modelling specific to the pumps used in this research. Chapter 3 outlines a technique to provide some guidance as to which operating point should be used to test the pump dynamics. Chapter 4 provides a thorough simulation study that confirms the feasibility of using dynamics to predict pump health using case drain leakage as a proxy. Chapter 5 evaluates the effectiveness of the engineering design performed in the simulation study on experimental pump dynamic data. The research project is summarized with future work suggestions in Chapter 6 and an Appendix section provides significant experimental data as well as a simple example to better visualize principal component analysis.

# Chapter 2 Nonlinear Dynamic Model

Chapter 2 details the derivation of a seventh order dynamic model based on previous modelling efforts. The system model is of a load sensing axial piston pump operating in a simple circuit where flow is controlled by a variable orifice and load pressure is simulated with another with a high speed valve that is responsible for the excitation of the system. The model is validated with experimental data from three worn pumps using a sensitivity analysis as a guide.

## 2.1 Description of System

Dynamic modelling is a modern, computationally efficient technique to not only mathematically represent a system but also to investigate system characteristics. It is commonly utilized for stability analysis, transient, and steady state analysis. One of the very first mathematical models of an axial piston pump was developed by Kavanagh (1987). It was shown to have good correlation with experimental testing for dynamic and steady state measurements of the swashplate angle.

Currently, many dynamic models of various hydraulic components exist in the literature. These models show good validation and have proven benefits in research. As a fundamental step in developing a condition monitoring device that utilizes pump dynamics as an indicator of condition, an investigation into how the dynamics of a pump correlate to leakage would be valuable. Experimentally, this is achievable but at significant expense, time, and difficulty. Controlling exactly how a pump fails is an obvious challenge.

Another useful method to investigate the effects of pump leakage and dynamic characteristics is to develop a validated nonlinear dynamic model of the pump and circuit components. A valid pump model is a time efficient tool for many types of analysis.

In this research, the dynamic model developed serves several purposes, which are to:

- Show the effects of leakage on pump dynamics
- Determine the best operating point to conduct dynamic testing
- Provide training data for the prediction algorithm

A dynamic model of the system depicted in Figure 2.1 was developed from fundamental fluid power and physics equations. Wagner (2014) developed a simplified dynamic model of an axial piston pump for the purpose of nonlinearity investigation. The model is detailed yet concise and shows very good validation accuracy when compared to experimental data. Wagner used experimental load pressure data as an input to the nonlinear model. This is a simple hydraulic circuit with a high speed control valve that changes orifice dimensions in a step fashion which results in a change in simulated load pressure.

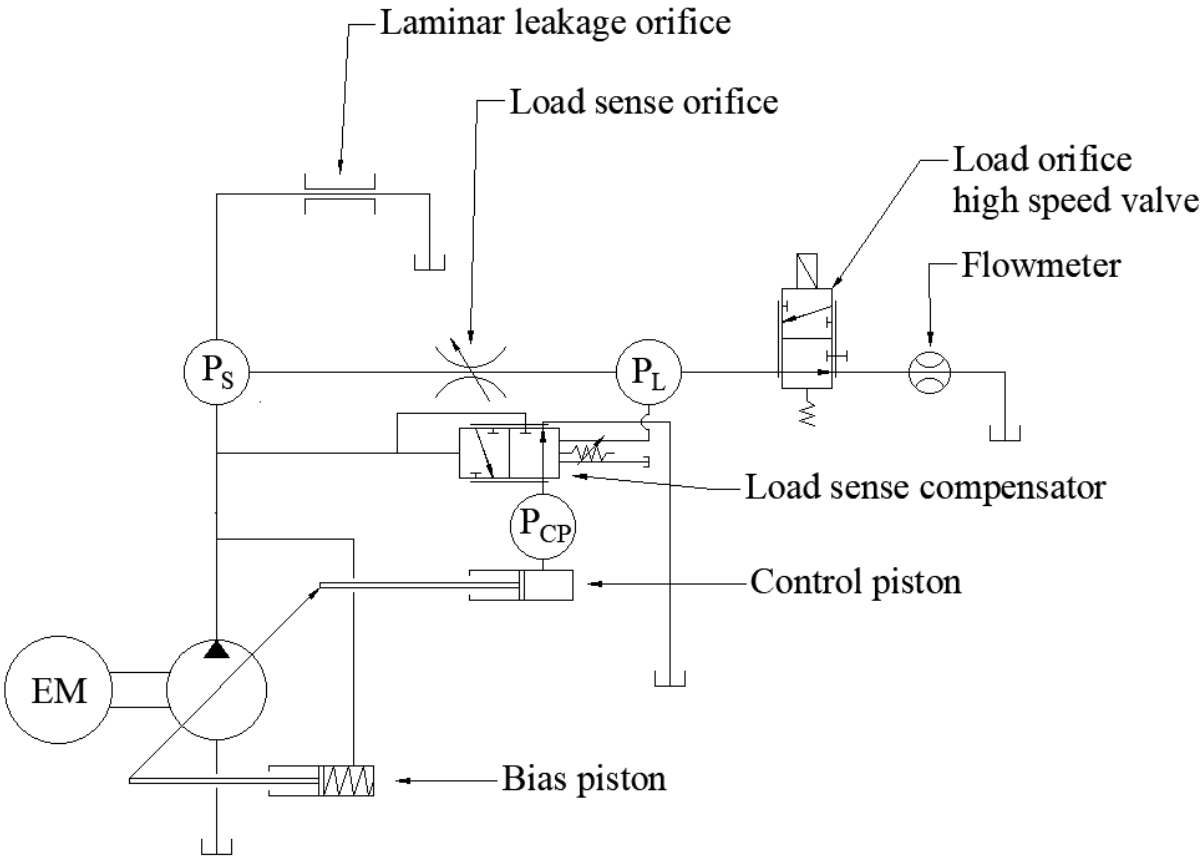


**Figure 2.1:** Load sense circuit for derivation of nonlinear dynamic model where as $P_s$ is the pump outlet pressure, $P_l$ the load pressure, and $P_{cp}$ the control piston pressure

## 2.2 Modelling System Volumes

Previous literature by Wagner (2014) and Manring and Mehta (2011) has highlighted the importance of modelling three circuit volumes, the pump outlet volume, $VB_{pump}$, the load volume, $VB_{load}$, and the control piston volume, $VB_{cp}$. Figure 2.1 illustrates the pressure within these volumes as $P_s$, $P_l$, and $P_{cp}$, respectively. A mathematical equation describing the pressure transient within a hydraulic volume is a combination of equations of state and conservation of mass flow rate (continuity equation). In reducing the continuity equation, isothermal flow is assumed; see Merritt (1967) for more details. Equation 2.1, from Merritt, assuming isothermal flow, is the resulting form after combining the continuity equation and the equation of state of a liquid:

$$\Sigma Q_{in} - \Sigma Q_{out} = \frac{dV_o}{dt} + \frac{V_o}{\beta}\frac{dP}{dt}. \tag{2.1}$$

The left side of the equation is simply the sum of flows in and out of the volume, $\frac{dV_o}{dt}$ accounts for the flow if a volume is expanding or contracting, $V_o$ is the nominal volume, $\frac{dP}{dt}$ is the change in pressure within the volume, $\beta$ is the effective bulk modulus of the volume, $\Sigma Q_{in}$ is the sum of the flows into the volume, and $\Sigma Q_{out}$ is the sum of the flows out of the volume.

For each of the three volumes modelled, equation 2.1 is rearranged and presented in a form to solve for the state variable, the pressure gradient within the volume. Applying equation 2.1 to model the pump volume yields

$$\dot{P}_s = \frac{\beta_{ps}}{VB_{pump}}\left(\Sigma Q_{VBpump}\right), \tag{2.2}$$

where $\Sigma Q_{VBpump}$ is the sum of all flows into and out of the pump volume, $\beta_{ps}$ is the effective bulk modulus of the pump volume, $VB_{pump}$is the pump volume, and $\dot{P}_s$ is the rate of change of pressure within the pump volume. It is important to note that $\beta_{ps}$is an effective bulk modulus and can be difficult to estimate since it is affected by entrained air and volume compliance. The pump volume accounts for all galleries and hose volumes that exist after the pumping piston volume in the barrel and before the load sense orifice. The pump volume is modelled with five flows given by

$$\dot{P}_s = \frac{\beta_{ps}}{VB_{pump}}\left(Q_{pump} - Q_{ls} - Q_{charge} - Q_{leak} - Q_{cpleak}\right). \quad 2.3$$

The pump volume equation includes the theoretical total pump flow calculated by the pump's flow gain and swashplate angle, $Q_{pump}$, $Q_{ls}$, the load sense flow (flow leaving the pump volume and passing across the load sense orifice), $Q_{charge}$, the charging flow which is the flow that enters the control piston, $Q_{leak}$, the pump leakage flow, and $Q_{cpleak}$, the control piston leakage flow. Each flow is modelled by equations 2.4-2.9 respectively. The pump flow is given as

$$Q_{pump} = f_{gain}\, tan^{-1}\left(\frac{Y_{max} - x_{cp}}{L}\right) \quad 2.4$$

where $Y_{max}$ is the maximum linear position of the control piston corresponding to a condition of no flow, $x_{cp}$ is the actual position of the control piston, and $L$ is the moment arm of the control piston. $f_{gain}$ is the flow gain of the pump given as flow per radian of swashplate angle.

Equation 2.4 results in a slightly nonlinear flow gain as shown in Figure 2.2.

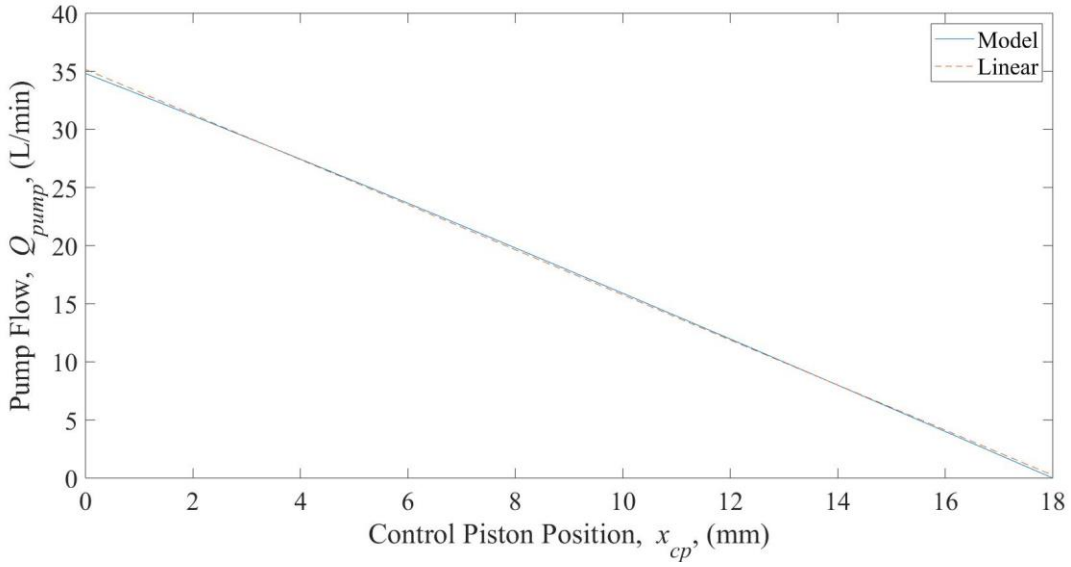


**Figure 2.2:** Flow gain comparison between linear and modelled (equation 2.4)

This yields an insignificant error as well as being a simple representation of the pump flow as a function of swashplate angle.

Merritt (1967) derives an equation for turbulent orifice flow for high Reynolds numbers and round orifices. The variable flow control valves in Figure 2.1 set the flow and simulated load and are assumed to have turbulent orifice properties. Merritt presents the general form for a turbulent orifice as

$$Q = C_d A_o \sqrt{\frac{2(P_1 - P_2)}{\rho}}, \tag{2.5}$$

where $C_d$ is the discharge coefficient of the orifice, typically near 0.60, $A_o$ is the orifice area, $P_1$and $P_2$ are the pressures before and after the orifices, respectively, and $\rho$ is the fluid density. Using this general form for a turbulent orifice, flow through the load sense orifice, $Q_{ls}$, can be modelled by

$$Q_{ls} = \sqrt{\frac{2(P_s - P_{load})}{\rho}} K_{ls}\,, \tag{2.6}$$

where $K_{ls}$ is a lumped parameter term and is simply the product of $C_{dls}$, the discharge coefficient of the load sense orifice, and $A_{ls}$, the hydraulic area of the load sense orifice. $P_s$ is the pump discharge pressure and $P_{load}$ is the simulated load pressure. Similarly, the turbulent orifice can be applied to the charging orifice. The charging orifice is the orifice created by the load sense spool and is responsible for metering the flow into the control piston. It can be represented by

$$Q_{charge} = C_d A_{charge} \sqrt{\frac{2(P_s - P_{cp})}{\rho}}, \tag{2.7}$$

where $Q_{charge}$ is the flow through the charging orifice, $A_{charge}$ is the effective charging orifice area that is covered in more detail in Section 2.4, $P_{cp}$ is the pressure inside the control piston volume, $C_d$ is the charging orifice discharge coefficient, and $P_s$ has been previously defined as the pressure within the pump volume.

The pump leakage is assumed to be laminar flow. It is modelled with a conductance term and a correction intercept. The intercept accounts for some flow at low pressure which was determined from extrapolating experimental data. The leakage flow, $Q_{leak}$, is represented by

$$Q_{leak} = R_{slope}(P_s - P_{tank}) + y_{int}\,, \tag{2.8}$$

where $R_{slope}$ is the conductance of the laminar leakage path, $y_{int}$ is the leakage flow intercept, and $P_{tank}$ is the system's tank pressure.

The control piston leakage is dependent on position. It is modelled as a laminar leakage path with a constant cross sectional area. However, the length of the leakage path changes as the control piston position changes. Equation 2.9 gives the control piston leakage, $Q_{cpleak}$, as a function of position:

$$Q_{cpleak} = \frac{C_{cp}(P_{cp} - P_{tank})}{-x_{cp}LP_{slope} + LP_{max}}, \tag{2.9}$$

where $LP_{slope}$ is determined by

$$LP_{slope} = \frac{LP_{max} - LP_{min}}{Y_{max}}. \tag{2.10}$$

$LP_{max}$ is the maximum position of the control piston leakage path, $LP_{min}$ is the minimum length of the leakage path, $LP_{slope}$ is the gradient of the leakage path with respect to control piston position, and $C_{cp}$ is a laminar leakage conductance specific to the control piston leakage path. Bitner (1986) modelled the control piston leakage path as the annulus between two cylinders and noticed that the leakage flow is significantly more when the cylinders are not concentric. Equation 2.9 is a simple rectangular orifice leakage path and does not account for leakage flow changes as the control piston nears its relief position or that the control piston is not centered on its guide.

A similar process can be performed for the load volume detailed in Figure 2.1. The general form of the state variable is defined by

$$\dot{P}_{load} = \frac{\beta_l}{VB_{load}}(\Sigma Q_{VBload}), \tag{2.11}$$

where $\dot{P}_{load}$ is the rate of change of pressure within the load volume, $VB_{load}$ is the load volume, $\beta_l$ is the load volume bulk modulus, and $\Sigma Q_{VBload}$ accounts for all flows in and out of the load volume.

$\Sigma Q_{VBload}$ can be represented with two flows: $Q_{ls}$ and $Q_{load}$. $Q_{ls}$ is the flow entering the load volume and has been previously derived as equation 2.6, and $Q_{load}$ which is the flow across the load orifice. Therefore, equation 2.11 becomes

$$\dot{P}_{load} = \frac{\beta_l}{VB_{load}}(Q_{ls} - Q_{load})\,. \tag{2.12}$$

Similar to the load sense flow, the load flow is modelled as a turbulent orifice equation with a lumped parameter term, $K_{load}$:

$$Q_{load} = \sqrt{\frac{2(P_{load} - P_{tank})}{\rho}} K_{load}\,, \tag{2.13}$$

where $K_{load}$ is simply the product of the load orifice area, $A_{load}$, and the discharge coefficient, $C_d$ , for the load orifice. $P_{load}$ is the pressure within the load volume and $P_{tank}$ is the system tank pressure.

The pressure gradient equation for the control piston in a general form is given by

$$\dot{P}_{cp} = \frac{\beta_{cp}}{VB_{Pcp}}\left(\Sigma Q_{VBcp}\right). \tag{2.14}$$

$\dot{P}_{cp}$ is the rate of change of pressure within the control piston volume, $\beta_{cp}$ is the effective bulk modulus of the control piston volume, $VB_{Pcp}$ is the volume of the control piston volume, and $\Sigma Q_{VBcp}$ is the parameter that accounts for all modelled flow in and out of the control piston. There are three potential sources of flow within the control piston volume. They can be included in equation 2.14 and in expanded form:

$$\dot{P}_{cp} = \frac{\beta_{cp}}{VB_{Pcp}}\left(\Sigma Q_{control} - A_{cp}\dot{x}_{cp} - Q_{CPleak}\right) \tag{2.15}$$

where $A_{cp}\dot{x}_{cp}$, the product of the control piston area and the control piston velocity, models the flow that accounts for the change in position of the control piston, and $Q_{CPleak}$ is from equation 2.9. $VB_{Pcp}$ is the control piston nominal volume and $\beta_{cp}$ is the effective bulk modulus of the control piston volume. $Q_{control}$ is the flow that acts to charge or discharge the control piston. It is a piecewise flow depending on the position of the load sense spool. If the load sense spool is positively displaced to the right (refer to Section 2.6, Figure 2.3), the flow in the control piston is considered to be charging; if it is displaced to the left, the flow is discharging from the control piston. Both flows can be modelled as flow through a turbulent orifice:

$$Q_{control} = C_d A_{chrg} C_{cc} \sqrt{\frac{2(P_s - P_{cp})}{\rho}} \text{ if } x_{ls} > 0\,, \tag{2.16}$$

and

$$Q_{control} = -C_d A_{dchrg} C_{dc} \sqrt{\frac{2(P_{cp} - P_{tank})}{\rho}} \text{ if } x_{ls} < 0\,. \tag{2.17}$$

$C_d$ is the discharge coefficient of the control piston charging or discharging orifice, $A_{chrg}$ is the charging orifice area, $A_{dchrg}$ is the discharging area orifice, $x_{ls}$ is the position of the load sense spool, and $C_{cc}$ and $C_{dc}$ are flow correction constants developed during model validation and detailed in Appendix A. Given the importance of the compensator as a controller, a more detailed model is outlined in Section 2.6. Equations 2.16 and 2.17 give the basic turbulent flow equations for general modelling purposes.

## 2.3 Modelling the Swashplate

Swashplate mechanics have been modelled extensively in prior literature. Kavanagh (1987) presents a mathematical swashplate model with good experimental validation both dynamically and at steady state. He discusses potential sources of error and notes that the linearity of the swashplate return spring can have a significant effect on dynamics. He also highlights the importance of modelling the reaction force of the pistons on the swashplate by performing sensitivity analysis on the associated parameters. Manring (2011) developed an extensive swashplate mechanics model with detailed reactionary forces. Wagner (2014) uses a simplified version of Manring's swashplate model and showed good dynamic response validation. The general state equation can be defined by

$$\ddot{x}_{cp} = \frac{1}{m_{cp}+m_{bias}}\Big[P_{cp}A_{cp} - P_s A_{bias} - k_{bias}x_{cp} - K_{ag}\dot{x}_{cp} - F_{bias} - \frac{C_1}{L}\tan^{-1}\left(\frac{Y_{max}-x_{cp}}{L}\right) + \frac{C_2}{L}P_s\Big]\,, \tag{2.18}$$

where $\ddot{x}_{cp}$ is the acceleration of the control piston, $m_{cp}$ and $m_{bias}$ are the control piston and bias piston masses, respectively, $A_{bias}$ is the bias piston area, $k_{bias}$ is the bias spring rate, $K_{ag}$ is the swashplate rotational damping, $F_{bias}$ is the bias spring preload, $L$ is the moment arm of the control and bias piston and $C_1$ and $C_2$ are additional torques on the swashplate and are detailed

by Wagner (2014). The swashplate inertia was neglected for simplicity and it was assumed that the damping term, $K_{ag}$, would account for friction in the cradle bearings of the swashplate as well as the damping of the swashplate rotation in hydraulic oil.

## 2.4 Modelling the Flow Compensator

The load sense compensator is an integral component to the system because it acts to control pump flow and load pressure. The compensator is a hydromechanical component that uses the pump pressure, load pressure, and margin spring setting to control flow and pressure within the pump control piston. Based on a simple force balance on the load sense spool, refer to Figure 2.3, the pump pressure is controlled to maintain margin pressure above the load pressure. The margin pressure of the load sense spool is determined by the preload setting of the margin spring. Wu (2003) describes the importance of the compensator because of its location within the control system loop of the load sensing pump. Because of this, the compensator was modelled with significant detail. The particular compensator that was modelled is illustrated in Figure 2.3. Physical measurements of the valve determine that the valve is technically an overlapped spool, meaning that in the center position all flow passages are closed. Merritt (1967) describes practical valve design and how, if the valve has some radial clearance, in order to be practically 'critically centered' it requires some overlap to compensate for the radial gap between the spool and bore. For simplicity, the valve is modelled as a strictly critically centered valve with no radial clearance. It was noticed that, with including valve overlap in the dynamic model, with no radial clearance, steady state error does occur. This is consistent with the valve characteristics that Merritt describes and practically makes sense since the valve may return to any position within the deadband zone and it is unlikely to return to the exact same position every time. Figure 2.3 illustrates the load sense spool and control piston relationship and shows the displacement conventions for modelling of both components.

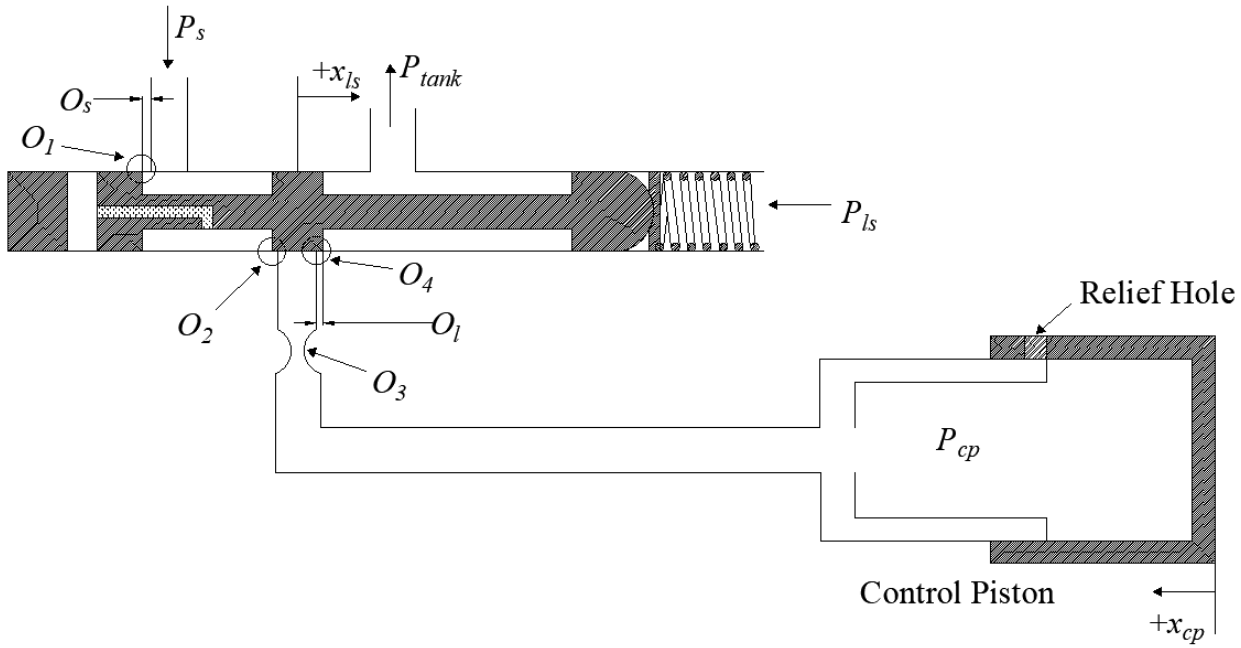


**Figure 2.3:** Load sense spool and control piston in fully extended position

The load sense spool is depicted in its centered position and is represented by $x_{ls}$. The control piston is shown in its startup position, $x_{cp}$, which corresponds to the maximum swash angle and maximum pump flow. The pressures illustrated include the pump pressure, $P_s$, control piston pressure, $P_{cp}$, the tank pressure, $P_{tank}$, and the load sense pressure, $P_{ls}$. Also shown is the control piston relief hole; this hole controls the maximum position of the control piston (corresponding to zero flow) by relieving control piston pressure upon being uncovered. Four orifices control the flow into and out of the control piston, these are defined in the charging and discharging cases: they are: $O_1$, the first load sense charging orifice area, $O_2$, the second load sense charging area, $O_3$, the load sense spool fixed damping orifice area, and $O_4$, the load sense spool discharging orifice area. Geometric parameters are the spool offset position, $O_s$, and the spool overlap, $O_l$.

In the charging case, $+x_{ls} > 0$ , the load sense spool moves to the right allowing pump flow to the control piston. As illustrated in Figure 2.3, the charging flow is controlled by three orifices in series, $O_1$, $O_2$, and $O_3$. $O_1$ and $O_2$ are variable orifices with a circular cross section and are a result of drilled passages being uncovered by the load sense spool lands. The third

orifice, $O_3$, is a fixed area orifice. The effective charging area, $A_{charge}$, of this series circuit can be given as

$$A_{chrg} = \sqrt{\frac{1}{\left(\frac{1}{O_1}\right)^2 + \left(\frac{1}{O_2}\right)^2 + \left(\frac{1}{O_3}\right)^2}} \,. \tag{2.19}$$

The discharging case is similar except that it is controlled by only two orifices in series, $O_3$ and $O_4$. The discharging effective area, $A_{dcharge}$, is given by

$$A_{dchrg} = \sqrt{\frac{1}{\left(\frac{1}{O_3}\right)^2 + \left(\frac{1}{O_4}\right)^2}} \,. \tag{2.20}$$

It is important to note that the damping orifice, $O_3$, is active in both the charging and discharging cases.

$$O_1 = \frac{(x_{ls} - d_{pso} - O_s + r_{pso})}{r_{pso}} \cos^{-1}(r_{pso}{}^2) - (x_{ls} - d_{pso} - O_s + r_{pso}) \left[\sqrt{(x_{ls} - d_{pso} - O_s)(-2r_{pso}) - (x_{ls} - d_{pso} - O_s)^2}\right] , \tag{2.21}$$

$$O_2 = \frac{(r_{pls} - x_{ls} - O_l)}{r_{pls}} \cos^{-1}(r_{pls}{}^2) - (r_{pls} - x_{ls}) \left[\sqrt{(2r_{pls}x_{ls} - x_{ls}^2)}\right] , \tag{2.22}$$

and

$$O_4 = \frac{(r_{pls} + x_{ls} + O_l)}{r_{pls}} \cos^{-1}(r_{pls}{}^2) - (r_{pls} + x_{ls}) \left[\sqrt{(-2r_{pls}x_{ls} - x_{ls}^2)}\right] \tag{2.23}$$

represent the areas of the variable orifices that control flow to the control piston. These equations are the result of circular geometry being covered or uncovered by the load sense spool. Geometric parameters include $r_{pso}$ and $d_{pso}$, the radius and diameter of the hole that is being covered or uncovered at $O_1$, and $r_{pls}$ and $d_{pls}$, the radius and diameter of the hole being uncovered at $O_2$ and $O_4$. The spool overlap, $O_l$, was included in the equations for clarity, however, its value was set to 0 to produce consistent results.

The resulting orifice area gains are graphically shown in Figure 2.4 and Figure **2.5**.

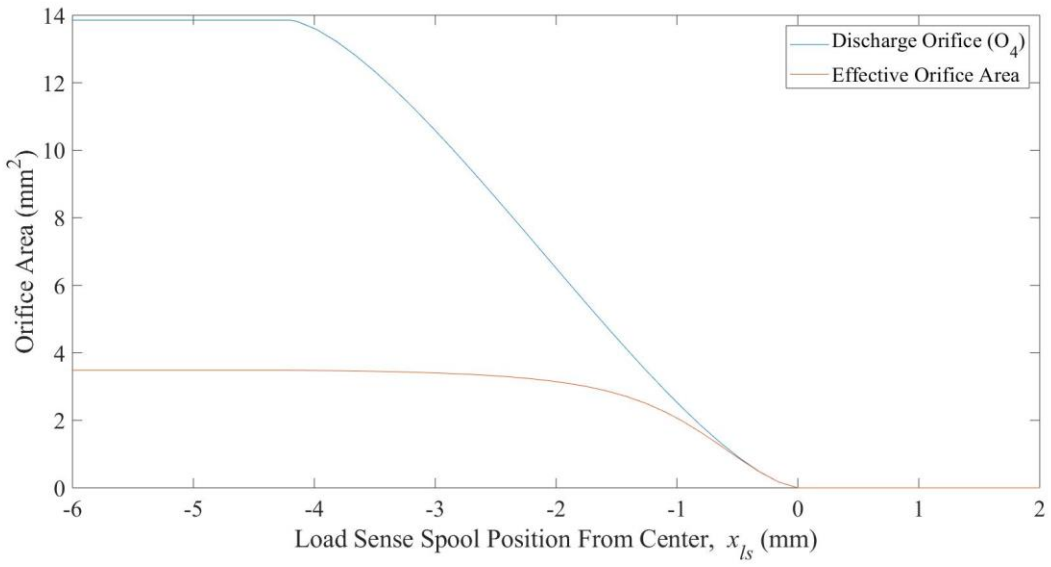


**Figure 2.4:** Effective discharge orifice area of orifice $O_4$

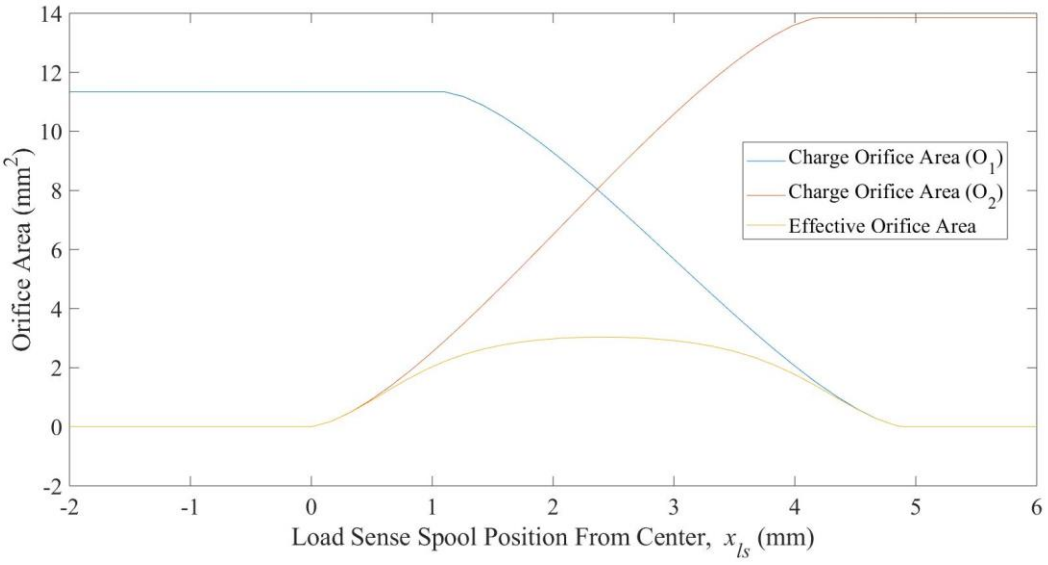


**Figure 2.5:** Effective charge orifice area of orifices $O_1$ and $O_2$

Lastly, the dynamics of the load sense spool are described. A simple sum of forces on the load sense spool results in the following second order differential equation:

$$\ddot{x}_{ls} = \frac{1}{m_{ls}}\left[A_{ls}P_s - A_{ls}P_m - A_{ls}P_{load} - k_{ls}x_{ls} - d_{ls}\dot{x}_{ls} + F_f\right]. \qquad 2.24$$

$\ddot{x}_{ls}$ is the load sense spool acceleration, $m_{ls}$ is the mass of the load sense spool, $A_{ls}$ is the cross sectional area of the load sense spool, $k_{ls}$ is the load sense spring constant, $d_{ls}$ captures the damping of the load sense spool, $\dot{x}_{ls}$ is the velocity of the load sense spool, and $F_f$ accounts for the flow forces acting on the load sense spool. Flow force modelling followed that of Wagner (2014) who neglected transient flow forces but was still able to acquire good model validation with a similar nonlinear model. The charging, $F_{chrg}$, and discharging, $F_{dchrg}$, flow forces can be modelled using

$$F_{chrg} = 2\left(P_s - P_{cp}\right)\frac{C_d^2}{C_c}\cos\alpha\, x_{ls}A_{chrg}C_{cc}\,, \qquad 2.25$$

and

$$F_{dchrg} = 2\left(P_{cp} - P_{tank}\right)\frac{C_d^2}{C_c}\cos\alpha\, x_{ls}A_{dchrg}C_{dc}\,, \qquad 2.26$$

respectively. $\alpha$ is the jet angle of the orifice, $C_c$ the contraction coefficient, and $C_{cc}$ and $C_{dc}$ are flow correction constants developed during model validation and detailed in Appendix A.

## 2.5 Sensitivity Analysis

Sensitivity analysis is an important tool for understanding how system parameters affect outputs. Outputs can be determined by the user and for this study they include characteristics of the dynamic response. Outputs can be features of the dynamic response such as percent overshoot, rise time, or they can simply be steady state values. The analysis simply involves varying a parameter by a small amount and determining how much an output changes. It can give insight into how accurate a parameter may need to be determined and consequently show if certain assumptions are valid. As a simple example, consider the case of a single automobile strut subject to a bump (step input). Characteristics of the struts' dynamics following the step input may be hypothesized to change with gas charge pressure. Perhaps the overshoot of the transient increases significantly with decreased charge pressure. A sensitivity analysis gives insight into this cause-and-effect relationship by determining how much of a change in one parameter (gas charge pressure) changes the output (shock overshoot). This gives insight about the effects of system parameters on specified outputs, provides information about how accurately parameters may need to be determined, and can guide instrumentation selection.

For this research, sensitivity analysis was utilized for several purposes. It is used to form a rough guide for the procedure of model validation. It will give insight into certain parameter assumptions that were initially made. As well, it will serve as a general analysis of which parameters are driving the system dynamics.

For model validation, two important characteristics were selected to guide the sensitivity analysis: the overshoot of the dynamic response and the rise time. The overshoot, $\%\, O.S.$, is calculated as

$$\%\, O.S. = \frac{Ps_{peak} - Ps_{SS2}}{Ps_{SS2} - Ps_{SS1}} \times 100\,, \qquad 2.27$$

where $Ps_{peak}$ is the peak of the pressure transient, $Ps_{SS1}$, is the steady state pressure value before the step, and $Ps_{SS2}$ is the steady state pressure after the step.

The rise time, $t_{rise}$, is calculated as the time it takes for the response to go from 10% to 90% of its final steady state value:

$$t_{rise} = t_{90\%} - t_{10\%}\,. \tag{2.28}$$

There are numerous ways to perform sensitivity analysis. For this research, since the sensitivity of parameters on the selected characteristics is to be compared relative to one another, relative sensitivity is used. Smith et al. (2008) describe several ways to perform sensitivity analyses and highlights relative sensitivity as appropriate for cross parameter comparison since it is dimensionless. The relative sensitivities of the overshoot and rise time are given by

$$S_{rOS} = \frac{\partial OS}{\partial \emptyset_i} \times \frac{\emptyset_i}{OS_{base}}, \tag{2.29}$$

and

$$S_{rtrise} = \frac{\partial t_{rise}}{\partial \emptyset_i} \times \frac{\emptyset_i}{t_{rbase}}, \tag{2.30}$$

respectively. The partial derivatives can be approximated as the slope due to small changes in $\emptyset_i$, the parameter of interest. $S_{rOS}$ and $S_{rtrise}$ are the relative sensitivities of the overshoot and rise time, respectively, of a parameter and are dimensionless values. $OS_{base}$ and $t_{rbase}$ are the values of overshoot and rise time with no parameter variation, or, base values. Having presented the theory behind the analysis, there exist two important considerations. The first involves the step size, or magnitude of change, in the base parameter. The second is the operating point at which the parameter sensitivity is assessed. In the case of a PCLS pump, the operating point is governed by a target flow and a target load pressure. Both targets can be met by choosing the size of the load and load sense orifice area. The following section details the selection of the change in step size for the parameters.

### 2.5.1 Step Size

Sensitivity analysis investigates how much of an effect a parameter has on a certain output characteristic. In this investigation, parameters were varied and how these parameter variations affected the overshoot and rise time was recorded. An important aspect of the analysis is the step size, or the delta change in a parameter given to determine differences in dynamic response characteristics. If the parameter change is too small, it will be sensitive to rounding

errors and noise, and if it is too big, then the sensitivity will change significantly over the parameter range.

Figure 2.6 illustrates how the sensitivity of a change in the pump volume bulk modulus changes with step size.

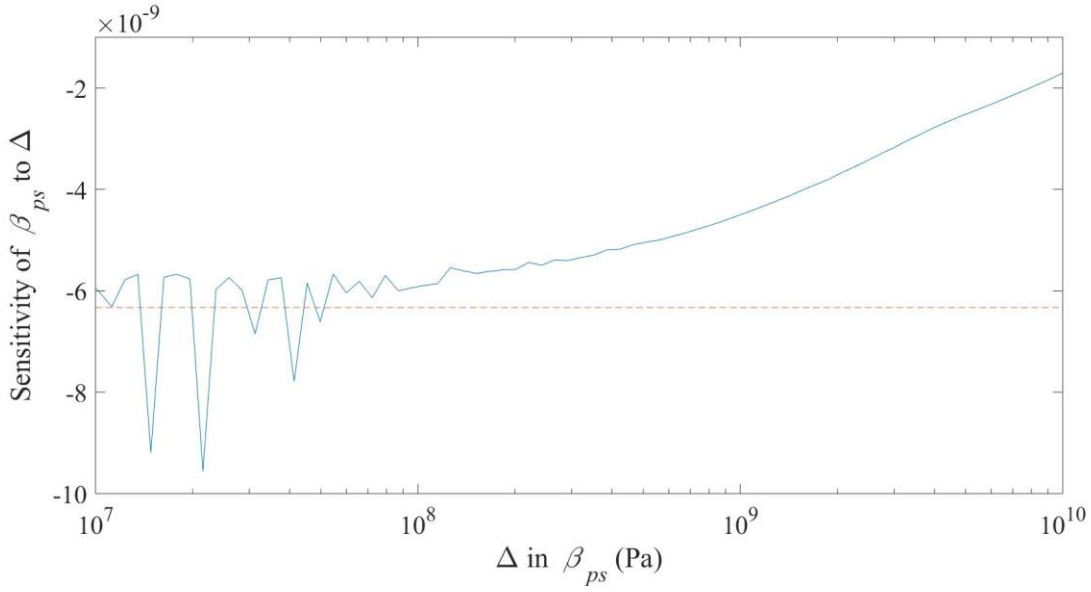


**Figure 2.6:** Step size determination for $\beta_{ps}$

As the step size gets smaller, the sensitivity becomes very sensitive to noise and rounding error. A larger step size has a large change in slope. A good step size from Figure 2.6 is approximately 0.1 GPa which equates to roughly 10% of the value of the pump volume bulk modulus (which is 1 GPa). A similar analysis can be done for the pump volume to determine cross parameter consistency with step size. This will allow for simplicity since each parameter can be varied the same amount.

Figure 2.7, a plot of the sensitivity of the load volume to changes in the load volume, shows similar results as Figure 2.6.

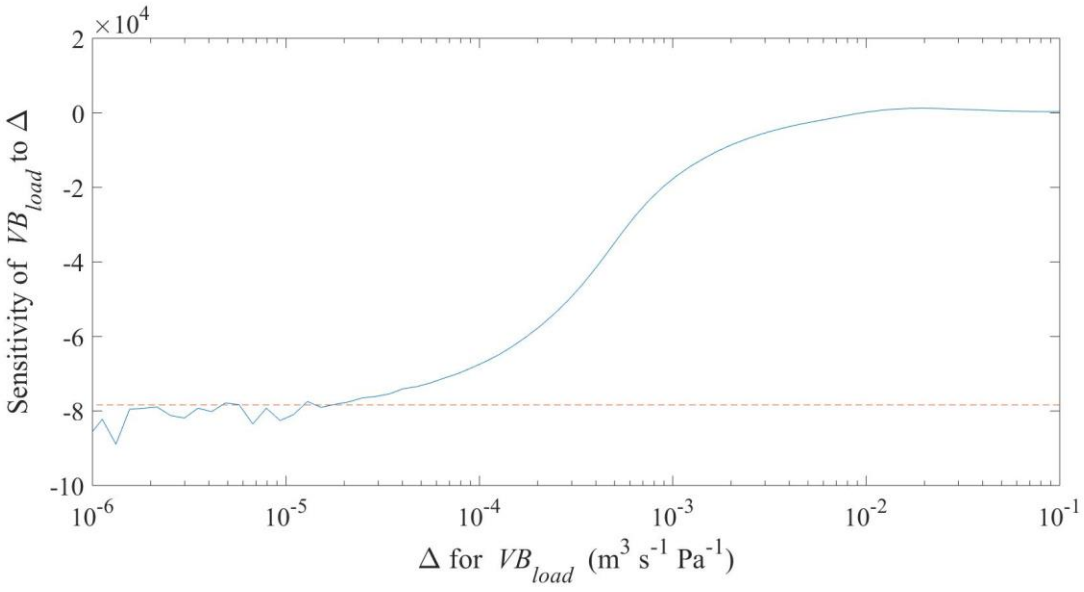


**Figure 2.7:** Sensitivity of $VB_{load}$

At very small delta values, noise and rounding error have a significant effect on the relative sensitivity. At larger step size selections, the slope of the sensitivity is quite steep and will show large changes in response characteristics. A good delta value for this parameter is $10^{-5}$ which corresponds to approximately 10% of the parameter $VB_{load}$.

### 2.5.2 Results

Having determined an appropriate step size, the next step is to determine the system operating point. Since the analysis is accurate for local operating points, it is known that parameter sensitivities can change significantly at different operating points. The majority of this research uses a step change to analyze pump response features. The sensitivity analysis is performed using a step in load pressure that gives similar output values to the experimental response data obtained and outlined in Appendix C. The target flow and pressures are given in Table 2.1.

**Table 2.1:** Operating point targets

| $P_{s1}$ (MPa) | $P_{s2}$ (MPa) | $P_m$ (MPa) | $Q_{pump}$ (L/min) | $R_{slope}$ ($m^3 s^{-1} Pa^{-1}$) | $y_{int}$ ($m^3 s^{-1}$) |
|---|---|---|---|---|---|
| 3.5 | 16 | 1 | 17.4 | 1e-12 | 4e-6 |

The operating points listed above were obtained by determining the correct load and load sense orifice constants that give the specified load pressure and flow. The leakage slope and intercept are values that give an average amount of pump leakage as compared to the experimentally worn pumps. Table 2.2 provides the results of the sensitivity calculations.

**Table 2.2:** Relative sensitivity analysis results for pump pressure response, highlighted in grey are parameters that show significant sensitivity

| Parameter | $SR_{OS}$ | $SR_{trise}$ |
|---|---|---|
| $\beta_{ps}$ | -0.5525 | 42.2388 |
| $\beta_l$ | 0.3555 | -198.3778 |
| $\beta_{cp}$ | -0.0272 | 27.0820 |
| $VB_{pump}$ | 0.5564 | 38.9635 |
| $VB_{load}$ | -0.4474 | -184.7628 |
| $V_{cp}$ | 0.0092 | -4.7558 |
| $\rho$ | 0.1788 | 38.6673 |
| $C_d$ | 0.4860 | -71.3267 |
| $R_{slope}$ | -0.1160 | -306.0437 |
| $k_{ls}$ | -0.2732 | -28.4740 |
| $F_{bias}$ | 0.0190 | -40.7526 |
| $k_{bias}$ | 0.0223 | -5004.3727 |
| $K_{ag}$ | -0.1767 | -39.9876 |
| $d_{ls}$ | 0.0124 | -13.4572 |
| $f_{gain}$ | 0.2546 | -18.0774 |
| $C_1$ | 0.0220 | -26.1765 |
| $C_2$ | -0.0352 | -177.4532 |

| | | |
|---|---|---|
| $y_{int}$ | 0.0180 | -31.6206 |
| $y_{max}$ | 0.1589 | -37.4541 |
| $C_{cp}$ | 0.0036 | -2.9049 |

The results in Table 2.2 and Table 2.3 show some parameters as having a large effect on the overshoot and rise time of the pump pressure transient. The pump discharge pressure response, $P_s$ , is very sensitive to the pump and load volumes ($VB_{pump}$ and $VB_{load}$ respectively) as well as the bulk modulus of the pump discharge volume, $\beta_{ps}$, and the load volume, $\beta_l$. In practice, the pump and load volumes can be determined with relatively good accuracy, however, the bulk modulus of each of the volumes is much more difficult to determine with confidence.

The load sense spring rate, $k_{bias}$ , was determined accurately through experimental testing. It is an important parameter for model validation since it has a large effect on overshoot at high pressures. Because its value was determined with confidence, this parameter can be used for validation but with a smaller threshold than unmeasurable parameters.

The pump and load volume modelled in the system have a large effect on the dynamic pump pressure measurements. With regards to model validation, they are especially important because their values are difficult to measure and because they have opposite effects to each other.

Table 2.3 presents the relative sensitivity results for the swashplate dynamics.

**Table 2.3:** Relative sensitivity analysis for swashplate transient

| Parameter | $SR_{OS}$ | $SR_{trise}$ | SS1 | SS2 |
|---|---|---|---|---|
| $\beta_{ps}$ | -0.7925 | 0.3338 | 0.0005 | -0.0010 |
| $\beta_l$ | 0.2010 | 0.1315 | 0.0002 | 0.0018 |
| $\beta_{cp}$ | -0.0068 | -0.6159 | 0.0004 | 0.0011 |
| $VB_{pump}$ | 0.7959 | 0.6640 | -0.0002 | 0.0011 |
| $VB_{load}$ | -0.2142 | -0.3027 | 0.0001 | 0.0018 |
| $V_{cp}$ | 0.0032 | -0.2834 | 0.0005 | 0.0000 |

| | | | | |
|---|---|---|---|---|
| $\boldsymbol{\rho}$ | 0.4371 | -0.0715 | -0.4872 | -0.4720 |
| $\boldsymbol{C_d}$ | 0.4059 | -0.3114 | 0.0003 | -0.0003 |
| $\boldsymbol{R_{slope}}$ | -0.0935 | 1.0824 | 0.0086 | 0.0395 |
| $\boldsymbol{k_{ls}}$ | -0.5956 | 0.2702 | 0.0008 | 0.0025 |
| $\boldsymbol{F_{bias}}$ | 0.0508 | -0.2010 | 0.0002 | 0.0018 |
| $\boldsymbol{k_{bias}}$ | 0.0153 | 0.3781 | 0.0002 | -0.0004 |
| $\boldsymbol{K_{ag}}$ | -0.1768 | 0.4923 | 0.0005 | 0.0014 |
| $\boldsymbol{d_{ls}}$ | 0.0171 | -0.1719 | 0.0006 | 0.0002 |
| $\boldsymbol{f_{gain}}$ | 0.7861 | -1.4489 | -0.9907 | -0.9877 |
| $\boldsymbol{C_1}$ | 0.0128 | -0.0197 | 0.0004 | -0.0003 |
| $\boldsymbol{C_2}$ | -0.0309 | 0.4919 | 0.0005 | -0.0001 |
| $\boldsymbol{y_{int}}$ | -0.0089 | 0.4791 | 0.0097 | 0.0087 |
| $\boldsymbol{Y_{max}}$ | 0.1290 | 0.4326 | 0.0003 | -0.0007 |
| $\boldsymbol{C_{cp}}$ | -0.0001 | -0.0727 | 0.0006 | 0.0000 |

The results differ from the pressure dynamics and can be referred to during model validation. Included in the sensitivity analysis results of the swashplate dynamics is the steady state characteristics of the response. SS1 is the steady state swashplate angle before the transient and SS2 is the angle after the transient. These results are useful for model optimization, specifically for the swashplate angle since the steady state angles depend on many parameters.

## 2.6 Model Validation Results

Model optimization involves adjustment of estimated parameters in order to match the nonlinear dynamic model outputs to experimental data. It is important to have a validated model since, ultimately, the training data supplied to the prediction algorithm are solely simulation data. Initially, base parameters were determined from geometric measurements as well as estimation from values found in the literature. This set of parameters is the base parameter set. Some of these parameters values were obtained with confidence, while others are known to exist within quite a broad range. The parameters with less confidence can be adjusted until the experimental dynamic model transients closely match the Simulink outputs. With no guidance this can be a

tedious and repetitive process. To create some guidance, a sensitivity analysis was performed on key parameters.

The primary goal of model validation is to ensure that the prediction algorithm outlined in Chapter 4 can be trained with a large amount of simulated pump response data rather than requiring experimental data. As will be outlined in a later section, the important outputs include the pump pressure response, control piston pressure, and swash angle. Model optimization is performed for the three outputs and collected experimental response data. Experimental data analysis is covered in much more detail in Appendix C, however, for model validation three dynamic response vectors from three different pumps which have various degrees of wear is performed. The nonlinear dynamic Simulink model inputs include the base parameter set and the flow and load orifice constants. The step input to the model is the step in load pressure. The base parameter set used for optimization is shown in Appendix A. The orifice constants are also determined in Appendix C. That is, for each experimental pump response the orifice constants were determined exactly from flow and pressure data using the turbulent orifice equation. Output signals of pump pressure, control piston pressure, and swashplate angle are used to assess the validity of the dynamic model. The optimization was performed using results from Section 2.5, sensitivity analysis, as guidance. Figure 2.8 - Figure **2.13** compare the response data from the nonlinear dynamic model subject to the same orifice constants and leakage amounts as determined from the experimental response data obtained from the three worn pumps.

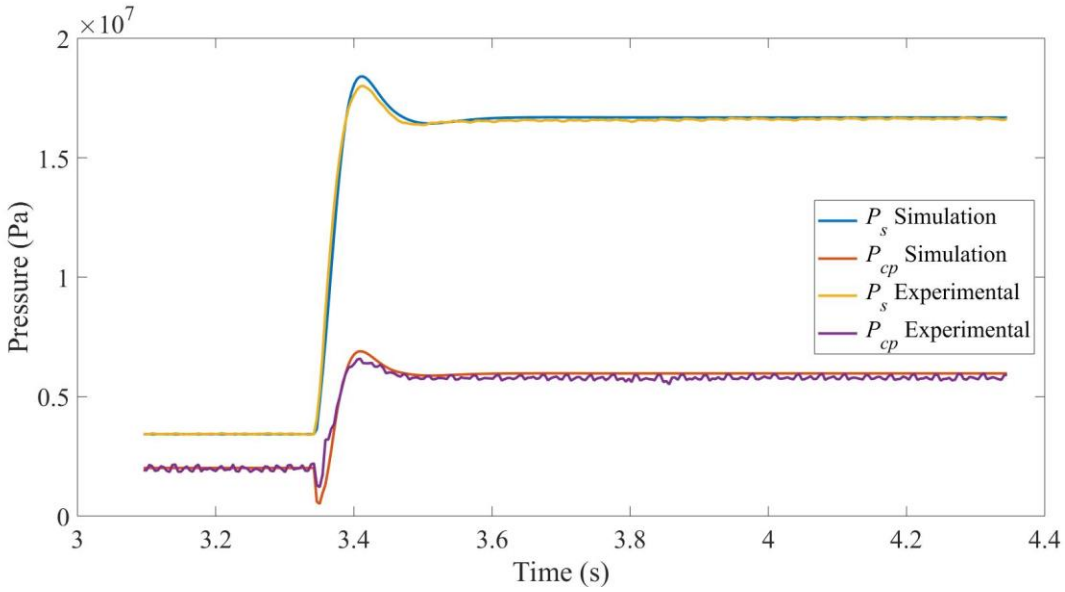


**Figure 2.8:** Pump 165 (most wear) pump pressure validation plot

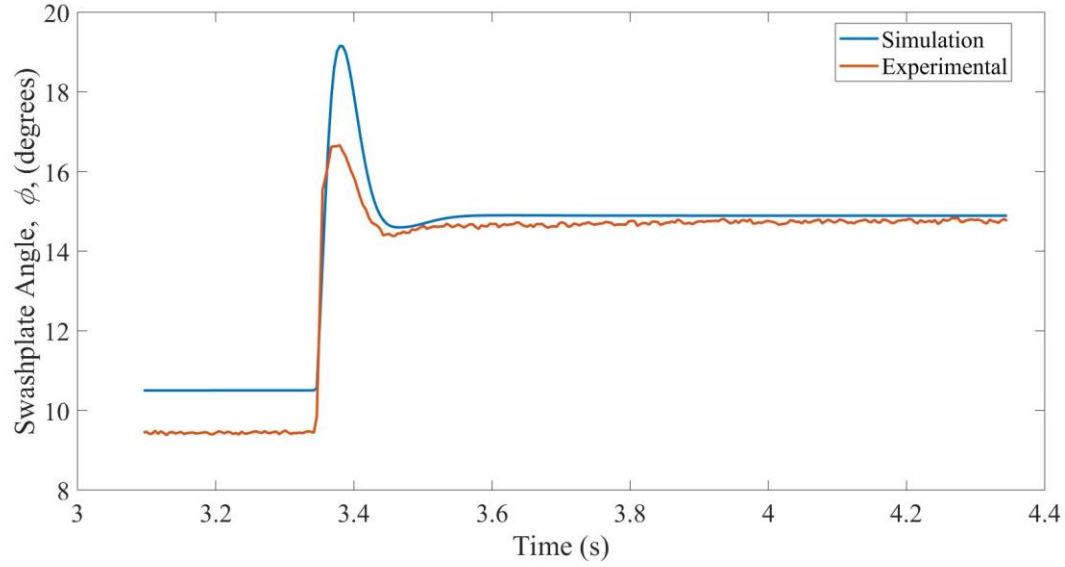


**Figure 2.9:** Pump 165 (most wear) swash angle validation plot

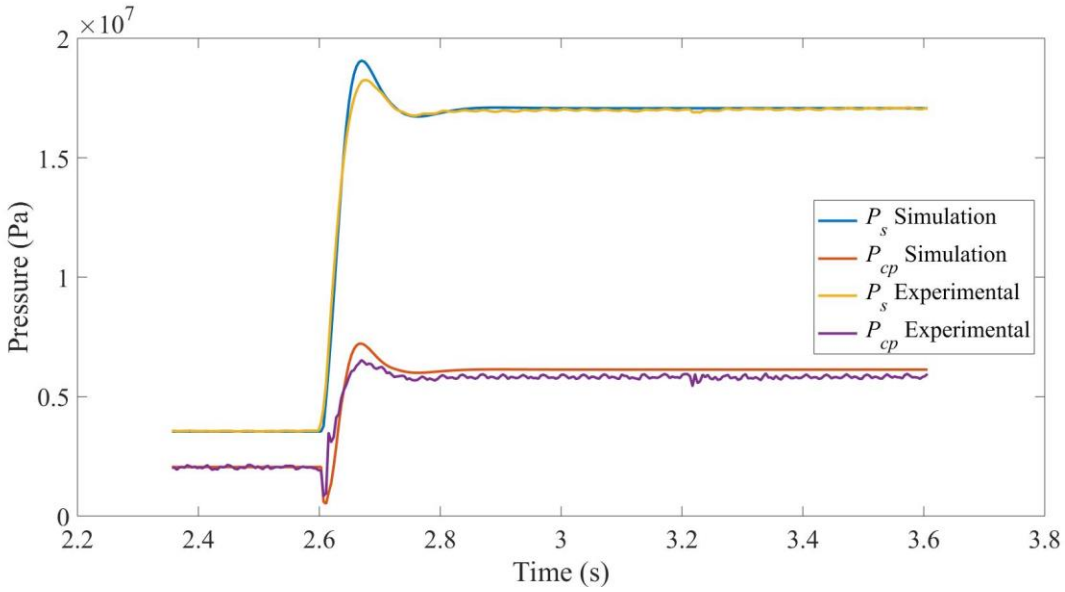


**Figure 2.10:** Pump 167 (mid wear) pump pressure response validation plot

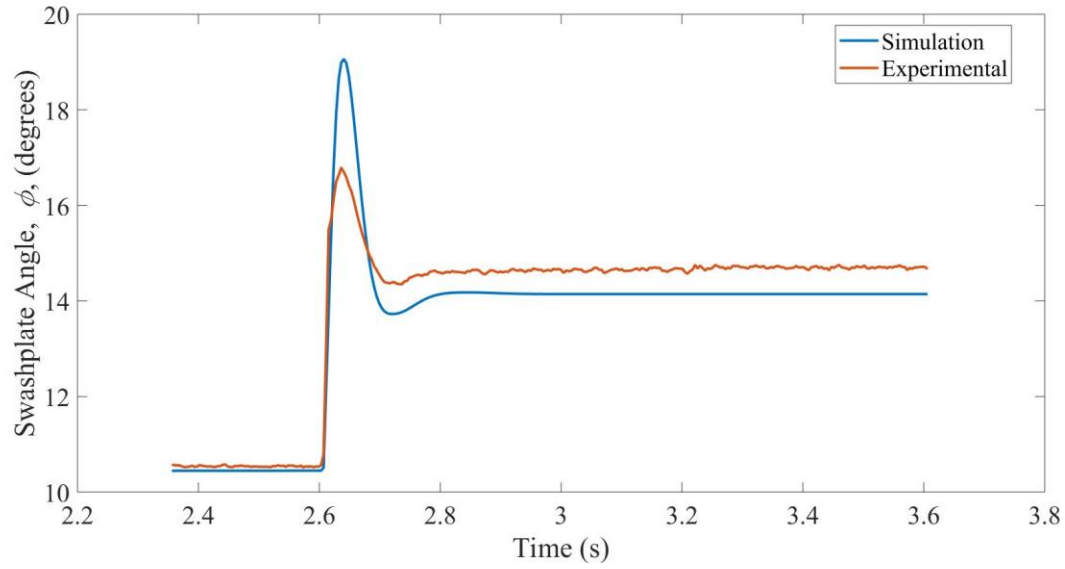


**Figure 2.11:** Pump 167 (mid wear) swash angle response validation plot

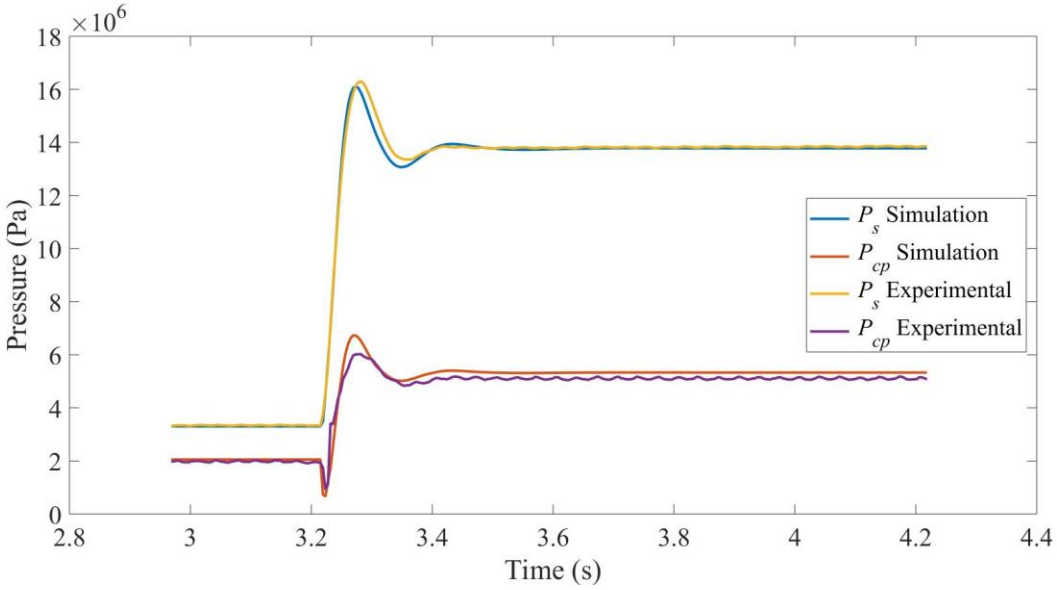


**Figure 2.12:** Pump 172 (mild wear) pump pressure response validation plot

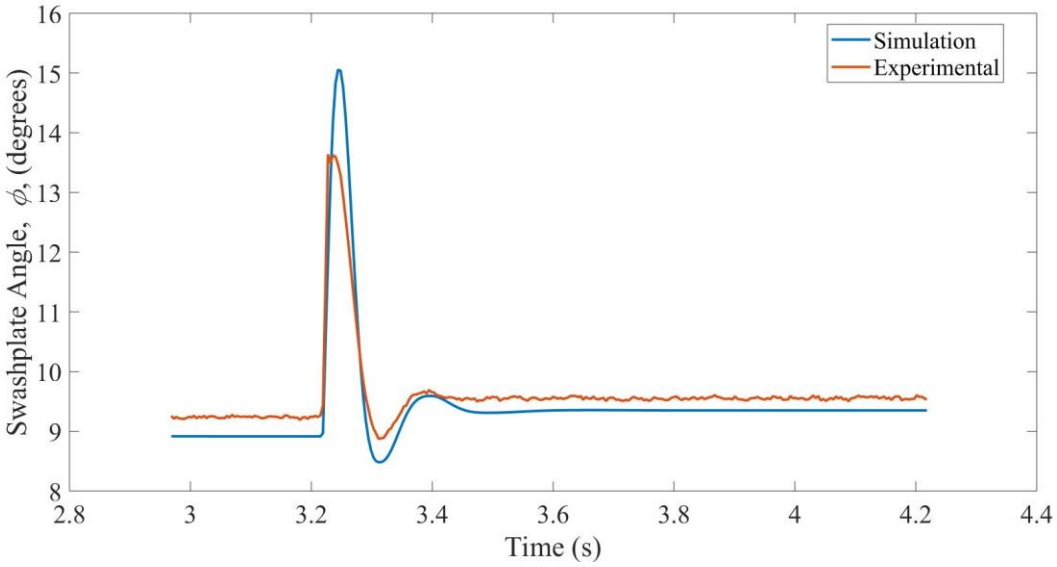


**Figure 2.13:** Pump 172 (mild wear) swash angle response validation plot

It is clear that the pressure response data have significantly better steady state and transient validation than that of the swash angle. A big unknown is how accurate this validation needs to be for the purposes of supplying data to the machine learning algorithm. In the best

case, the validation matches perfectly, however, this can be difficult and tedious. In Figure 2.8 - Figure **2.13** it is clear that the nonlinear dynamic model results replicate the *trends* in response data as the experimental results show. For example, observing the difference between the most worn and least worn pump, the swash angle response has significantly more overshoot and oscillation than the worn pump. The nonlinear dynamic model seems to capture this trend.

# Chapter 3 Operating Point Investigation

The main objective of Chapter 3 is to determine an optimal operating point for the step input excitation. A linearized model of the 7th order system is developed and an analysis on pole movement through root locus is performed. The movement of the dominant poles is shown to be much more significant at higher pressures. This simply means that, within a linear range, changes in leakage have more of an effect on the dominant poles of the system at higher pump or load pressures. The chapter concludes with the recommendation to perform dynamic testing at the highest possible pressure but to also avoid signal saturation.

## 3.1 Linearization

In developing a condition monitoring device, an important consideration is the operating point at which the device will test the dynamics of the pump. Different test operating points can affect the resolution of the leakage. For example, at higher flows and pressures, perhaps the changes in pump dynamics as a result of variations in leakage are greater than at lower flows and pressures. Another consideration is the resolution at different operating points with confounding variables. Perhaps the influence of bulk modulus on dynamics is significantly less at higher pressures and flows. In order to determine this, the system was linearized at certain operating points. Appendix D provides the complete linearized equation set for the 7th order system. At the specified operating points, small changes in the leakage parameter were provoked in order to investigate pole movement. Since the poles give insight into the dynamics of the system, large movements in poles may be representative of large changes in dynamics, depending on which poles move and in which direction. This was confirmed with a simple root mean square error of the dynamics using the nonlinear dynamics model. The 7th order system of equations is rearranged and listed as state equations.

$$\dot{x}_1 = x_2 = \text{Load sense spool position} \tag{3.1}$$

$$\dot{x}_2 = \frac{1}{m_{ls}}\left[A_{ls}x_7 - A_{ls}P_m - A_{ls}x_6 - k_{ls}x_1 - d_{ls}x_2 - 2(x_7 - x_3)\frac{C_d^2}{C_c}\cos(jetangle)\, x_1 C_{cc} A_{chrg}\right] = \text{Load sense spool velocity} \tag{3.2}$$

$$\dot{x}_3 = \frac{\beta_{cp}}{V_{cp} + x_4 A_{cp}} \left( C_d x_1 C_{cc} K_{chrg} \sqrt{\frac{2(x_7 - x_3)}{\rho}} - A_{cp} x_5 - \frac{K_{cp}(x_3 - P_{tank})}{-x_4 LP_{slope} + LP_{max}} \right)$$
$$= \text{Pressure in control piston} \qquad 3.3$$

The load sense spool operates close to its null position. The orifice area gradients are different in the positive and negative directions, see Section 2.4. For simplicity, leakage in the control piston was added to force the load sense spool to operate only in the positive direction, this leakage exists in axial piston pumps, although, its exact experimental magnitude for this research was unknown. The orifice area gradient in the positive direction is a cumulative area of orifices in series. This was simplified for the linearization by approximating the slope of the orifice area gradient from the total effective charging area plots.

$$\dot{x}_4 = x_5 = \text{Control piston position} \qquad 3.4$$

$$\dot{x}_5 = \frac{1}{m_{cp} + m_{bias}} \left[ x_3 A_{cp} - x_7 A_{bias} - k_1 x_4 - K_{ag} x_5 - F_{bias} - \frac{C_1}{L} \tan^{-1}\left( \frac{Y_{max} - x_4}{L} \right) + \frac{C_2}{L} x_7 \right]$$
$$= \text{Control piston velocity} \qquad 3.5$$

$$\dot{x}_6 = \frac{\beta_l}{VB_{load}} \left( \sqrt{\frac{2(x_7 - x_6)}{\rho}} K_{ls} - \sqrt{\frac{2(x_6 - P_{tank})}{\rho}} K_{load} \right) = \text{Pressure load volume} \qquad 3.6$$

$$\dot{x}_7 = \frac{\beta_{ps}}{VB_{pump}}\left( f_{gain}\tan^{-1}\left(\frac{Y_{max}-x_4}{L}\right) + f_{int} - \sqrt{\frac{2(x_7-x_6)}{\rho}}K_{ls} - C_d x_1 C_{cc} K_{chrg}\sqrt{\frac{2(x_7-x_3)}{\rho}} \right.$$

$$\left. - (R_{slope}(x_7 - P_{tank}) + y_{int}) - \frac{C_{cp}(x_3 - P_{tank})}{-x_4 LP_{slope} + LP_{max}} \right)$$

$$= \text{Pressure pump volume} \qquad 3.7$$

The initial conditions used for linearization were obtained using the nonlinear dynamic model. To assess the linearization accuracy, a state space model was developed and implemented in Simulink. The state space model and nonlinear dynamic model were excited with a small perturbation where the magnitude of this step being a factor of the load orifice constant. To assess the linearization accuracy at a specific operating point, the step was reduced and how well the linearized model matched the nonlinear dynamic model was assessed. This investigation was performed by assessing the pump outlet pressure.

## 3.2 State Space Results

Figure 3.1 shows the results of the nonlinear dynamic model compared to the linearized state space model for decreasing step sizes specified in the figure legend.

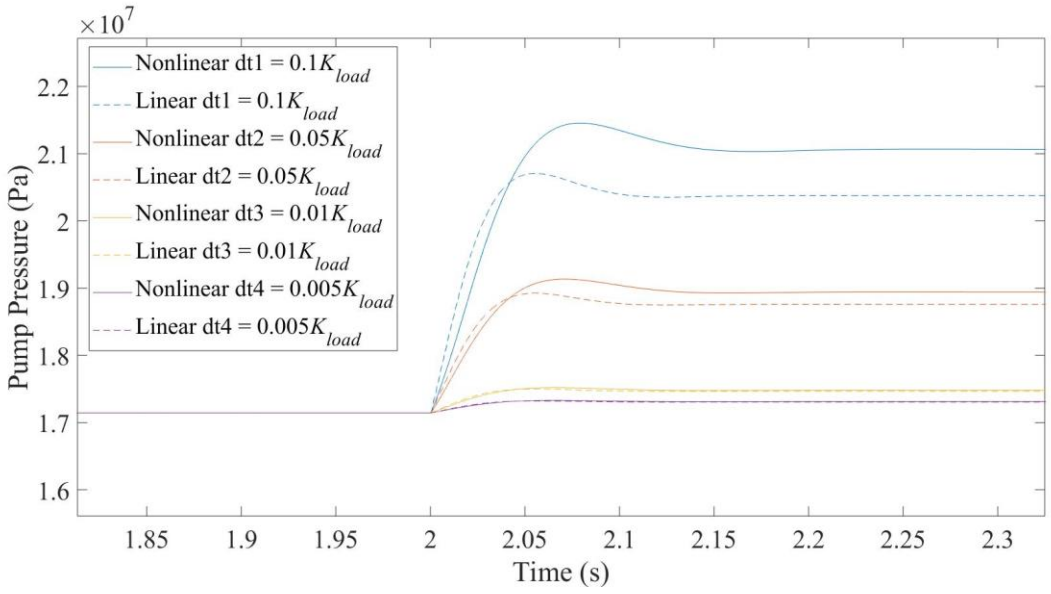


**Figure 3.1:** Assessment of linearization accuracy

As expected, the linearization accuracy improves as the step size is reduced. Since the model is 7th order, it can be approximated as linear within a very small range.

## 3.3 Root Locus Plots for Best Leakage Resolution

Selecting an operating point involves certain considerations. The best operating point to test the dynamics of the pump would be one at which the effects of bulk modulus are minimal but the effects of leakage are at a maximum. Observing the root locus plots, and how the poles move with small variations in a parameter at different operating points, can give insight into the best operating point. Since the linearization has been shown to be accurate, an investigation into operating point selection can now be performed. Five operating points were selected. These operating points were selected at a constant mid-range flow with increasing load pressure and are summarized in Table 3.1.

**Table 3.1:** Operating point summary

| State | IC1 | IC2 | IC3 | IC4 | IC5 |
|---|---|---|---|---|---|
| $\dot{x_1}$ (mm) | 4.94 | 4.74 | 4.88 | 4.96 | 5.06 |
| $\dot{x_2}$ (mm$^2$) | 0 | 0 | 0 | 0 | 0 |

| | | | | | |
|---|---|---|---|---|---|
| $\dot{x_3}$ (MPa) | 2.20 | 3.88 | 5.56 | 7.24 | 8.93 |
| $\dot{x_4}$ (mm) | 7.87 | 6.55 | 5.21 | 3.86 | 2.50 |
| $\dot{x_5}$ (mm) | 0 | 0 | 0 | 0 | 0 |
| $\dot{x_6}$ (MPa) | 3.019 | 8.557 | 14.10 | 19.66 | 25.22 |
| $\dot{x_7}$ (MPa) | 4.026 | 9.563 | 15.11 | 20.66 | 26.23 |

Figure 3.2 and Figure 3.3 are root locus plots for the bulk modulus and leakage, respectively. For each plot, an operating point was selected and the parameter being analyzed was varied. The resulting plots show how the poles move when each parameter is varied at that operating point.

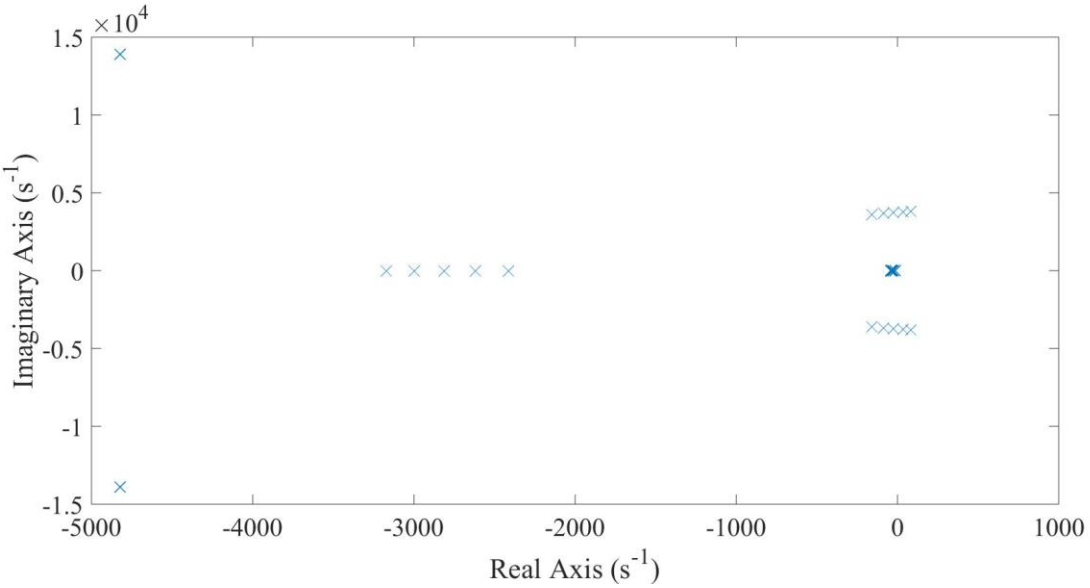


**Figure 3.2:** Root locus plot for system at high pressure (IC5) and with variations in bulk modulus

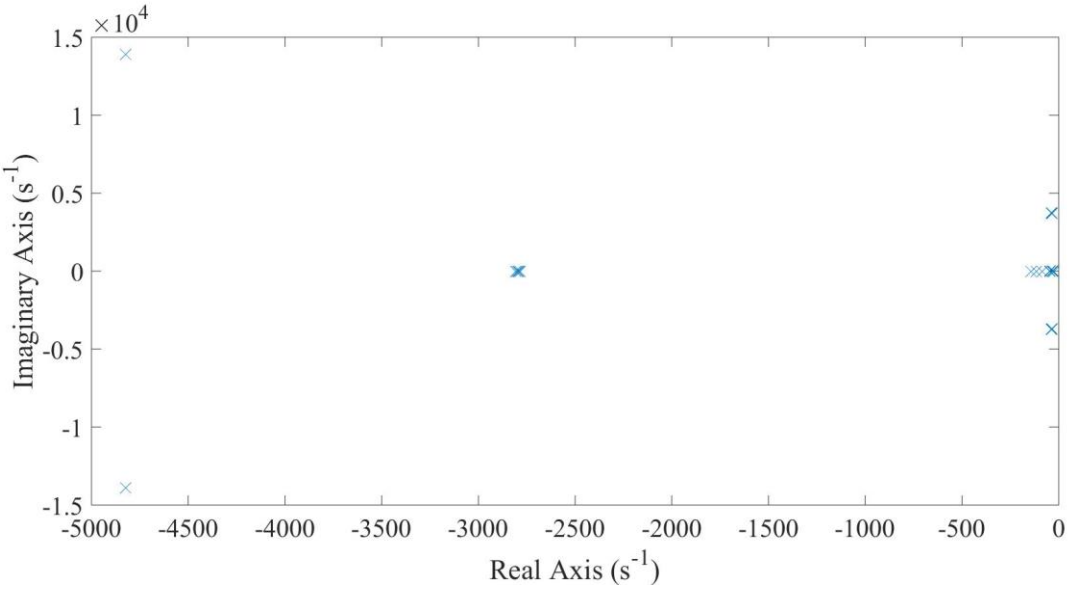


**Figure 3.3:** Root locus plot for system at high pressure (IC5) and with variations in leakage

The poles were inspected and for both leakage and bulk modulus, the poles to the far left of the plot do not move. Plots shown in Figure 3.4 and Figure 3.5 use a smaller horizontal axis range to highlight the movement of the dominant poles for both parameter variations.

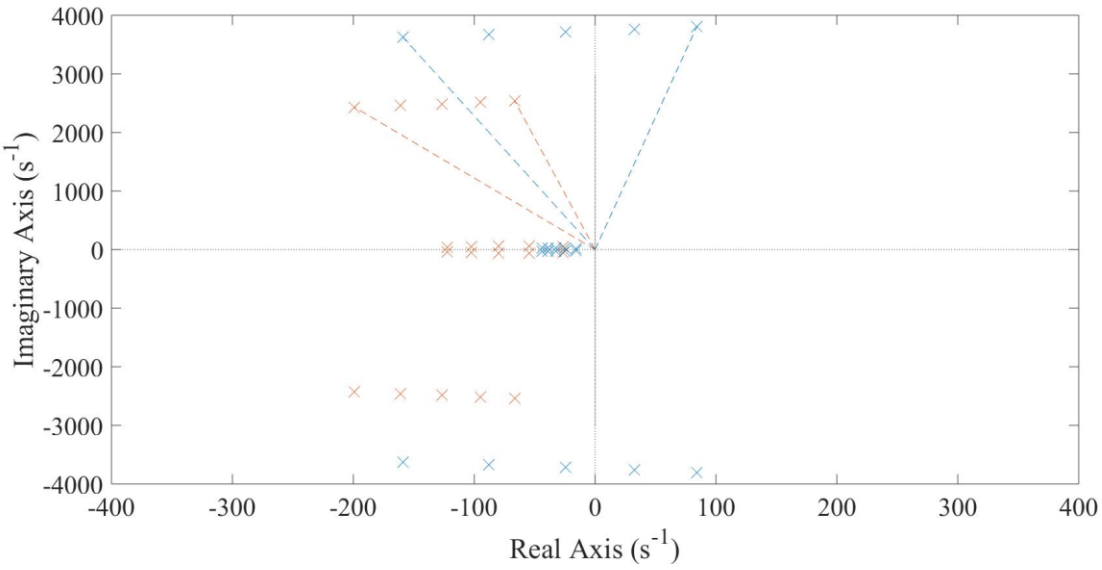


**Figure 3.4:** Pole movement at high and low pressure as $\beta_{ps}$ changes: blue is at high pressure (IC5) and red is at low pressure (IC1)

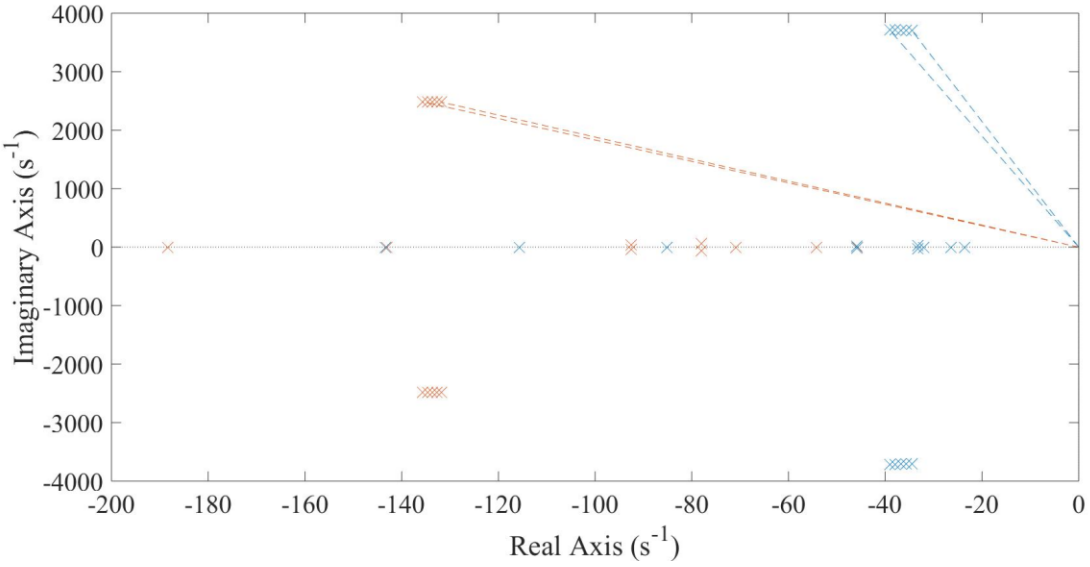


**Figure 3.5:** Pole movement at high and low pressure as $R_{slope}$ changes: blue is at high pressure (IC5) and red is at low pressure (IC1)

Figure 3.4 and Figure 3.5 illustrate the dominant pole movement as the initial conditions change to reflect low and high pressures. In Figure 3.4, as the pump bulk modulus parameter, $\beta_{ps}$, is varied, the blue colored poles (high pressure) move significantly more than the red colored poles (low pressure). Figure 3.5 shows similar pole movement when the leakage parameter is varied, although to a lesser degree. The red colored poles move slightly at low pressures with changes in leakage while the blue colored poles, at higher pressure, move much more noticeably. It is important to reiterate that the root locus plots are being used to observe the *change* in the dominant pole position at the different operating points. In addition, more pole movement may not necessarily mean larger changes in dynamics, however, this analysis provides preliminary guidance.

From this analysis it was decided to excite the pump at the largest possible load pressure without the swashplate hitting its mechanical travel limit. This was achieved by maintaining a pump flow of roughly half of its full flow specification.

# Chapter 4 Simulation Study

Chapter 4 investigates the effectiveness of a machine learning algorithm to predict the leakage conductance, $R_{slope.}$ The initial sections illustrate the effects of parameter changes on the dynamics of the pump. Principal Components Analysis is introduced and shown to be simple but effective for data reduction resulting in simpler regression. PCA is used to reduce the dimensionality of a large dataset created with the validated dynamic model outlined in Chapter 2, simplifying a linear regression used to predict pump leakage. The training dataset is optimized and an analysis is performed to determine which pump dynamic signals give the best predictive capabilities of leakage. The best predictive performance is a result of using the pump pressure transient, the control piston transient, and the dynamics from the swashplate angle.

## 4.1 General Effects of Key Parameters on Dynamic Response

Using the validated nonlinear dynamic model of the load sensing system, an investigation was performed to observe how the dynamics change when highly sensitive parameters are varied. This is a simple visual introduction to the data that is used in subsequent sections for training the machine learning algorithm.

Signal outputs that give the best results are described in Section 4.8.1 and were determined to be the pump pressure, control piston pressure, and the swashplate angle. Figure 4.1 - Figure **4.6** illustrate changes in dynamic outputs as the leakage parameter, $R_{slope}$, changes within a reasonable range for a pump. This range was derived from experimental data covered in Appendix C.

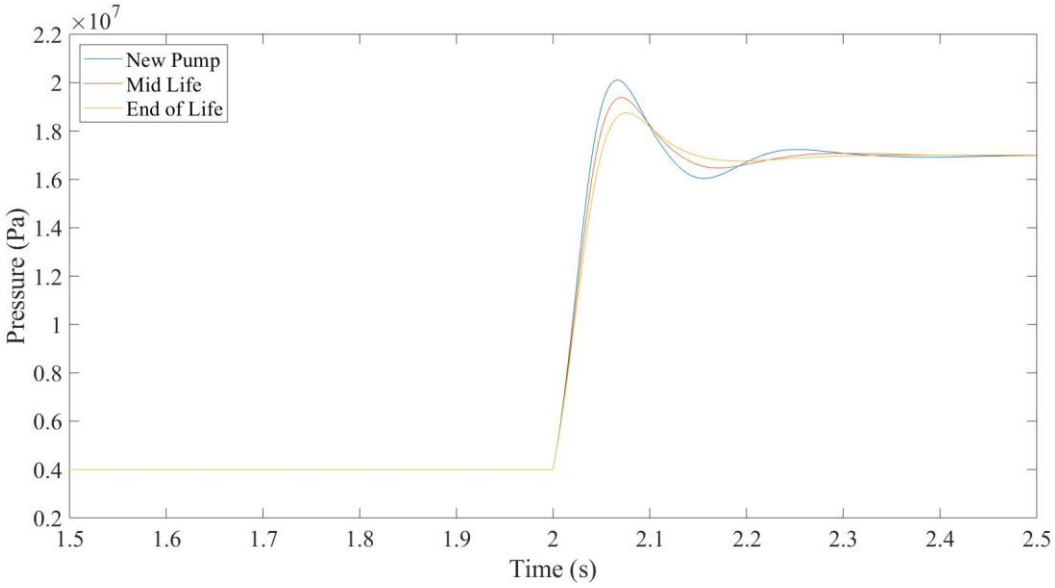


**Figure 4.1:** Plot of pump pressure dynamics with changing leakage parameter

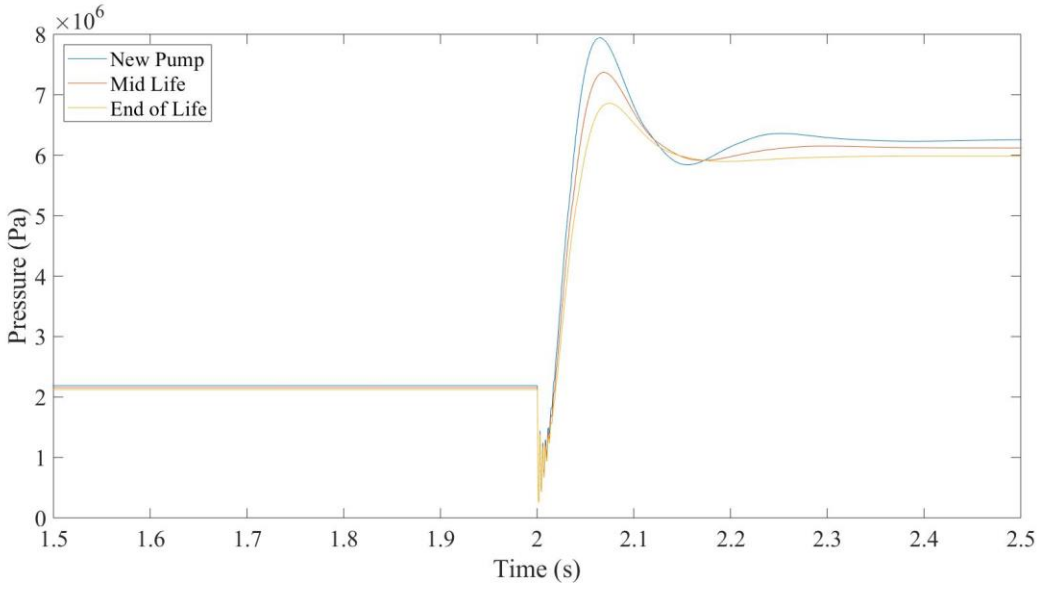


**Figure 4.2:** Control piston pressure dynamic changing due to leakage

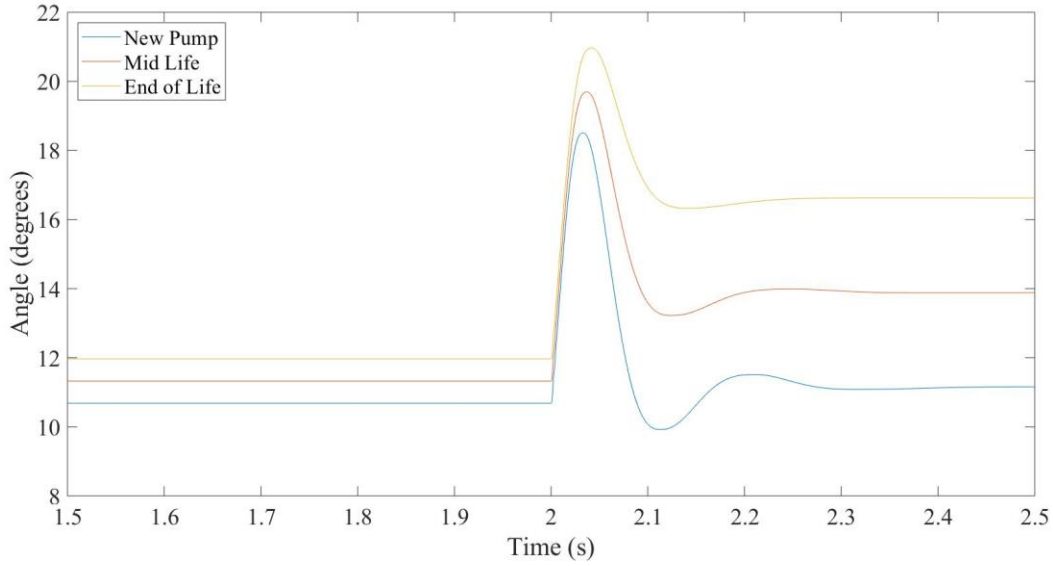


**Figure 4.3:** Swash angle dynamics changing due to leakage

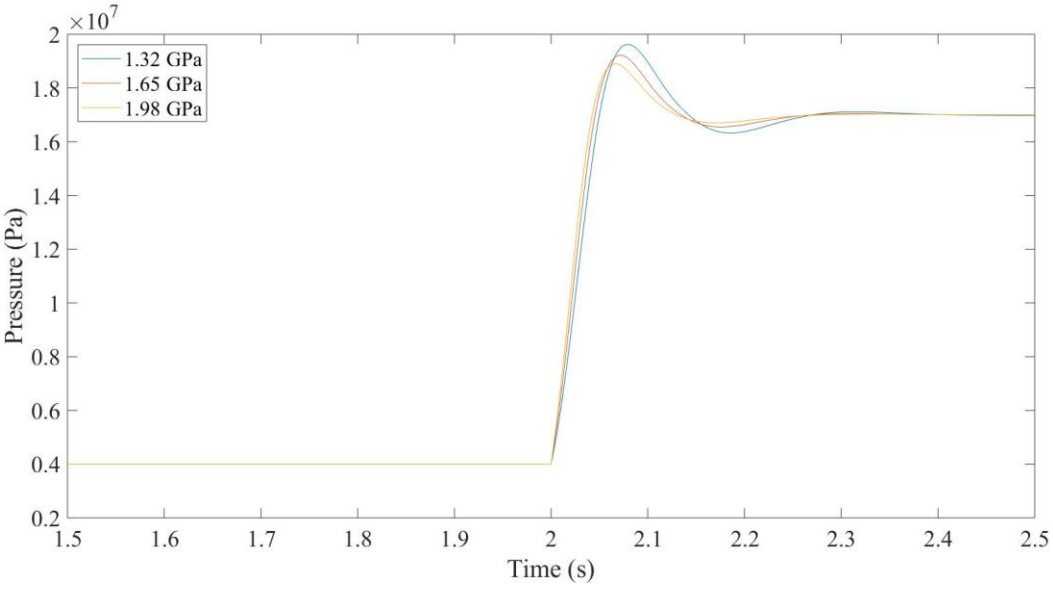


**Figure 4.4:** Pump pressure dynamic variation due to bulk modulus change

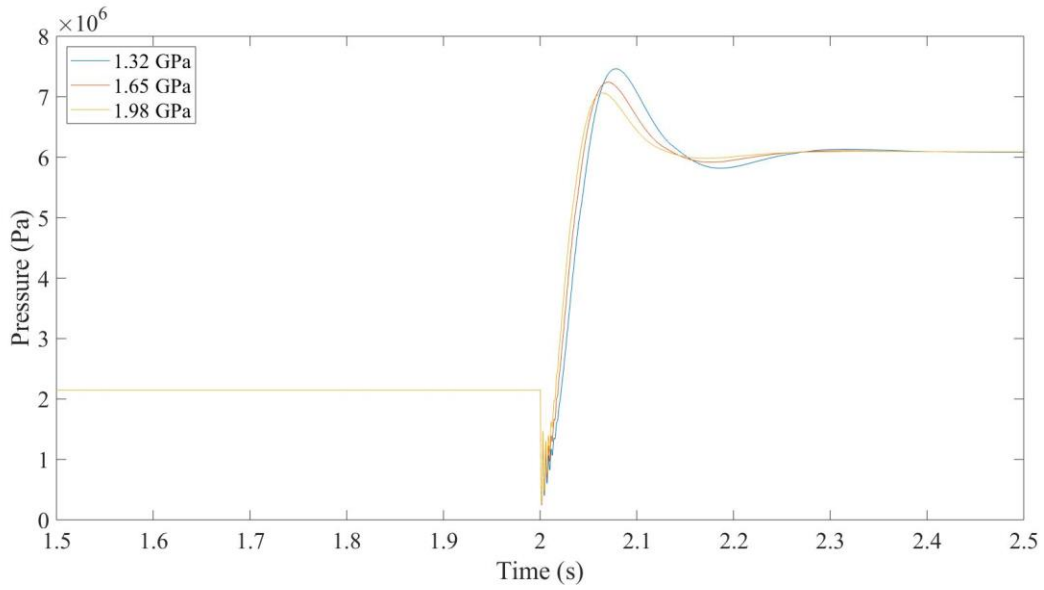


**Figure 4.5:** Control piston pressure dynamic variation due to bulk modulus change

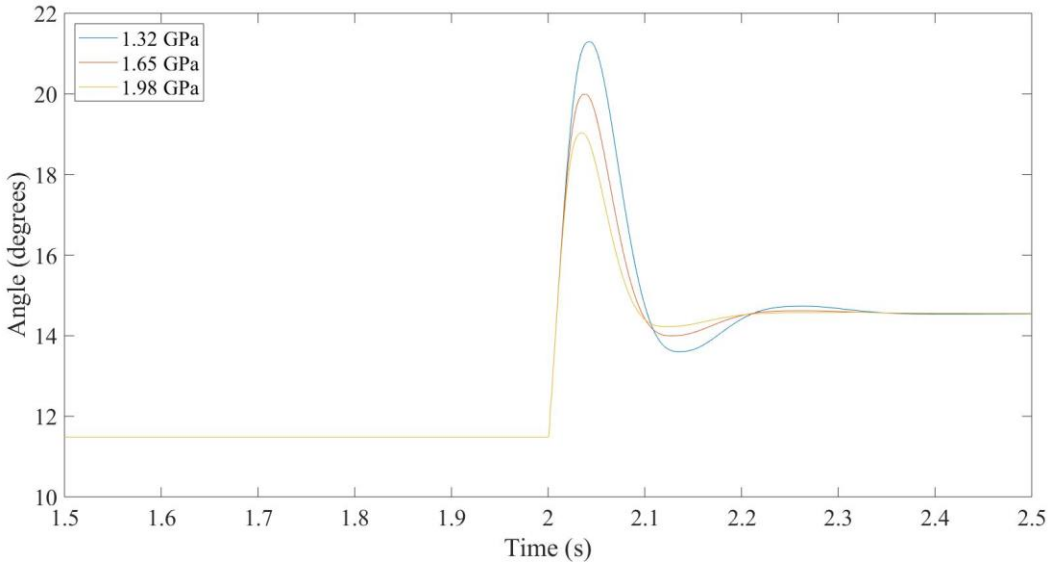


**Figure 4.6:** Swash angle dynamics changing with bulk modulus variations

The changes in the dynamic portion of the output transient when leakage conductance and bulk modulus change are very similar. If the plots were unlabeled, it would be difficult to tell which dynamic changes result from leakage and which result from variations in bulk modulus. The dynamics show some differences in steady state swash angle and control piston pressure after the step in load pressure. With leakage, given a higher load pressure, the pump

must increase its swash angle in order to maintain the same flow since the load sensing orifice does not change. At a larger swash angle, the control piston pressure is slightly lower because the bias spring force is not as large at larger swash angles. At this stage it may be hard, using common dynamic features, to determine, given a series of response data, if the data change from leakage or bulk modulus.

## 4.2 Confounding Variables

This section explains how the number of parameters that have a significant effect on the response can be reduced through practical design. This is an important step that reduces the number of confounding variables that a machine learning algorithm will eventually sort through. Confounding variables can decrease predictive performance by adding unknowns to the data.

Ideally, the leakage parameter would have significantly higher sensitivity than all other parameters. This would mean that the dynamics of the pump would change dramatically with small changes in leakage but would show very little change with large variations in other parameters. The sensitivity analysis performed in Section 2.5 shows that this is not at all the case. In reality, other parameters have much higher sensitivity than even the leakage conductance term. Table 4.1 lists parameters that have significant effects on the dynamics as quantified by the rise time and overshoot.

**Table 4.1:** Selected confounding variables

| | |
|---|---|
| $\boldsymbol{\beta_{ps}}$ | Bulk modulus of pump volume |
| $\boldsymbol{\beta_{l}}$ | Bulk modulus of load volume |
| $\boldsymbol{\beta_{cp}}$ | Bulk modulus of control piston volume |
| $\boldsymbol{VB_{pump}}$ | Pump volume |
| $\boldsymbol{VB_{load}}$ | Load volume |
| $\boldsymbol{R_{slope}}$ | Leakage conductance |
| $\boldsymbol{\mu}$ | Dynamic viscosity of fluid |

Since it is the change of the parameter that needs to be minimized, some parameters in Table 4.1 can be eliminated through practical design. During machine operation, load volumes can change significantly. The pump volume may change based on design but it is not as likely to change as the load volume. The proposed condition monitoring device should be a retrofitted hydraulic component that tests the pump dynamics at fixed pump and load volumes. This effectively eliminates two highly sensitive parameters from Table 4.1, $VB_{pump}$, and $VB_{load}$.

Another parameter to consider is the viscosity of the fluid. This can change significantly with fluid temperature. This confounding variable can simply be overcome by performing testing at constant operating temperature. This is currently common practice in machine performance testing.

The remaining confounding variables are the bulk modulus of each of the modelled system volumes. Bulk modulus has been shown to change significantly during machine operation due to aeration of the hydraulic fluid, fluid pressure, and compliance of the volume Merritt (1967). Bulk modulus is difficult if not impossible to determine without significant instrumentation.

A method of feature extraction can help classify changes in pump dynamics as being a result of a change in certain parameters, while also changing these three confounding variables. The next section introduces a basic machine learning algorithm that can extract features from large amounts of data as well as reduce data dimensionality called Principal Components Analysis.

## 4.3 Creating the Training Dataset

The training dataset acts as the foundation for principal components analysis. Principal components analysis detects features in the dataset and uses these features to predict pump leakage given a new dynamic response vector. The training dataset was created with specific variations in the four variables described in Section 4.2, the three bulk moduli are confounding whereas the leakage conductance parameter is the parameter that will be predicted as it indicates wear in the pump. The other inputs used in creating the dataset are the remaining constant parameters necessary to run the dynamic model as well as the orifice constants that set the target pump flow and discharge pressure. The flow remains constant, however the load pressure is

increased in a step input fashion. Appendix C summarizes the step size, flow, and pressure targets that were selected.

The response data are created by using random uniform variations in each of the parameters and within a desired range. The range of bulk modulus for each volume was not determined exactly for the experimental system. Gholizadeh (2013) outlines how the bulk modulus of hydraulic oil is difficult to determine as it is dependent on many factors including entrapped air, compressibility of hoses, and operating pressure. Gholizadeh presents a new model for the low pressure range of hydraulic oils which shows that at higher pressure, there is much less variation in bulk modulus. In creating the simulation data, it was decided to apply a generous range of 20% to the base bulk modulus value to account for expected significant changes. The range of the leakage parameter, $R_{slope}$, was determined using experimental data. The lower range accounts for pumps with very little leakage, as would be the case for a new pump, and the larger range accounts for severely worn pumps. This range encompasses the experimentally worn pumps.

A Monte Carlo approach was used to create a large training dataset. A variation was made in each of the four parameters listed, within the specified range, and the output data of the simulation were obtained. All other parameters were held constant. The output data include the pump discharge pressure, control piston pressure, and swashplate angle. Each output response vector was concatenated to form a single compact data vector that contains all of the selected output information of the pump. The parameter variations are maintained as factors of the median value of that parameter. They will be referred to as 'parameter factors' and are dimensionless. For example, a variation in $\beta_{ps}$ that corresponds to the maximum value would be recorded as $Y_{bps}$ = 1.2, that is, the base value of $\beta_{ps}$ is multiplied by a factor of 120%. Factors for each of the four parameters are recorded and indexed to their corresponding output data vector. For each output data vector, there will be four 'factors', one for each of the four parameters and the magnitude being the multiplicative value for the median values. Table 4.2 summarizes the median values of the four parameters and the minimum and maximum values once each parameter is multiplied by its corresponding factor.

**Table 4.2:** Parameter range

| Factor | Parameter | Median | Min | Max |
|---|---|---|---|---|
| $Y_{bps}$ | $\beta_{ps}$ (GPa) | 1.75 | 1.4 | 2.1 |
| $Y_{bl}$ | $\beta_{l}$ (GPa) | 1.4 | 1.12 | 1.68 |
| $Y_{bcp}$ | $\beta_{cp}$ (GPa) | 1 | 0.8 | 1.2 |
| $Y_{rslope}$ | $R_{slope}$ [$m^3 s^{-1} Pa^{-1}$] | 5.965e-12 | 5.965e-14 | 1.187e-11 |

It is important to note that the designed leakage prediction algorithm predicts the dimensionless factor $Y_{rslope}$, not the actual conductance parameter $R_{slope}$.

## 4.4 Principal Components Analysis

The application of Machine Learning techniques to assess significant amounts of data has become much more prevalent. One technique, in particular, has been used successfully in pattern recognition and data reduction. Principal Components Analysis (PCA) is a statistical procedure that uses an orthogonal transformation to determine directions within a dataset of significant variance. Refer to Appendix E for a simple two-dimensional example that explains PCA. In this research, PCA assists in designing a leakage prediction algorithm by reducing the dimensionality of the training dataset and ultimately improving the overall algorithm's predictive performance.

A dataset of 1000 samples is created, each dynamic sample a result of some degree of variation of each of the four parameters, the pump leakage slope and the three system volume bulk moduli. Refer to Section 4.3, creating the training dataset, for more details. The original dimension of each sample was linearly interpolated from the simulation results with 300 data points, reduced to 299 having removed the first data point of each data vector. Concatenating the pump pressure, $P_s$, control piston pressure, $P_{cp}$, and swash angle, $\emptyset$, vectors results in a 1000*897 matrix, denoted as $\boldsymbol{X}$. Figure 4.7 illustrates just the pump pressure dynamic response training data. Each dynamic pressure vector is a result of some variation in each of the four parameters previously discussed. Changing the four parameters does not have an effect on the steady state pump pressure, however, there are significant changes in the dynamics.

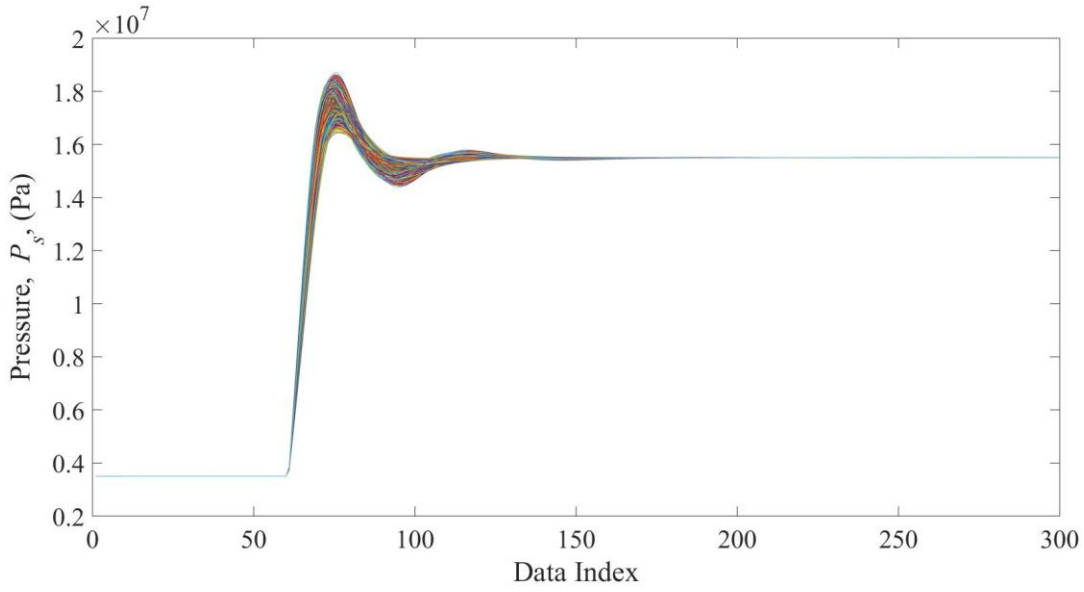


**Figure 4.7:** Sample of pump pressure data vector

The first step in performing PCA is to normalize the data by subtracting the data mean and dividing by its standard deviation.

$$\boldsymbol{X_{norm}} = \frac{\boldsymbol{X} - \boldsymbol{X_{mean}}}{std(\boldsymbol{X})} \tag{4.1}$$

The covariance of this normalized data is then

$$\boldsymbol{\Sigma} = cov(\boldsymbol{X_{norm}}). \tag{4.2}$$

From the covariance matrix of the normalized data, the eigenvalues, $\boldsymbol{\lambda}$, and eigenvectors, $\boldsymbol{U}$, are determined. The eigenvectors represent orthogonal directions of variance within the data and the corresponding eigenvalue is a measure of the relative magnitude of variance in each direction. These are sorted by eigenvalues.

The data can now be transformed into principal components using the following expression.

$$\boldsymbol{X_{pc}} = \boldsymbol{XU} \tag{4.3}$$

The columns of $\boldsymbol{U}$ represent directions of the largest variance present in the fully dimensioned data set. Certain columns may be more affected by leakage or bulk modulus values. In order to determine which of these new dimensions, or principal components, explains the most variance that also correlates with a parameters of interest, the Pearson linear correlation coefficient (PCC) (Guyon and Elisseeff 2003) can be utilized. This method ranks each principal component by its correlation to each parameter by a dimensionless coefficient that ranges from +1.0 to -1.0 where +1.0 corresponds to high positive correlation, 0 corresponds to no correlation. and -1.0 corresponds to high negative correlation. As an example, in the full data set, the first principal component, that explains the most variance, may strongly correlate to bulk modulus but have weak correlation to leakage. This principal component would not be a good one to use in a regression to predict leakage but would be much better in a regression at predicting bulk modulus. The principal components of $\boldsymbol{X_{pc}}$ were reordered from strongest to weakest based only on their correlation with the each of the parameters used in the training data. This results in four different Principal Component matrices, one for each parameter. These contain the same essential data, however the vectors are reorganized by decreasing correlation to each parameter.

## 4.5 PCA Process Flow Chart

For clarity, a flowchart, Figure 4.8, has been created to summarize the process of predicting the leakage parameter. This process is used in this Chapter to perform the analysis contained within.

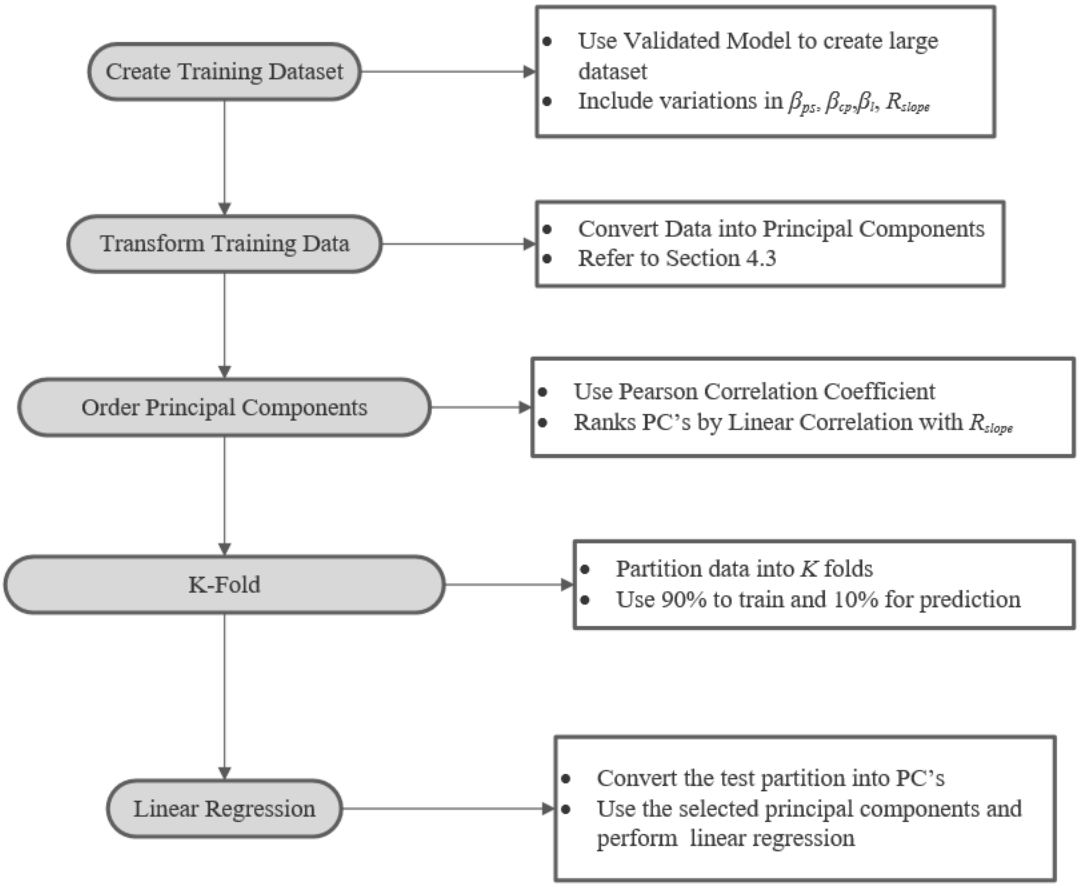


**Figure 4.8:** PCA process flowchart

## 4.6 Initial Investigation of PCA Applied to Pump Response Data

A first consideration having converted the original training dataset into principal components is the magnitude of the eigenvalues of the data. The eigenvalues corresponding to each principal component are a measure of how much variance each principal component describes of the original dataset. The two-dimensional example in Appendix D clearly illustrates how the largest eigenvalue describes the high correlation between $X_{pc1}$ and $y$ while the other significantly smaller eigenvalue describes the noise added to the data. This can mean that strong eigenvalues, and consequently strong principal components, describe important trends in data while weaker ones describe less important trends and even unimportant noise. This is important in data reduction because, as Appendix D describes, the two-dimensional data can be reduced to

one dimension without a significant loss in information. Investigating the strength of principal components from the training dataset created by the pump dynamic model may provide valuable information about the data. Figure 4.9 plots the variance described by each principal component.

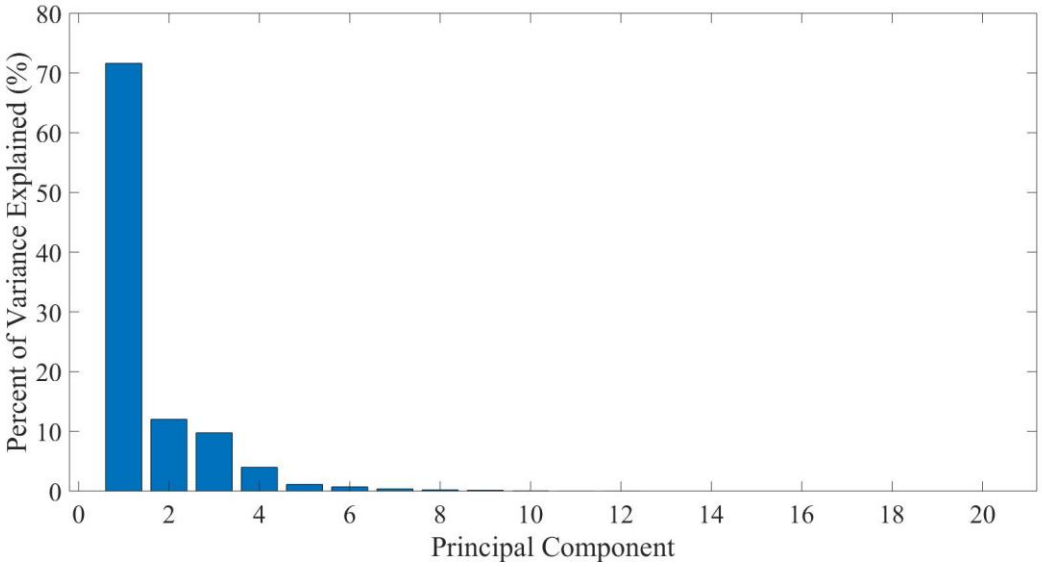


**Figure 4.9:** Variance described by each principal component

It is clear that there is a steady decline in strength for each principal component. This shows that roughly nine principal components can describe the majority of the variance present in the original dataset.

Performing the transformation given by equation 4.3 results in a number of principal components that equals the fully dimensioned training dataset. Each principal component correlates to a feature of the original dataset. A feature may be a change in part of the dynamic response that is a result of a parameter changing. In order to assess the correlation between principal components and parameters, the correlation of each principal component to each of the four variables can be assessed. The linear correlation of each variable (through the parameter factors) to each principal component can be measured using the Pearson Correlation Coefficient. The first three strongly correlated principal components, unique to each parameter, are plotted for each of the variables.

The correlation of each principal component to each parameter is shown in Figure 4.10 for the first three principal components and are ordered by their strength of correlation to the selected parameter.

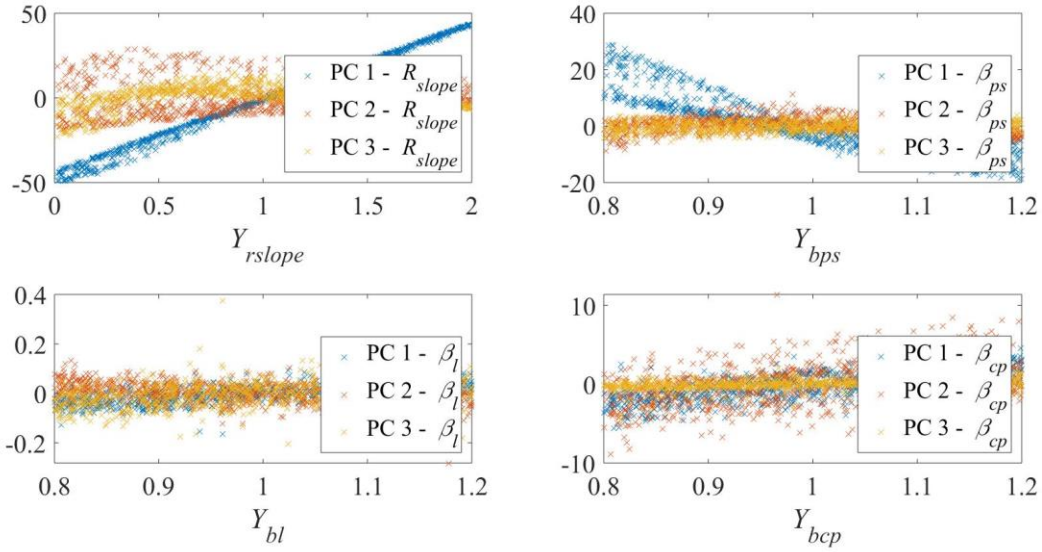


**Figure 4.10:** Correlation of each parameter factor to their strongest three PC's

It is visually clear in Figure 4.10 that PC 1 has the strongest linear correlation to the $R_{slope}$ facotr, this is also confirmed as it ranks highest by the Pearson correlation coefficient. It is important to note that each subplot plots the first three strongest principal components to the parameter selected.

Reordering each principal component by its correlation with each parameter results in the plot depicted in Figure 4.11.

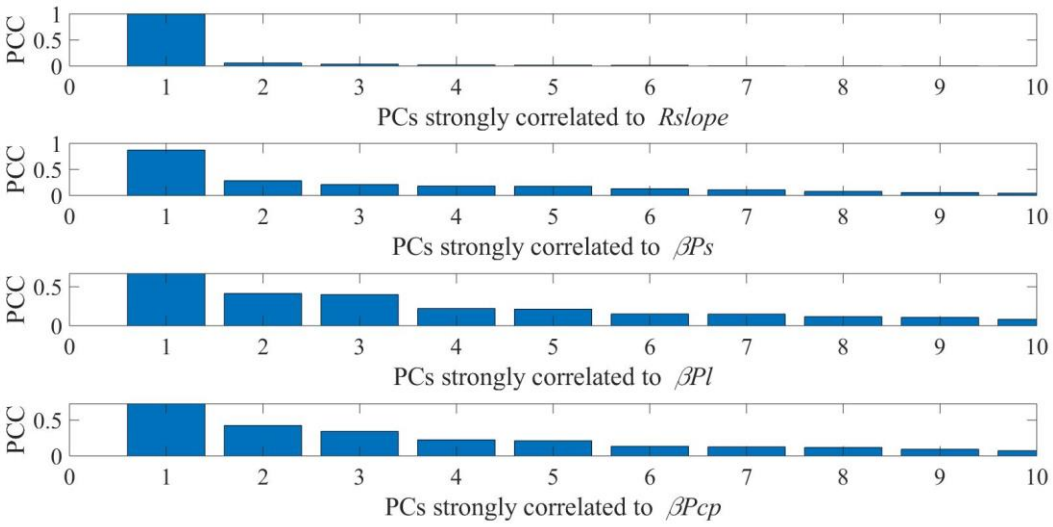


**Figure 4.11:** PC correlation (measured by PCC) to each parameter for the strongest ten principal components of each parameter

It is important to note that PC 1 from the first subplot is not the same principal component as PC 1 from the second subplot. PC 1 of the first subplot corresponds to the principal component that most strongly correlates to the leakage parameter, $R_{slope}$. As previously mentioned, the first principal component has the largest correlation to pump leakage and the remaining have much less correlation. Observing the plot for the bulk modulus of the pump volume, the first principal component has strong correlation with pump volume bulk modulus, but the remaining components have much less. It is important to clarify that Figure 4.11 illustrates strictly linear correlation of principal components with each of the parameters but does not show the variance explained by each of the principal components to the entire dataset.

Figure 4.12 directly corresponds to Figure 4.11 as it shows how much variance each of the principal components describes in the entire dataset.

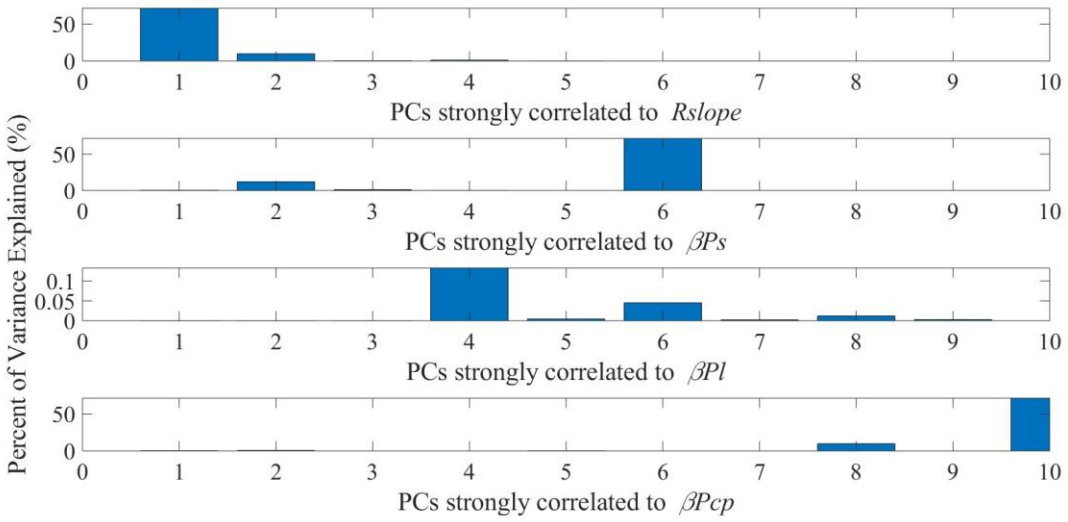


**Figure 4.12:** Plot of variance described by each principal component of the entire dataset

It is clear that the principal component most strongly correlating to leakage also describes the most variance within the entire dataset.

## 4.7 Regression and Prediction

It has been shown how the training dataset has features that correlate with the four outlined variables. This section describes how a linear regression using the transformed dataset (select principal components) can be used to predict the leakage factor of a new output data vector.

As was performed for the training dataset, given a new data vector with known parameter factors, the vector is converted into principal components. The fully dimensioned dataset, $\boldsymbol{X}$, was shown to be a 1000*897 matrix where the number of rows corresponds to the number of pump samples, and the columns correspond to the length of each response vector. The principal components matrix, $\boldsymbol{X_{pc}}$, is of the same dimensionality. Depending on how many principal components are selected, a linear regression is performed using the specified dimensioned data. That is, a new matrix, $\boldsymbol{X_{reg}}$, derived from selecting columns (or principal components) of $\boldsymbol{X_{pc}}$ will be a column vector if one principal component is used or an 897- columned matrix if all of

the original data are used. Padding the matrix with ones to facilitate matrix operations has been omitted for clarity.

$$\boldsymbol{X_{reg}} = \boldsymbol{X_{pc}}(:, i) \tag{4.4}$$

The corresponding leakage factors of the training data, $Y_{reg}$, is a vector of values with a length corresponding to the amount of pump response samples used.

$$Y_{reg} = Y_{reg}(1{:}m), \tag{4.5}$$

where $m$ is the number of pump samples selected. The least squares solution from the training data is

$$\boldsymbol{W} = (\boldsymbol{X_{reg}^T X_{reg}})^{-1} \boldsymbol{X_{reg}^T} Y_{reg}. \tag{4.6}$$

Using the parameters in matrix form, $\boldsymbol{W}$, and given a new data vector, $X_{new}$, the leakage factor for the new data vector can be predicted by

$$\hat{Y}_{rslope} = X_{new} \boldsymbol{W}. \tag{4.7}$$

To assess the prediction accuracy, a simple root mean squared error is calculated based on the calculated value of $\hat{Y}_{rslope}$, and the actual leakage factor, $Y_{rslope}$ as follows:

$$RMSE = \sqrt{(Y_{rslope} - \hat{Y}_{rslope})^2}. \tag{4.8}$$

The above process is applicable to a single new pump response data vector, however, using matrix form, it can be efficiently applied to a number of new pump response vectors. The regression errors determined in this section come from predicting the pump leakage factors for many response vectors and it is important to note that since the leakage factor is dimensionless, RMSE is also dimensionless. The process used in partitioning the training data is K-fold cross validation, the data is divided into K segments, all but one segment of data is used to derive the weights matrix, $\boldsymbol{W}$, (commonly referred to as the training set) and the remaining data are used as a performance assessment (validation set). This is then repeated for the other segments. For the simulation study of Chapter 4, a value of 10 was selected for K. This has been shown in literature to be a good general value Kohavi (1995). This corresponds to 900 pump response vectors for training and 100 response vectors for validation. The regression error is calculated as the root-mean-square error (RMSE) and for each partition of data, the RMSE is calculated. The process is repeated K times and a mean value of the RMSE is obtained. This is the error value used for the assessment of PCA in the following sections.

## 4.8 Regression with PCA Results

From the analysis in Section 4.7, K-fold cross validation was performed and a linear regression to predict the leakage factor of the pump using principal components strongly correlated with $R_{slope}$.

Figure 4.13 compares the RMS error using the strongest overall principal components and the strongest correlated to leakage. The regression error for the first principal component is exactly the same because the first strongest overall PC is also the most correlated with leakage. When the second principal component is added for both cases, the RMS error for the overall strongest principal components does not decrease very much. This principal component is strongly correlated with some other feature within the data and has little correlation to leakage.

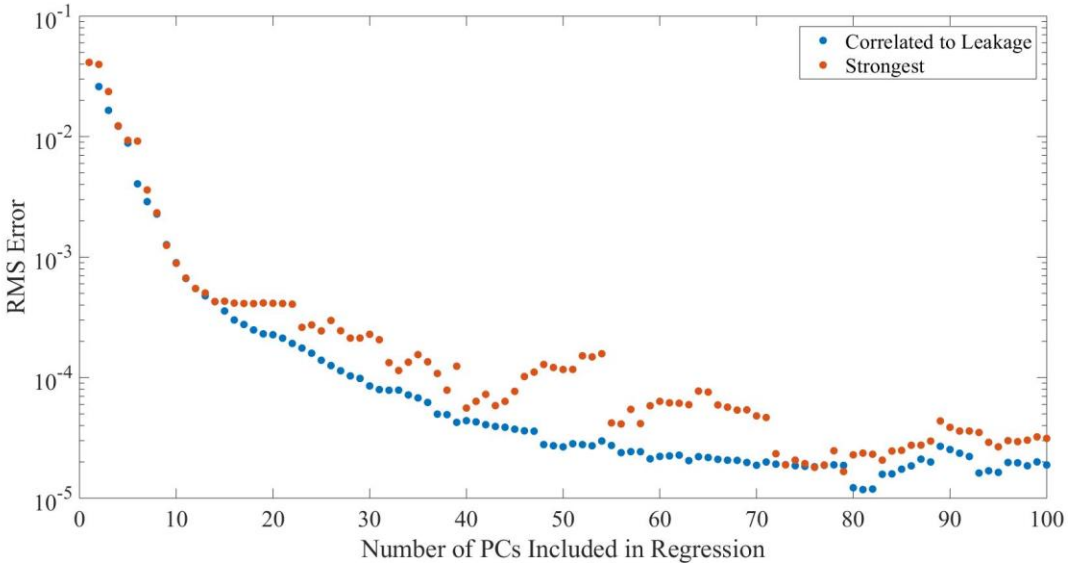


**Figure 4.13:** Strongest PC's compared with correlated PC's

From Figure 4.13 it is clear that in order to obtain the best prediction results of the leakage factor, some number of principal components that strongly correlate to leakage is optimal. This method will give the best regression error using the smallest number of principal components which ultimately means using less data in performing the linear regression.

In an attempt to understand what components of the original data that PCA is recognizing as features, Figure 4.14 illustrates the weight of each principal component on the data vector

index. The data index from 1-300 is composed of the pump pressure signal, from 301-598 is the control piston pressure signal, and 599-897 is the swash angle dynamic response.

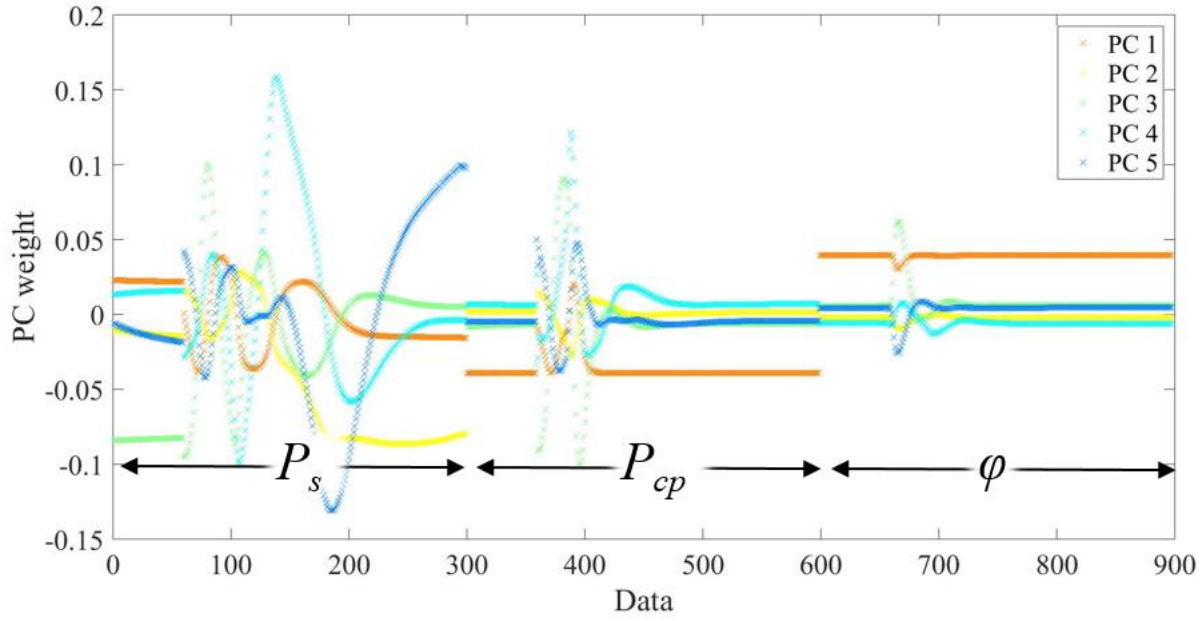


**Figure 4.14:** PC weights

The first principal component, in orange, has large weight for the swash angle steady state values. The remaining principal components rely on other features of the response.

PCA can be used to reduce data dimensionality. It is relatively simple to reduce dimensionality of the pump response dataset. By selecting a number of principal components that correlate strongly with leakage, the regression is performed on a significantly reduced dataset. For example, if the first 15 principal components are used, and referring to Figure 4.13, the regression error from this small data set is only slightly higher than if all 40 principal components are used. The number of principal components to use directly affects the resulting regression error. This is open ended and would depend on the condition monitoring device design parameters.

### 4.8.1 Signal Selection

A necessary step in the design of a condition monitoring device utilizing pump dynamics is determining which sensor information is important. Three general outputs were selected, $P_s$

the pump pressure response, $P_{cp}$ the control piston pressure response, and $\varphi$ the swash angle dynamic response. These specific outputs were selected because they are easy to measure on a pump once instrumentation is setup and do not require significant instrumentation to acquire. The prediction capabilities of the leakage prediction algorithm are assessed using various combinations of the base pump outputs. Figure 4.15 shows the results of this analysis.

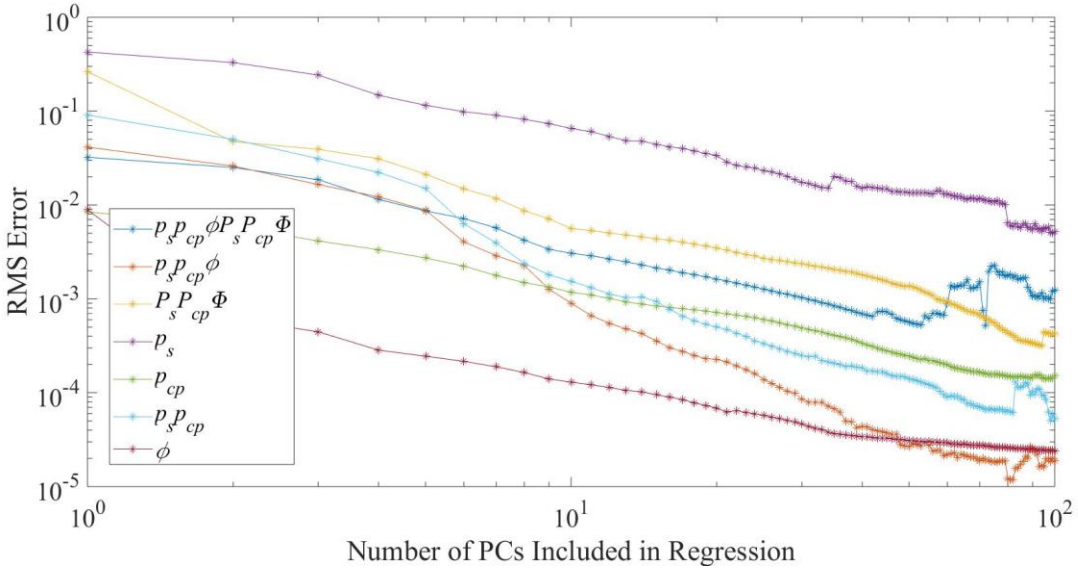


**Figure 4.15:** Sensor regression where capitalized parameters represent frequency data and lowercase represent time domain

The investigation uses combinations of output information including frequency and time series data. The swash angle data perform the best with very little information (low number of principal components). Using just control piston pressure gives low error and combining this with the pump discharge pressure, the error is further reduced. The lowest error when including 100 PC's is produced by using a combination of the pump pressure, control piston pressure, and the swash angle data. The less correlated principal components, when added to the regression, can have good or bad effects on the regression depending on how they correlate with leakage and other features of the data.

### 4.8.2 Effects of Training Dataset

The amount of training data required to result in good regression error has obvious importance. There exist numerical issues with this type of analysis. Problems arise when

performing a regression on data where the weights matrix is rank deficient. Specific to performing PCA, this occurs when the amount of data vectors that make up the dataset is close to or less than the number of principal components. Since this is not the focus of research, this was overcome by using the pseudoinverse (pinv) function in Matlab. Pinv has been shown to produce good results when a matrix can have many solutions (rank deficient).

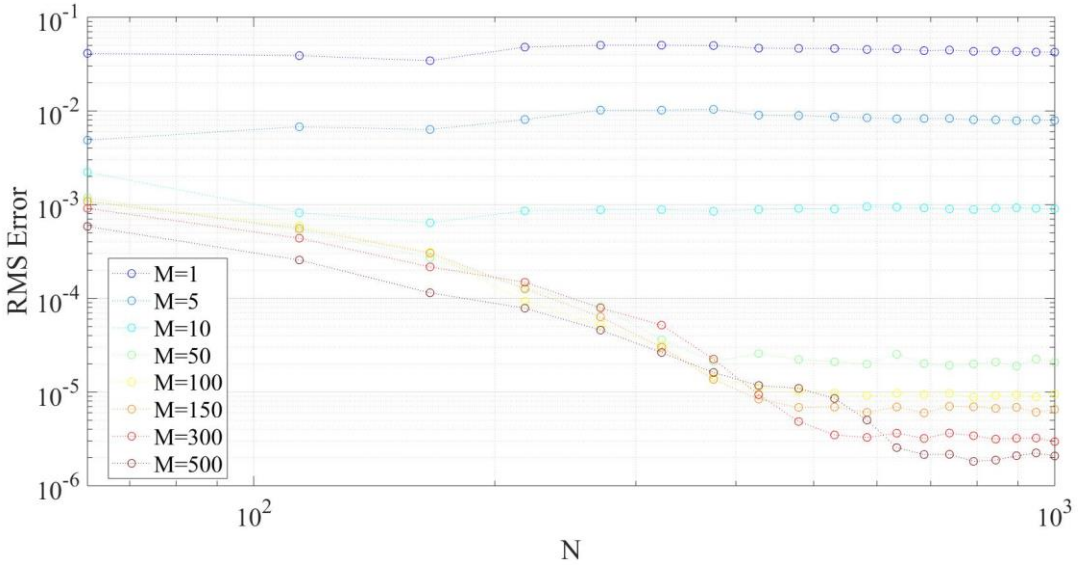


**Figure 4.16:** Training data and regression where M is the number of principal components and N is the number of pumps or training data vectors

Figure 4.16 illustrates trends between regression error and amounts of training data. In general, the fewer principal components included in the regression, the less improvement in regression as more training data are provided. This has obvious benefits since a reduction in data dimensionality can result in a reduction in training data (and the cost associated with its generation). The improvement in regression error is consistent until approximately 700 training samples are included and at this point, the error does not improve. Using 1000 data samples is a good compromise for further investigation of the leakage prediction algorithm.

### 4.8.3 Noise Addition

In order to make the leakage predictive algorithm more robust, some considerations need to be made. A component of the algorithm, PCA, detects features within data, and it can

determine steady state patterns, dynamic patterns, and non-random noise. From the preceding analysis, it is clear that, with a clean training data set, the main feature that the designed algorithm is using to predict pump leakage is the steady state swash angle. Practically, this may be as simple as using a swash angle sensor and collecting steady state information from an operating pump as a predictive technique. This may require certain calibration procedures, and additionally, swash angle sensors are not commonly used and thus, retrofitting would be difficult. Another consideration is the form of the actual data that will eventually be used for leakage prediction.

The simulation study uses simulation data to train and predict. In actuality, the device will utilize simulation data for training purposes but will be given experimental pump dynamic data for actual pump leakage prediction. Typically, experimental data will contain noise and other errors. These errors can manifest in the form of steady state differences and sensor noise. If the regression heavily relies on steady state information, the algorithm may have good predictive capabilities using simulation data, however, given noisy experimental data, it may fail. If the regression could be trained to rely solely on dynamic information, the potential to predict pump health via a simple dynamic pressure measurement may be possible. To accomplish this, the clean training dataset can be manipulated to remove any patterns that occur from steady state data. The obvious pattern is that the pump swash angle must operate at a larger angle (more flow) to compensate for leakage. If this pattern is purposely hidden, the regression will adapt to rely on other features, the goal being the dynamic portion of the data vector. Three types of 'noise' were then added to the training data to remove any steady state patterns present. These include a bias (shift), gain (multiplication), and random noise. A simulation study outlines the effects of noise addition to the training data set and ultimately, the effects on regression.

The noise was chosen with guidance from the experimental data results. The potential bias and gain error within the experimental results was used as a range for the uniform noise distribution applied to the training data. The random noise was estimated from the experimental data signals as well. The noise analysis performed in this section is a feasibility study that generally shows that if the expected response data are noisy then it is best to train the algorithm with noisy data. Chapter 5 uses actual experimental data and a practical investigation into the magnitudes of noise addition to training data is conducted.

Figure 4.17 to Figure **4.19** illustrate how the original training dataset has been corrupted with three types of noise

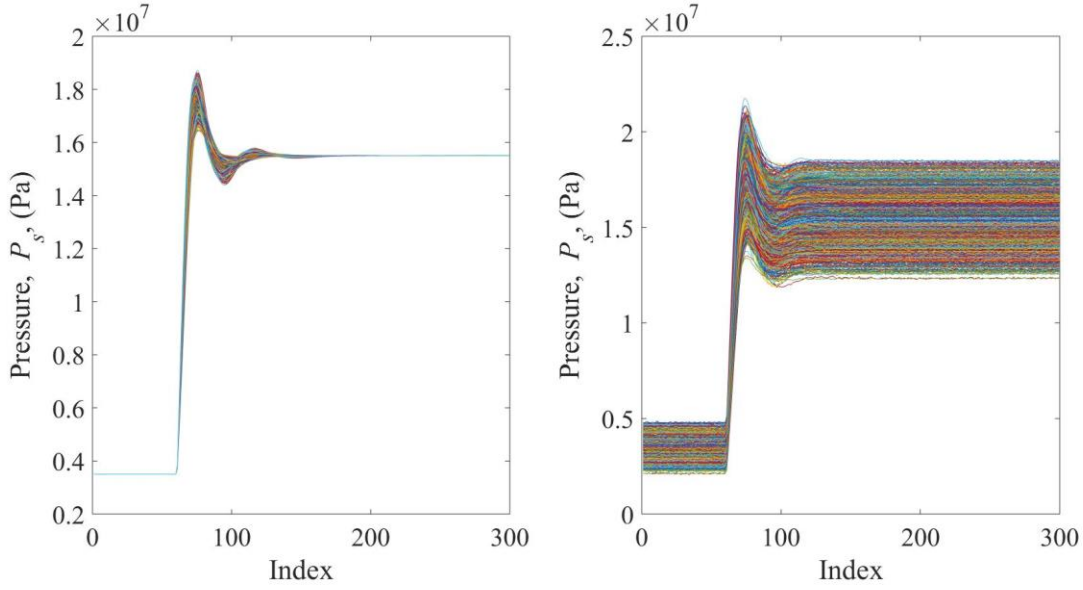


**Figure 4.17**: Noise corrupted pump pressure signal, on the left illustrates no noise corruption and the right has been corrupted with the designed noise

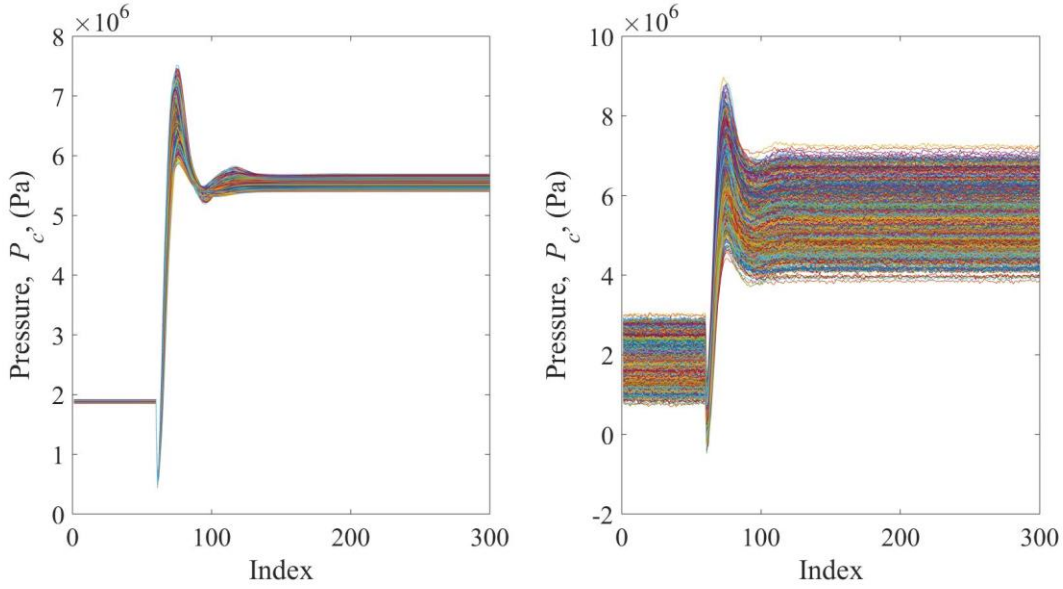


**Figure 4.18:** Noise corrupted control piston pressure signal

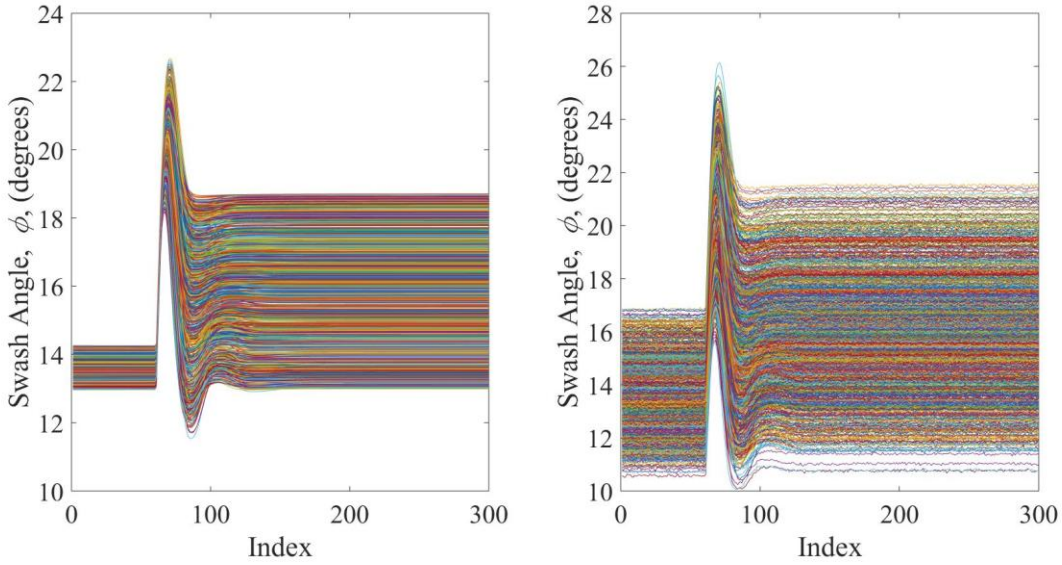


**Figure 4.19:** Noise corrupted swash angle sensor signal

After noise corruption, the same process is carried out to transform the now ‘noisy’ data into principal components and perform a regression using the principal components strongly correlated with leakage.

The following investigation compares the performance of the algorithm using noisy versus clean training data on predicting the leakage factor of a random noise corrupted signal. A single clean data vector is corrupted with the noise outlined previously. Figure 4.20 gives a

visual portrayal of the noise corruption of the original clean data vector.

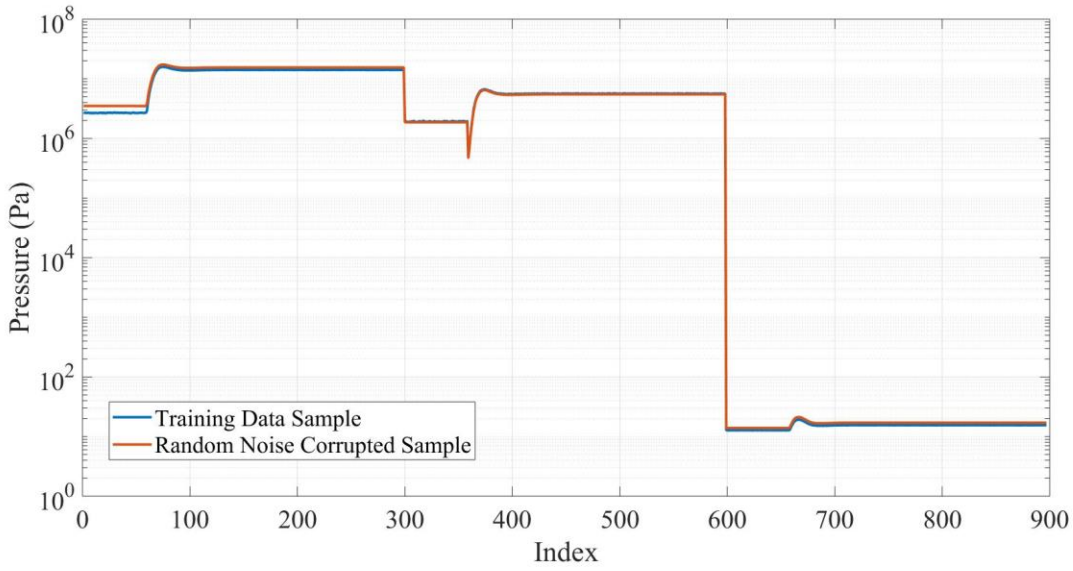


**Figure 4.20:** Clean and noisy data sample used in regression

The regression scheme is then trained twice, once with clean data and a second time with noisy data and the leakage factor, $Y_{rslope}$, of the single noise corrupted vector is predicted. The prediction error is shown in Figure 4.21 for different numbers of principal components.

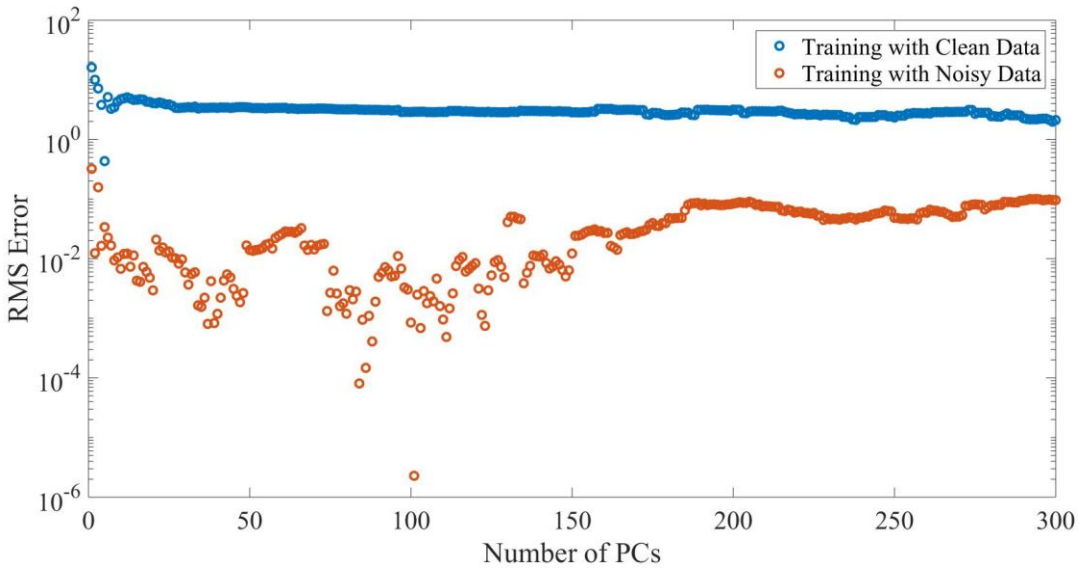


**Figure 4.21:** Comparison of training data performance for a single noisy sample

Figure 4.21 illustrates a significant difference in error using noisy and clean training data. If one were to input a noisy response vector in order to predict the leakage or one with some degree of measurement error, the above analysis would suggest to train the algorithm with noisy data.

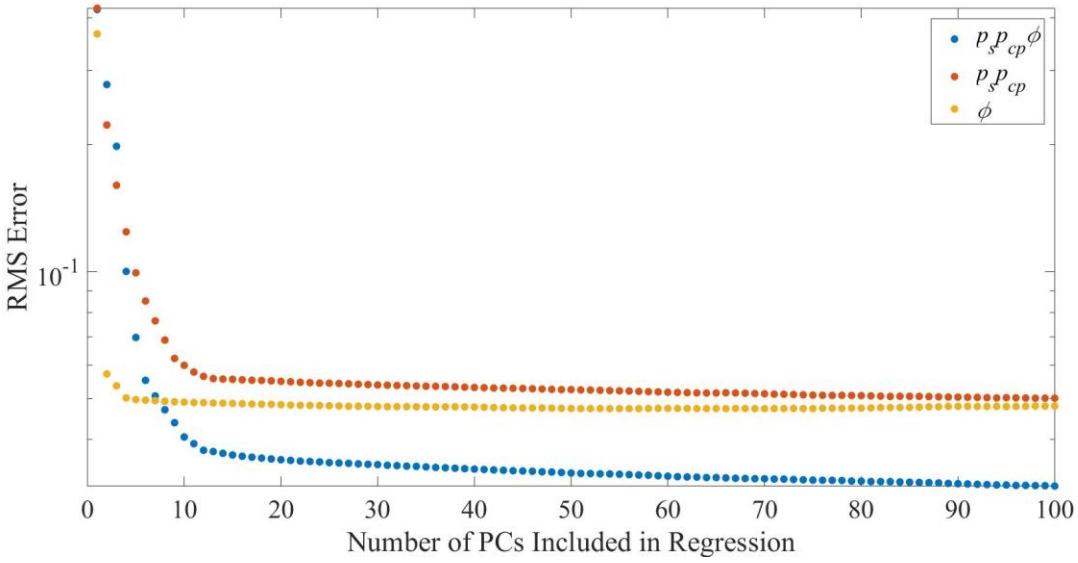


**Figure 4.22:** Prediction error of different signal combinations and training with a noisy dataset

Figure 4.22 shows the regression error for different numbers of principal components given a noisy training data set and using K-fold cross validation. The regression error is significantly higher than with clean training data, however, it is not unreasonable. The best signal combination, when training with noisy data, remains unchanged.

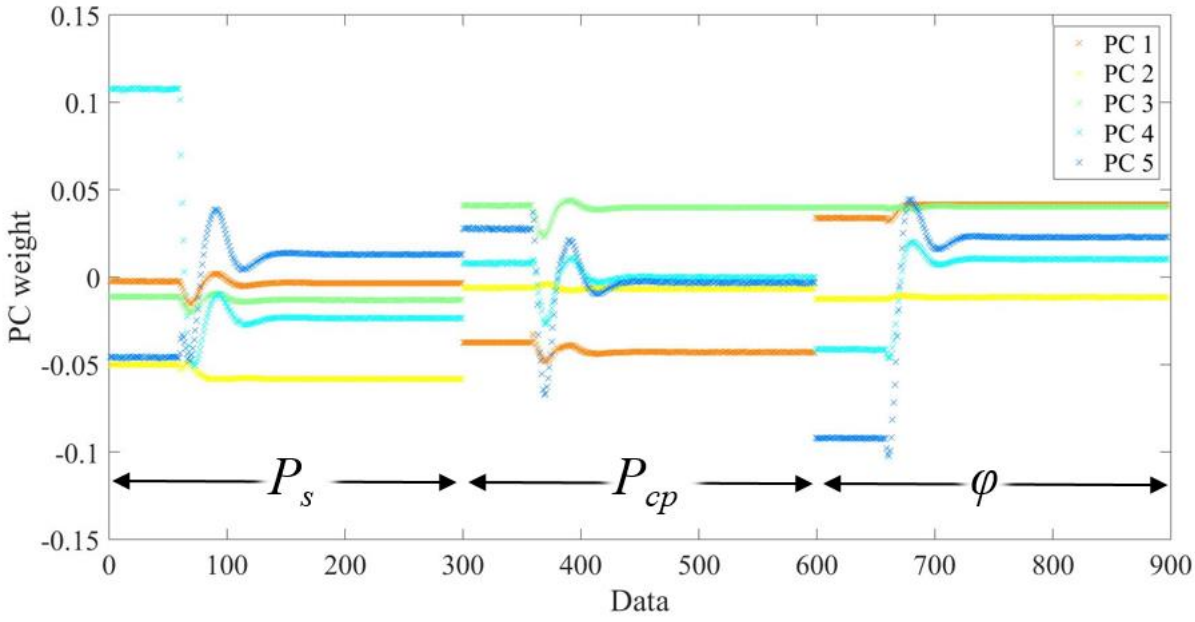


**Figure 4.23:** Weights of principal components for noisy dataset

Figure 4.23 illustrates the weighting of each principal component using a noise corrupted dataset. The first principal component carries a lot of weight with the swash angle steady state information.

This section uses strictly simulation analysis to outline the design considerations of a condition monitoring device that relies on pump dynamic sensor information to predict case drain leakage. Since the design is strictly simulation based, it cannot account for all considerations when given experimental data. Chapter 5 details the evaluation of the leakage prediction algorithm using simulated training data and experimental response information and details further algorithm optimization.

# Chapter 5 Experimental Response Data

This chapter uses the algorithm design framework developed in the simulation study in Chapter 4 to assess the leakage prediction capabilities using experimental pump data. The chapter begins with a general introduction of the experimental data captured, then investigates filter design for the raw pump data. The noise investigation performed in Chapter 4 is expanded for the experimental data and a larger study is conducted. A comparison of using only pressure versus all three signals is performed. The later sections of the chapter investigate using different experimental pump signals as well as assessing the performance of the algorithm with small steps in load pressure at various operating points.

## 5.1 Experimental Response Data General Observations

As previously mentioned, this chapter focuses on using experimental response data to assess the effectiveness of the leakage estimation algorithm. The dynamic data from 3 pumps with varying levels of case drain leakage were obtained. Two assessments of the algorithm are performed. The first uses large step response data, which is the dynamic response of the pump to a single large change in load pressure, and the second is small step response data. Small step response data are response data for small, incremental increases in load pressure. To begin, the pump condition is summarized in Table 5.1 and is more detailed in Appendix A.

**Table 5.1:** Summary of pump condition

| **Pump** | **Condition** |
|---|---|
| Pump 165 | Beyond Service Limit |
| Pump 167 | At Service Limit |
| Pump 172 | Below Service Limit |

An example of the pump response data obtained is displayed in Figure 5.1 - Figure **5.3**. Refer to Appendix A for a more detailed data analysis.

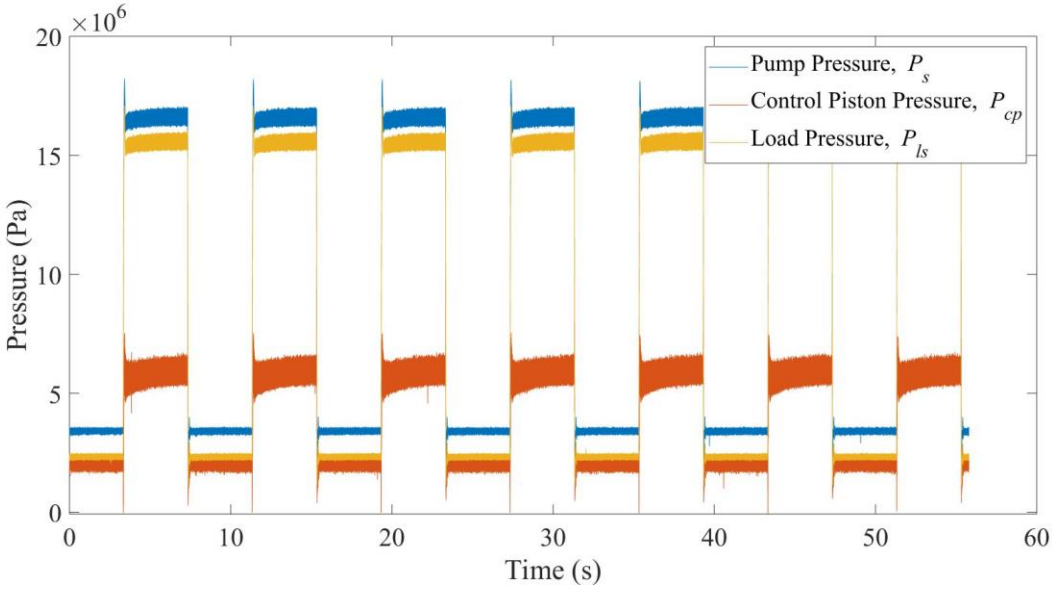


**Figure 5.1:** Large step dynamic pressure response data for pump 165

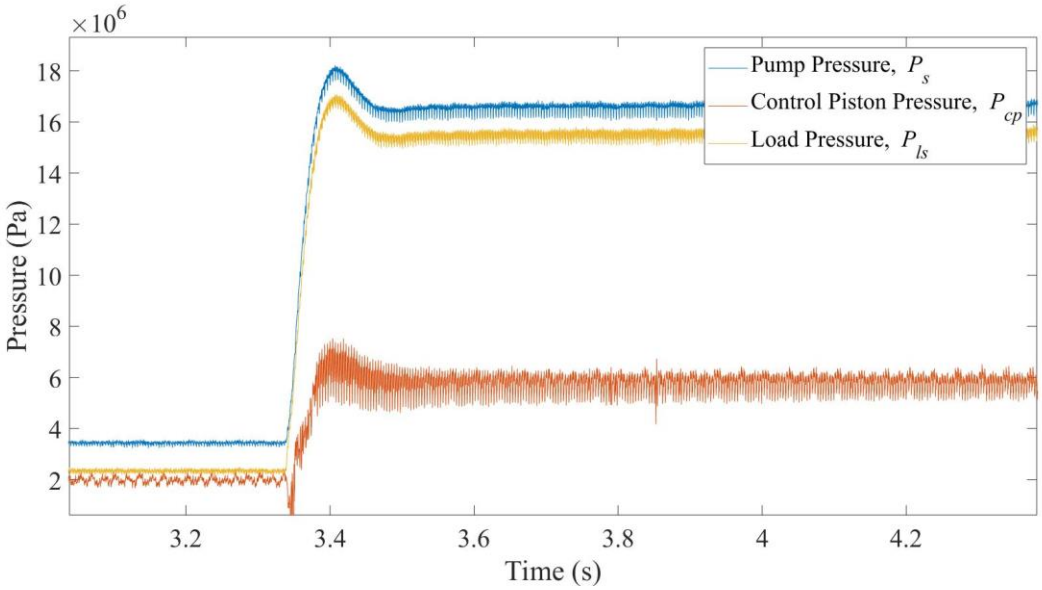


**Figure 5.2:** Magnified portion of pressure response data for pump 165 highlighting pressure dynamics

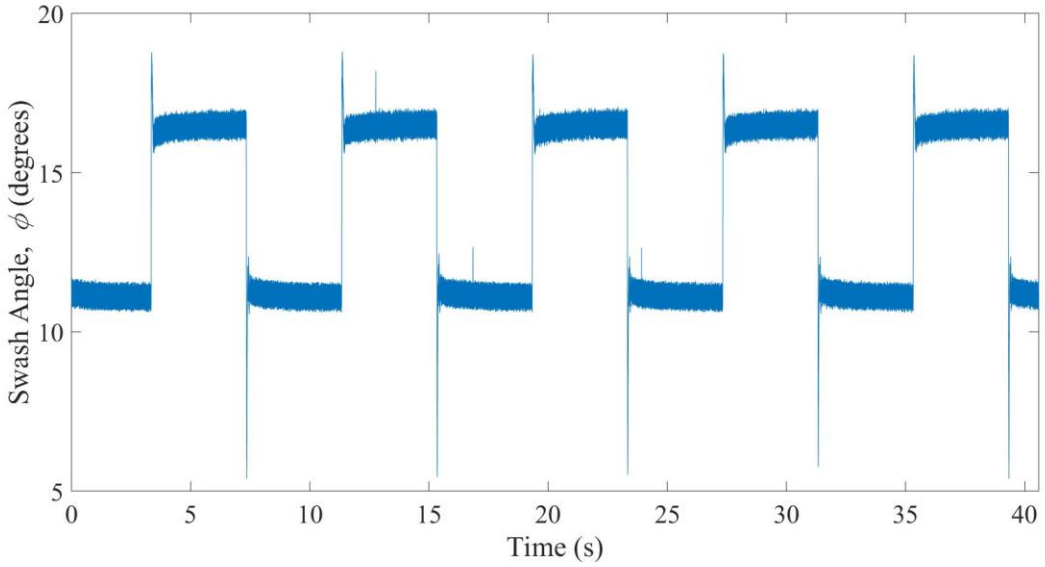


**Figure 5.3:** Large step dynamic swashplate angle data from pump 165

The following chart summarizes the prediction algorithm process. It is slightly different than in Section 4.7 since this process uses experimental pump data.

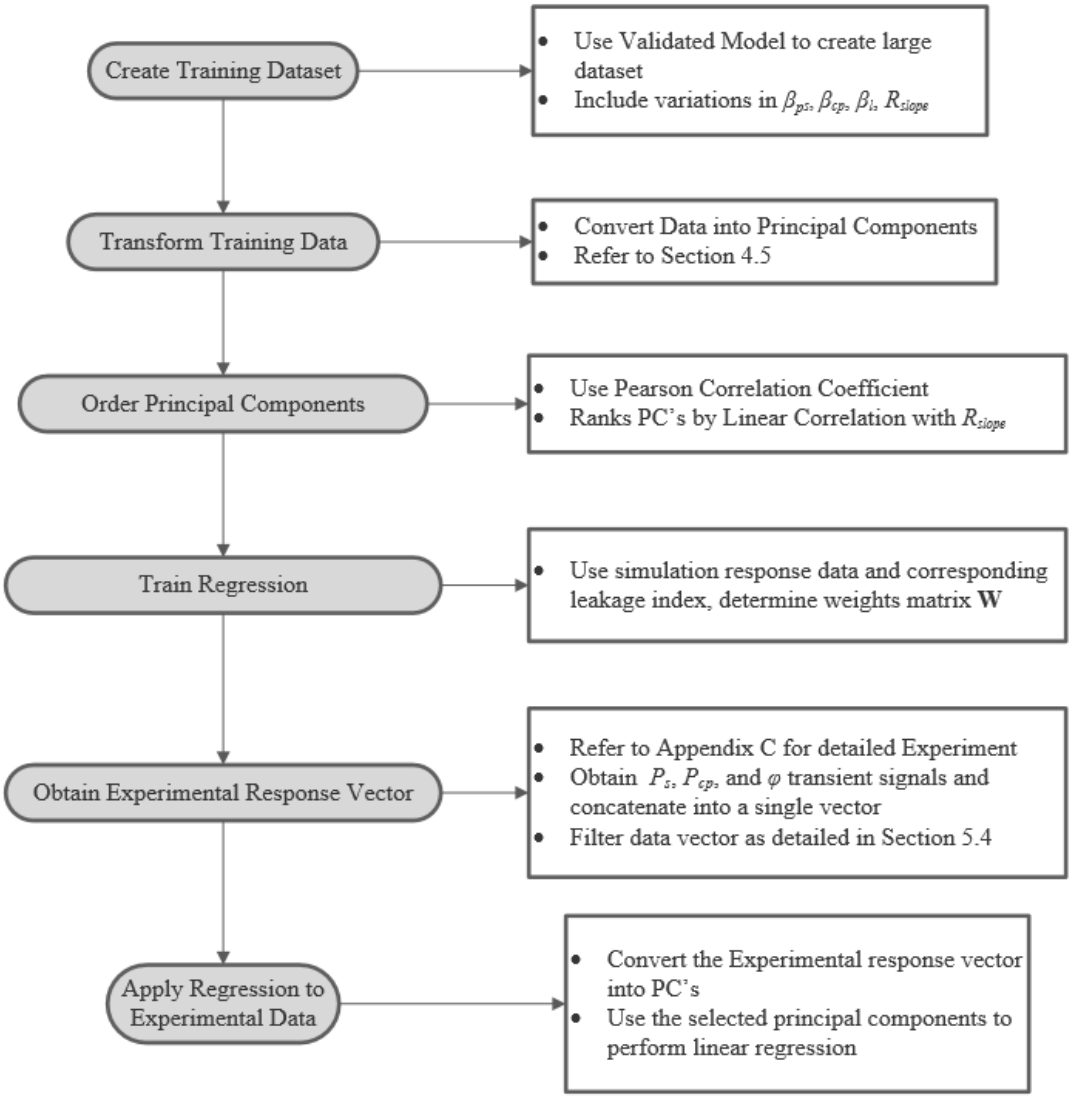


**Figure 5.4:** Process to predict pump leakage factor using PCA with simulated data applied to an experimental response vector

## 5.2 Filtering Experimental Data for All Signals

The experimental data collected contains significant noise. Upon closer inspection, it was observed that the wide noisy pressure signals seen in Figure 5.5 and Figure 5.6 are a result of a combination of noise and pump ripple.

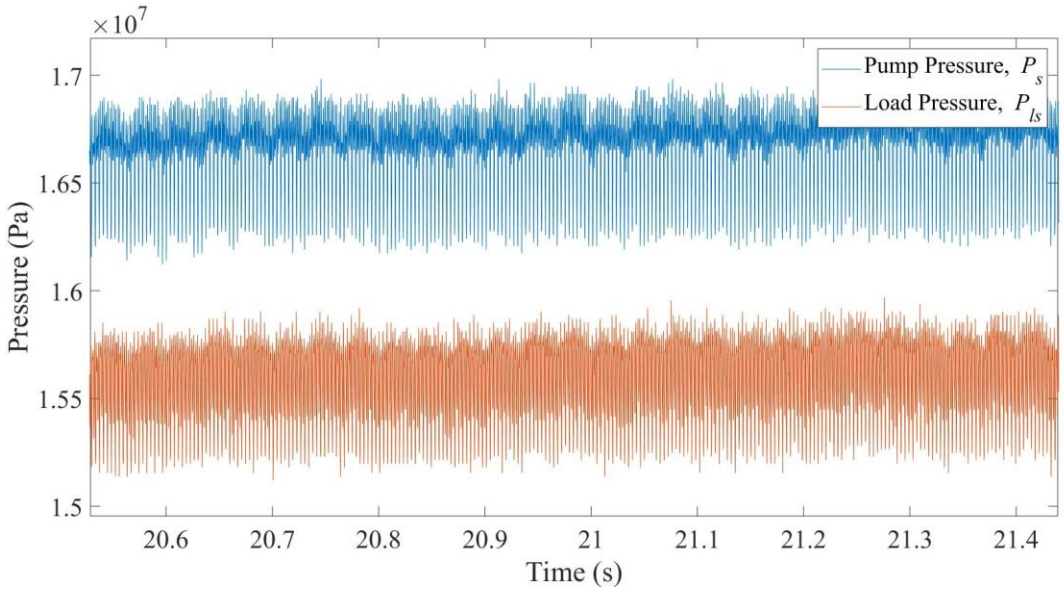


**Figure 5.5:** Close up view of pressure data from pump 165

Figure 5.5 shows a repeating pattern. To ensure consistency, the ripple was also inspected on the pump with minimal wear, Pump 172. The pump ripple appears very similar for both worn and new pumps. This is likely due to even wear. Li (2005) shows similar results but also shows how with a single worn piston, the pump ripple can change.

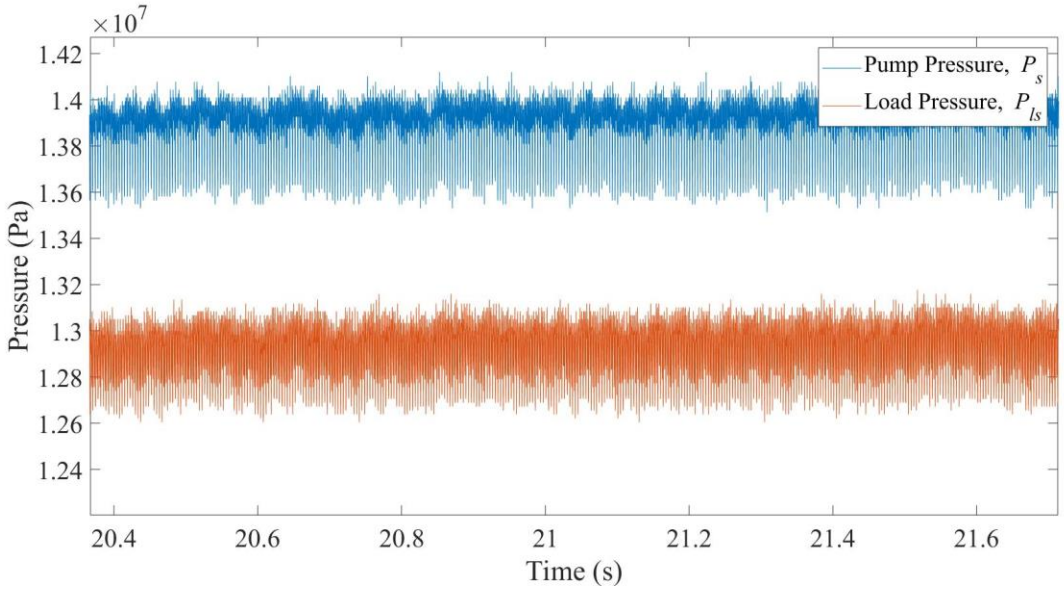


**Figure 5.6:** Pump ripple inspection for pump 172

It was expected that using a low-pass digital filter to remove the pump ripple and noise would improve results. In evaluating the effectiveness of the leakage estimation algorithm on experimental data, an analysis of filtering cutoff frequency was determined to be of importance. This analysis is unique to the experimental evaluation since the simulation data in Chapter 4 are clean.

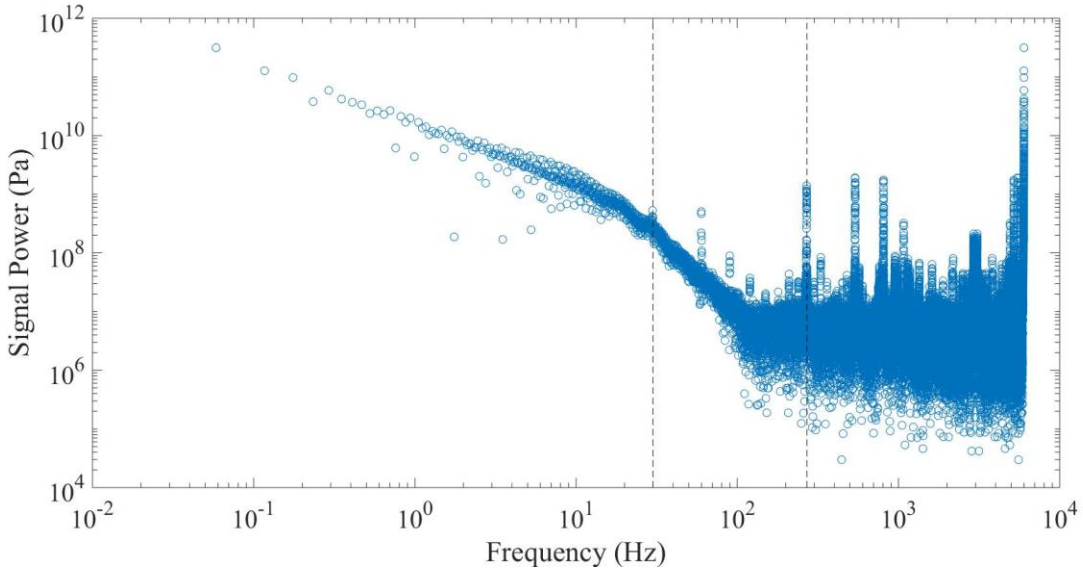


**Figure 5.7:** FFT of experimental pump outlet pressure data from pump 165, the first from the left vertical marker indicates the pump rotational frequency (30 Hz) and the second marks the piston pumping frequency (270 Hz)

Figure 5.7 plots the magnitude of the frequencies present in the experimental data. The first vertical mark denotes the pump rotational frequency, roughly 30 Hz, and the second marks the pumping piston frequency, 270 Hz (9 times the pump rotational frequency). Filtering the data is an important step because it can have significant effects on the prediction accuracy. For this research, a low pass filter will remove high frequency content that could be attributed to sensor noise. Determining the cutoff frequency is essential: too low and valuable information is removed, and too high the algorithm uses a very noisy data sample. It is important to note that the dynamic model training data do not include pump ripple but the experimental data do. It was decided to attempt to predict the leakage of an experimental response data vector using four different cutoff frequencies and evaluating the RMS error to determine which cutoff frequency

performs best. This was done for a single data sample from each pump. Figure 5.8 – 5.10 evaluate the effectiveness of the predictive algorithm for different data filters.

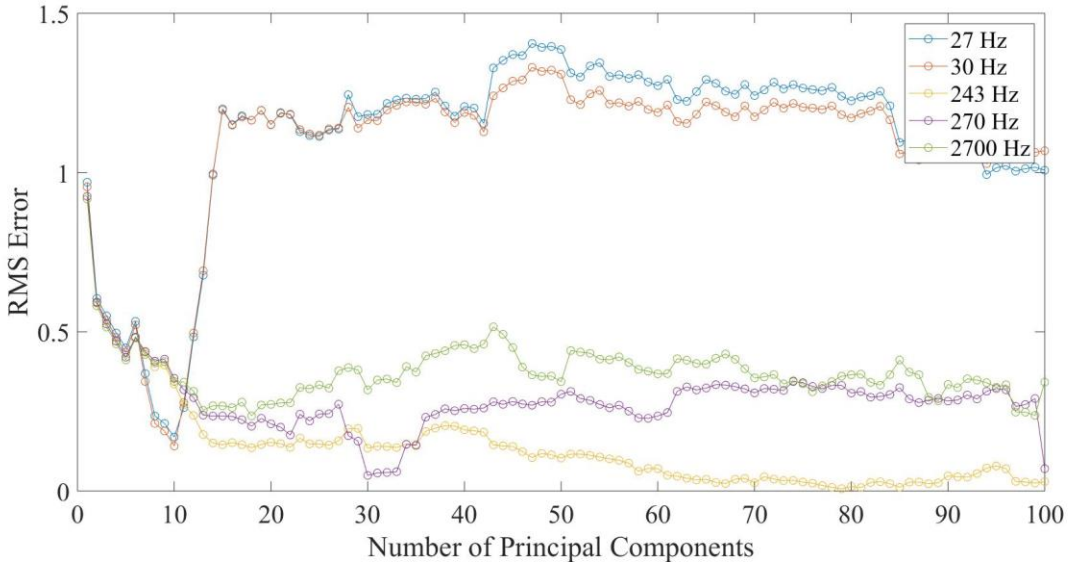


**Figure 5.8:** Pump 165 filter analysis

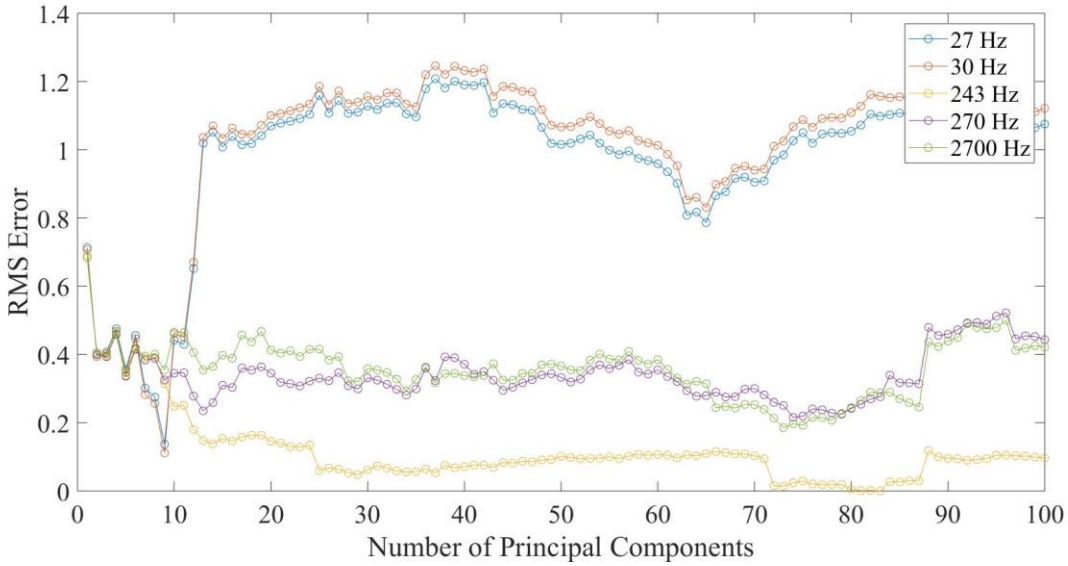


**Figure 5.9:** Pump 167 filter analysis

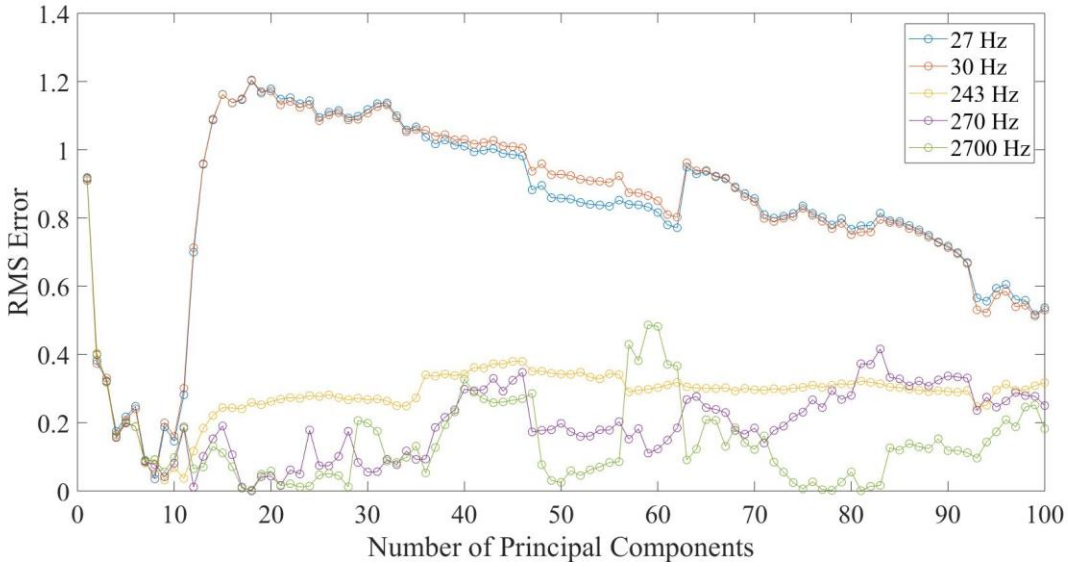


**Figure 5.10:** Pump 172 filter analysis

The specified frequencies are cutoff frequencies and correlated to the frequencies shown in Figure 5.7. The cutoff frequencies for the low pass filter are outlined in Table 5.2.

**Table 5.2:** Cutoff frequencies

| Cutoff Frequency | Frequency (Hz) |
|---|---|
| 90% of Pump frequency | 27 |
| Pump frequency | 30 |
| 90% of Piston frequency | 243 |
| Piston frequency | 270 |
| High frequency | 2700 |

It is clear that the selection of a cutoff frequency in the design of the low pass filter is essential to prediction effectiveness. Using a cutoff frequency at or below the pump rotational frequency removes important information and results in a very ineffective prediction of the leakage factor.

Removing only very high frequencies, essentially not filtering the data, gives sporadic results across the three pumps. Filtering only high frequency gives good RMS error for pumps

167 and 172, however, it does not give the best results for pump 165. Filtering at 243 Hz, 90% of the piston frequency gives good results for all pumps. The RMS error across different numbers of principal components is very consistent. There is not much random change in RMS error when new principal components are added. Filtering at 270 Hz, the piston frequency, gives good RMS error, however, the results vary significantly when adding principal components.

## 5.3 Training Dataset

This section outlines the creation of the training dataset for leakage prediction with experimental data. The training data in Chapter 5 are acquired much differently than in the simulation study of Chapter 4. As discussed in Chapter 4, the inputs to the dynamic model to create the training dataset include variations in the bulk modulus, leakage factor, the constant parameter set to run the model, and orifice flow constants to set the flow and pressure of the pump. In this Chapter, the experimental response data are obtained first. The experimental data outputs are used to calculate the orifice flow constants as summarized in Appendix C. A simulated training dataset was created to capture the characteristics of all three worn pumps. To create the training set, the base parameter set is the same as that used in Chapter 4, however, the flow and load pressure orifice constants are different. This is because, for each pump, the orifice constants are different despite attempts to keep them constant. The results are reviewed in Appendix C.

Since the orifice constants vary for each pump, it was decided to use the median of the range of the values. This is also detailed in Appendix C. Since the orifice constants are not calculated exactly from each experimental response for each pump, it may be useful to illustrate the response validation using these values.

The flowchart in Figure 5.11 clarifies how the training dataset was obtained.

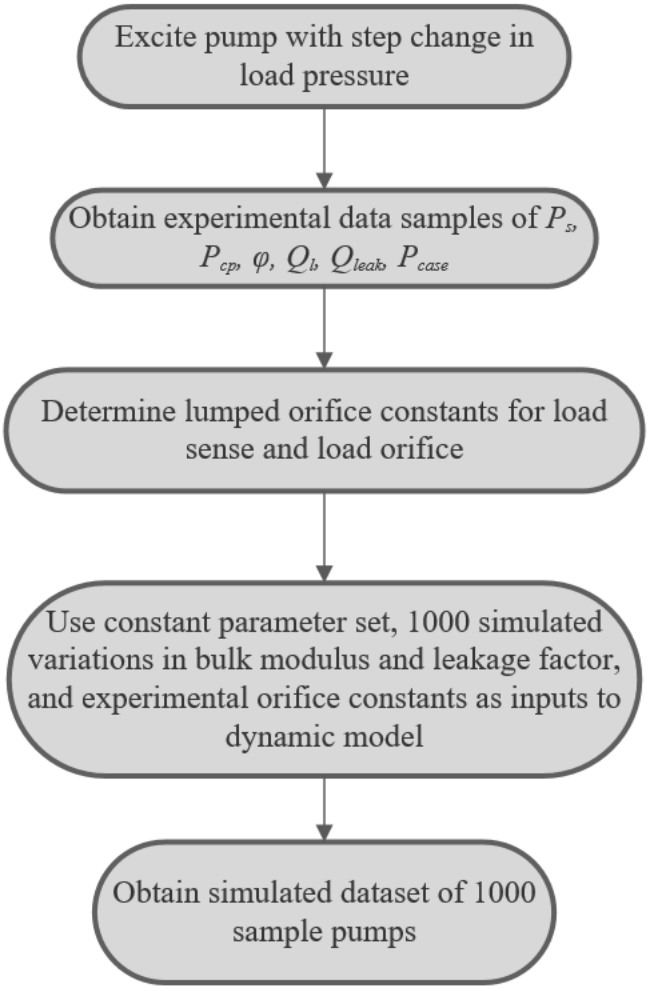


**Figure 5.11:** Flow chart of method to create training dataset for experimental evaluation of predictive capabilities of the algorithm

## 5.4 Noise

Section 4.8.3 of Chapter 4 highlights the importance of corrupting the clean training data with noise before the PCA is performed. This section uses experimental data to give a detailed outline of the noise addition to the clean training data before PCA is applied. Three different sensor combinations are evaluated because it is unsure if different amounts of noise will give better results for each signal set. The combinations are summarized in Table 5.3.

**Table 5.3:** Sensor combination summary

| Combination | Advantages | Disadvantages |
|---|---|---|
| $P_s P_c \emptyset$ | Evaluated as having the lowest prediction error | Implementation of 3 sensors |
| $P_s P_c$ | Potential to assess pump health with simple pressure measurements | Error may be high |
| $\emptyset$ | Potential to assess pump health with single, low-cost sensor | Error may be high |

In order to obtain some preliminary range of magnitude for added noise, the experimental step data was evaluated. Section 4.8.3 outlines how this preliminary range was determined.

## 5.5 Determination of Range of Noise Addition for each Signal

In order to determine an approximate range of noise to add to the training dataset, the experimental results were evaluated. Figure 5.12 - Figure **5.14** plot a single data sample collected from each of the worn pumps for each signal. The plots are for a large step input in load pressure and the noise range derived from the plots is only applicable to the large step data. These data are also filtered for presentation purposes. An initial noise range can be derived from each plot for each sample.

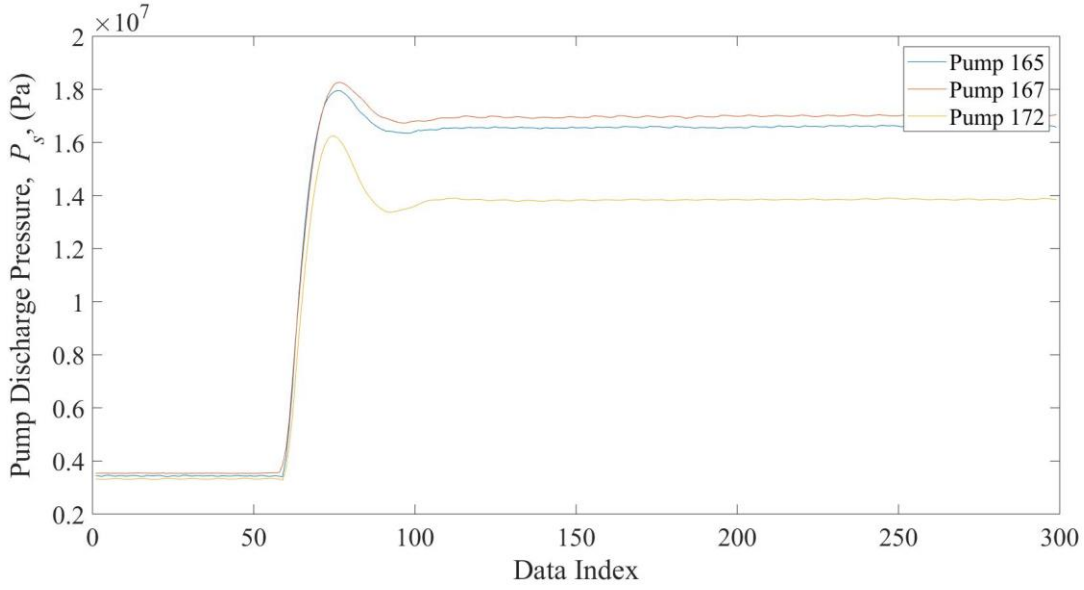


**Figure 5.12:** Filtered pump pressure dynamic sample for each pump

Figure 5.12 and Figure 5.13 show a marked difference in steady state pump discharge pressure between the pumps after the large step input to load pressure. Figure 5.14 shows similar dynamics for pumps 165 and 167 with noticeable steady state error. The swash angle response of pump 172 is expectedly different than the worn pumps 165 and 167 because the pump is not compensating for leakage by settling at a larger swashplate angle. Further discussion of the differences is provided in Appendix C.

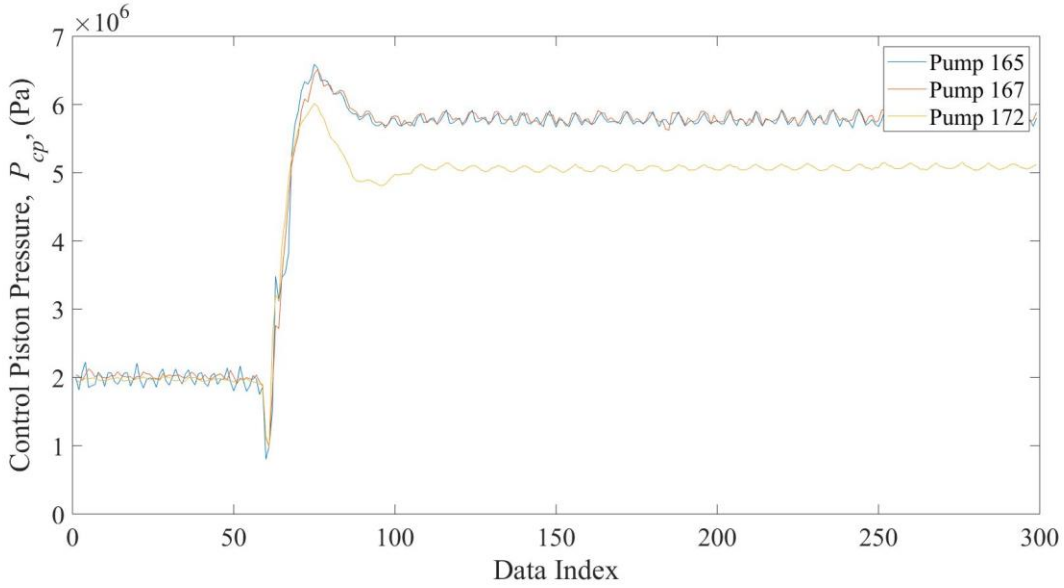


**Figure 5.13:** Filtered control piston pressure dynamic sample

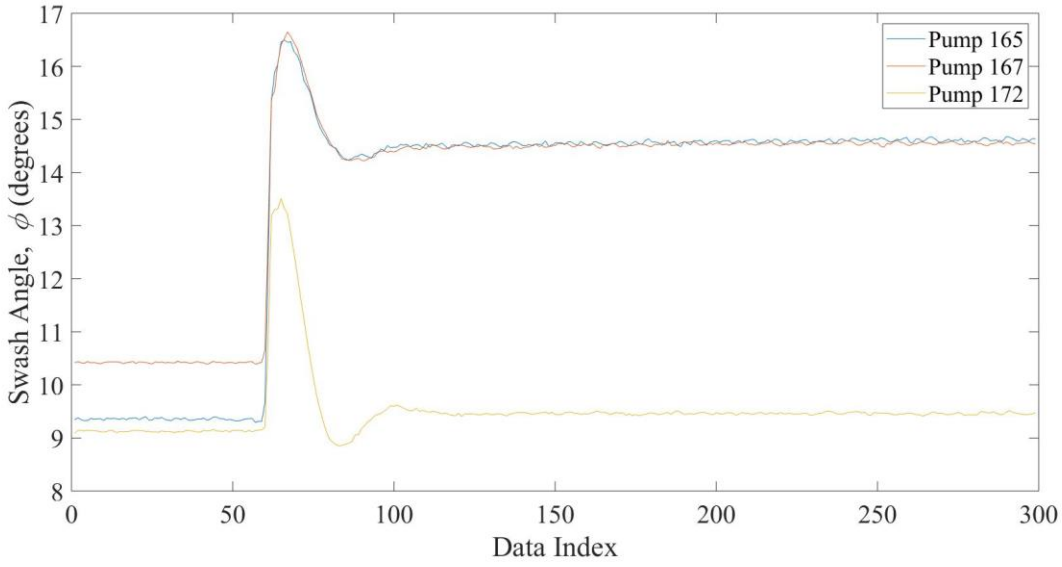


**Figure 5.14:** Filtered swash angle sample dynamics

Appendix A describes the differences in pump pressure, while each pump is subject to the same load sense and load orifice, as a result of a change in margin pressure, a phenomenon requiring further study. For the purposes of this research, noise can be added to account for this difference. Sections 5.5.1 - 5.5.3 outline the optimized noise addition to the training data. Each section evaluates the addition of three types of noise, gain, bias, and random noise.

### 5.5.1 Noise Optimization for all Signal Data Combinations using Experimental Data

The first noise assessed is that in the form of a bias error. A general range for the bias error was determined and applied to the training data. Bias error appears to have no effect on the predictive capabilities of the algorithm. Figure 5.15 illustrates how the prediction capabilities of the algorithm do not show any obvious trends while the range of bias is increased.

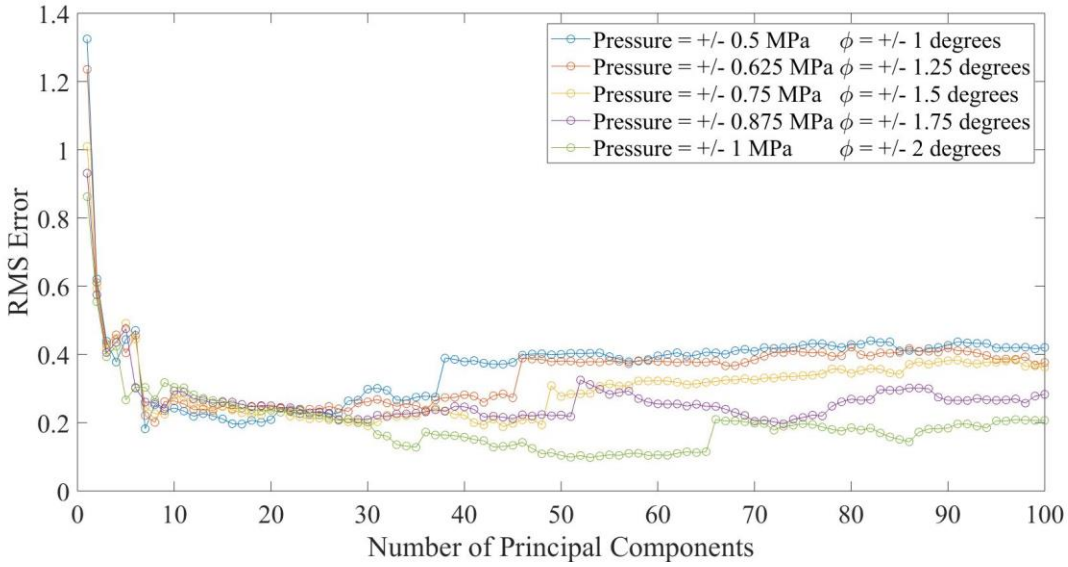


**Figure 5.15:** Pump 165 RMS error when training data are corrupted with random bias

The results in Figure 5.15 are for pump 165, however, the other two pumps show similar results.

A random gain applied to the training data can remove any relationship between the steady states before and after the step. Different signal combinations may respond differently to a random gain. For example, using only pressure data may require using a larger gain when corrupting training data then with using just swashplate data. It is known that an important component of the swashplate data is the steady state values. Corrupting this signal with significant gain may remove this strong relationship and result in high regression error.

The values for gain are drawn from a normal distribution with a specified standard deviation. The noise is mean centered at unity. Figures 5.16 – 5.18 give the RMS error when different magnitudes of random gain are added to the training data

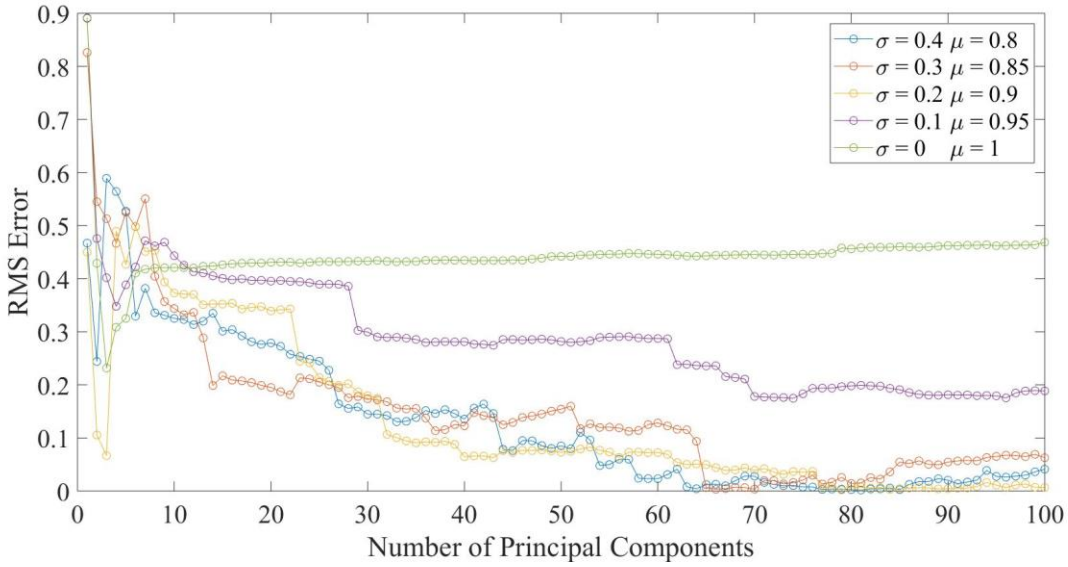


**Figure 5.16:** Pump 165 RMS error for different amounts of gain applied to training data

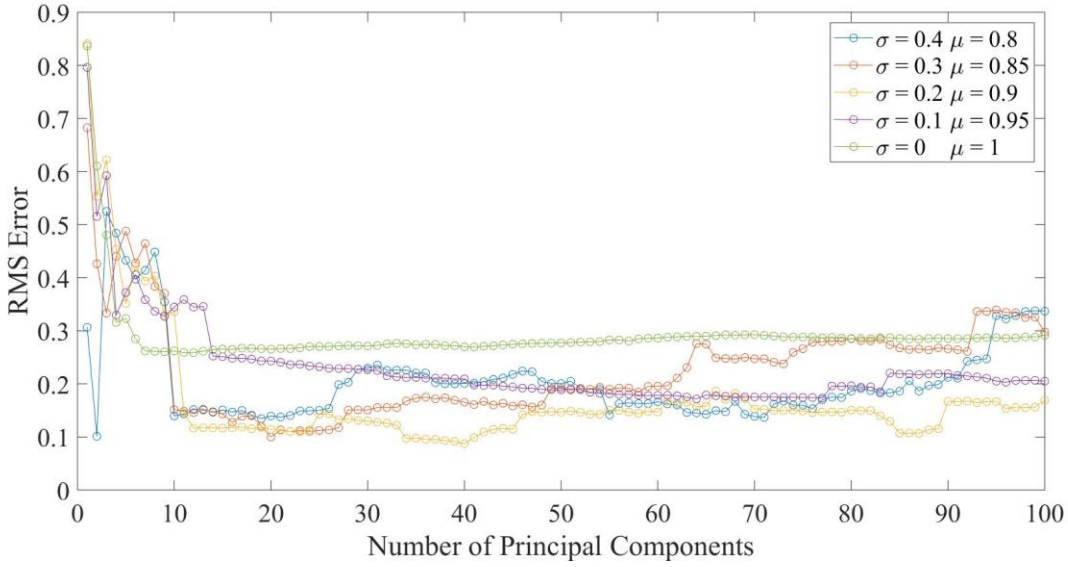


**Figure 5.17:** Pump 167 RMS error for different amounts of gain applied to training data

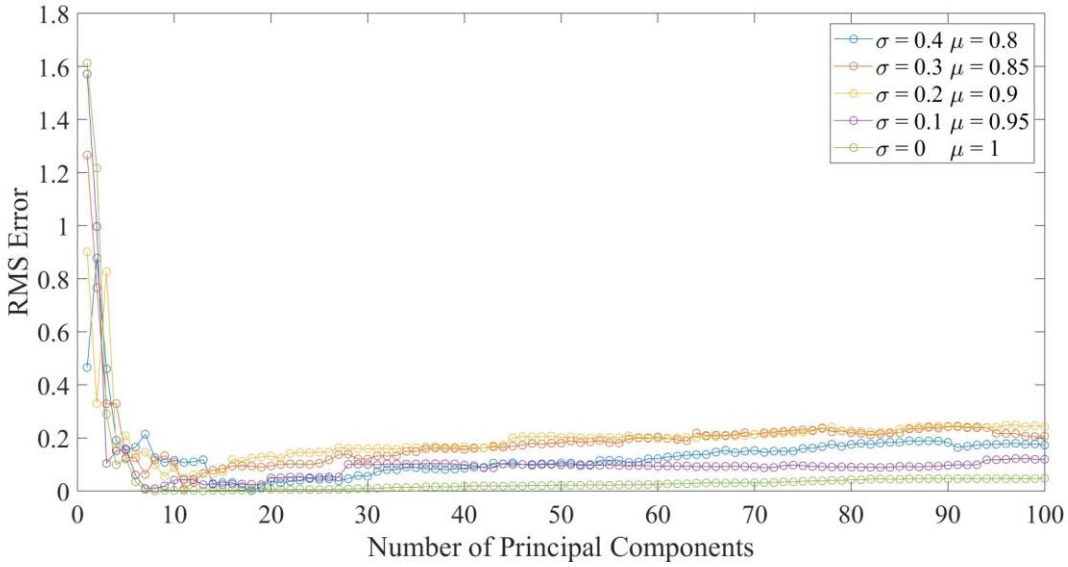


**Figure 5.18:** Pump 172 RMS error for different amounts of gain applied to training data

Pumps 165 and 167 show the best results when some amount of gain is added to the training data. The opposite is true for pump 172. It appears that no gain applied to the training dataset gives the lowest RMS error. The amplitude of random noise is also investigated and the results are shown in Figure 5.19 - Figure **5.21**.

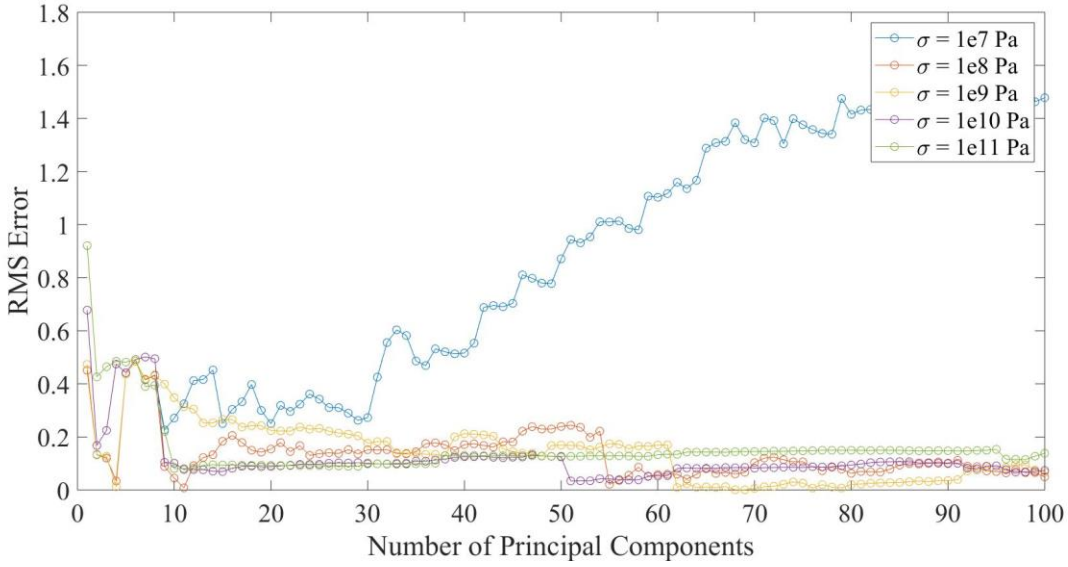


**Figure 5.19:** Pump 165 RMS error with random noise added to training dataset

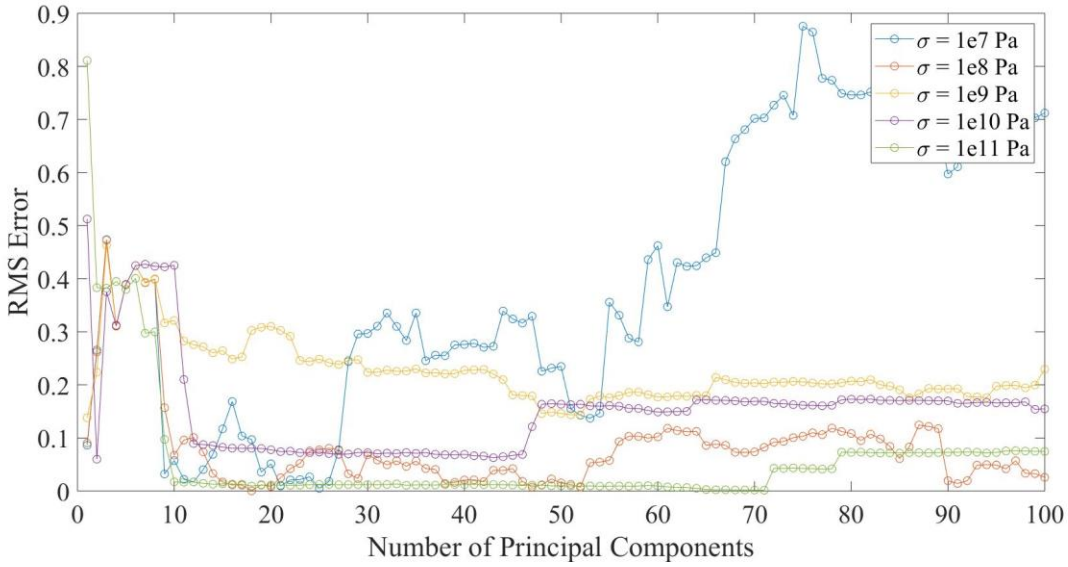


**Figure 5.20:** Pump 167 RMS error with random noise added to training dataset

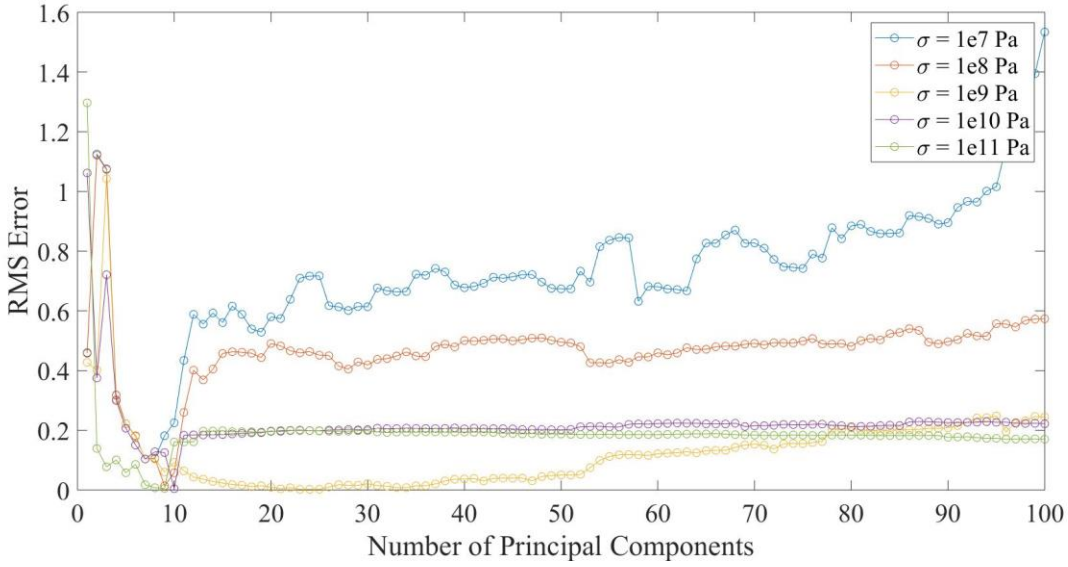


**Figure 5.21:** Pump 172 RMS error with random noise added to training dataset

Observing the previous plots, a base set of noise was selected. For the gain, a standard deviation of 0.9 was used and for the random noise a standard deviation of 1e10. Applying the optimized

gain values, Figure 5.22 shows the predictive performance of the algorithm when using all pump experimental sensor data.

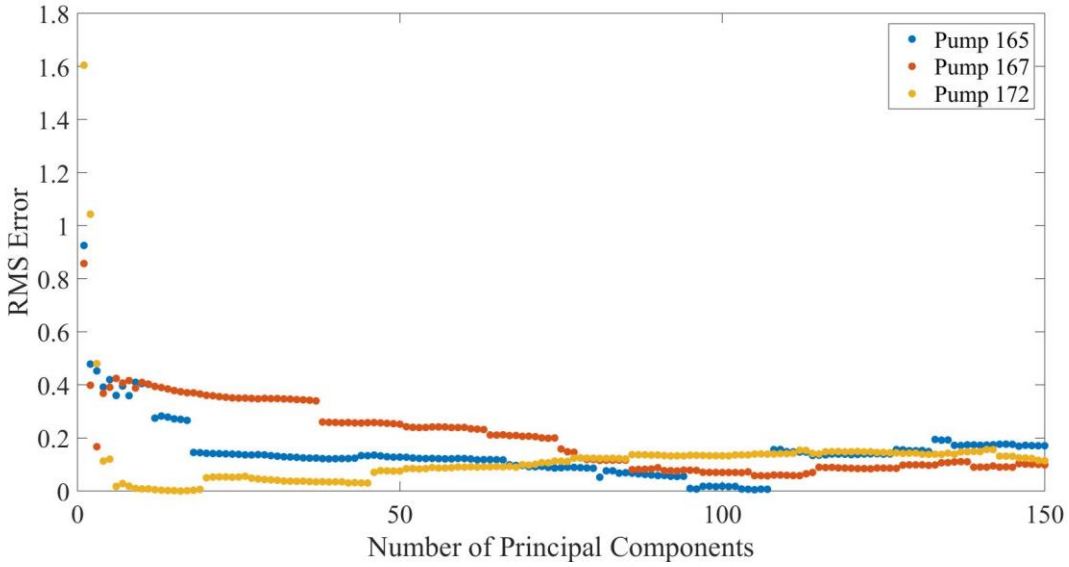


**Figure 5.22:** Optimized error results using algorithm to predict pump leakage

The predictive capabilities of the algorithm fall below an RMS error of 0.2. This can be interpreted as having less than 20% error in estimating the leakage factor of the pump.

### 5.5.2 Noise Optimization for Pressure Response using Experimental Data

When the swash angle response data is excluded from the regression, and the prediction is done on only pressure data, the RMS error is significantly higher (as expected). The performance appears to give the best RMS error for pump 167, the mid-life classified pump. This may be because the training data are median centered and would match most closely to Pump 167.

Figure 5.23 shows the predictive performance of the algorithm with optimized noise values using only experimental pump pressure data.

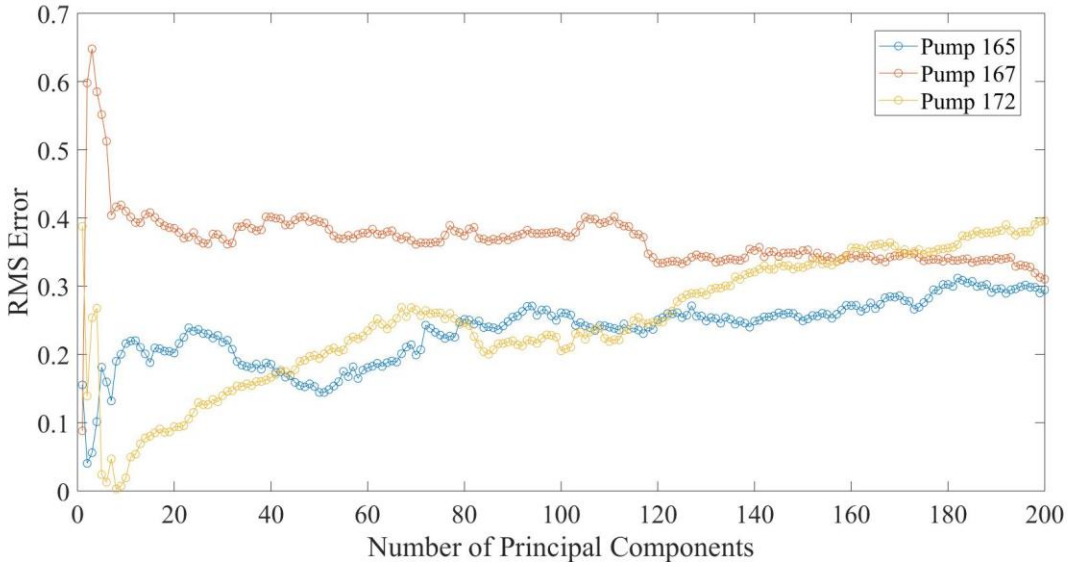


**Figure 5.23:** RMS error for prediction using only pressure data

Performing a similar gain analysis as done with the full signal content data, Figure 5.24 - Figure **5.26** illustrate how the application of certain magnitudes of gain to the training dataset affects the algorithm predictive capabilities for each pump.

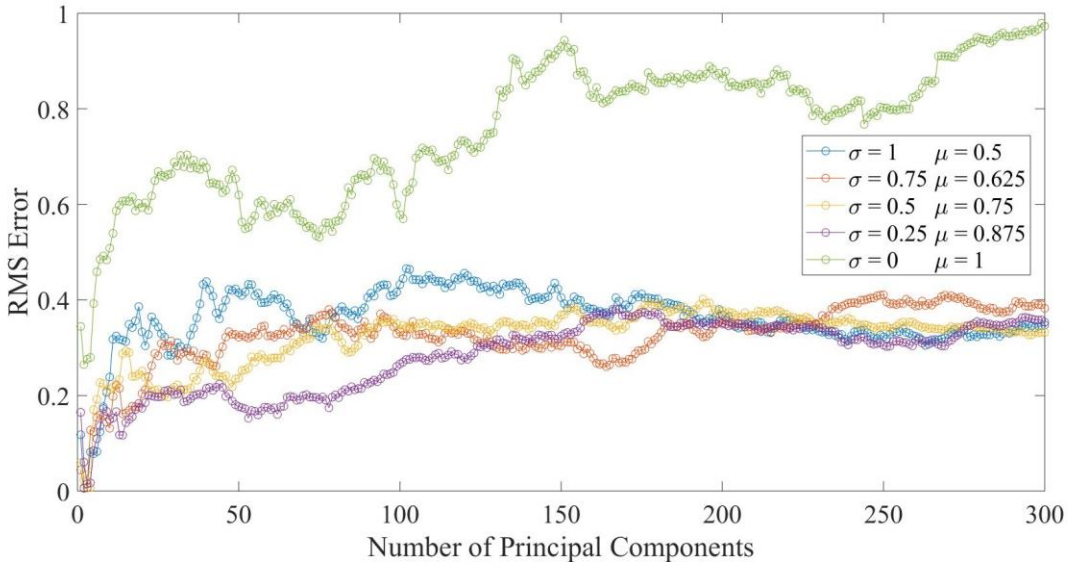


**Figure 5.24:** Pump 165 RMS error for different gains applied to training dataset

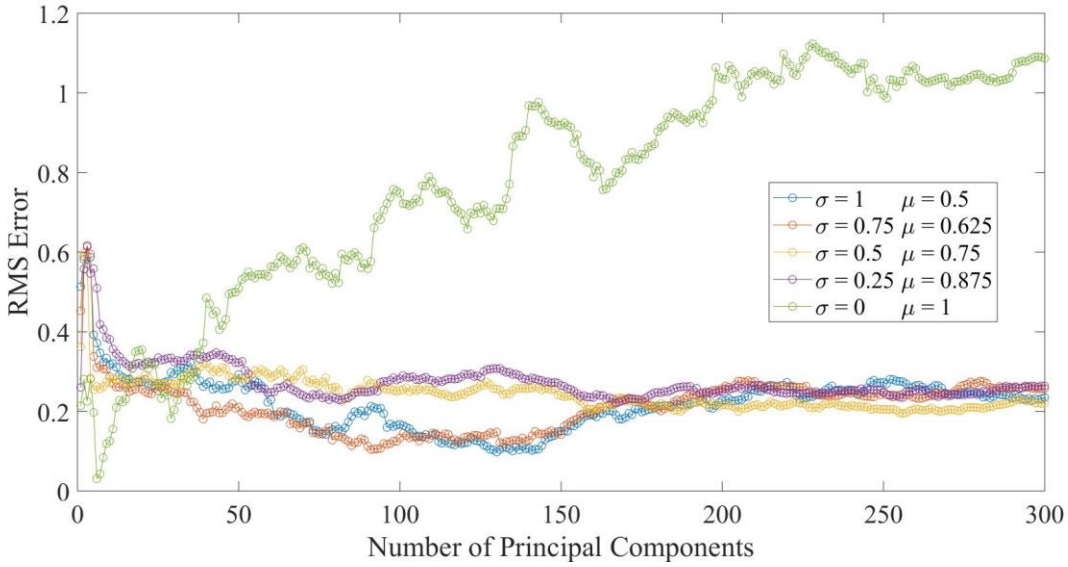


**Figure 5.25:** Pump 167 RMS error for different gains applied to training dataset

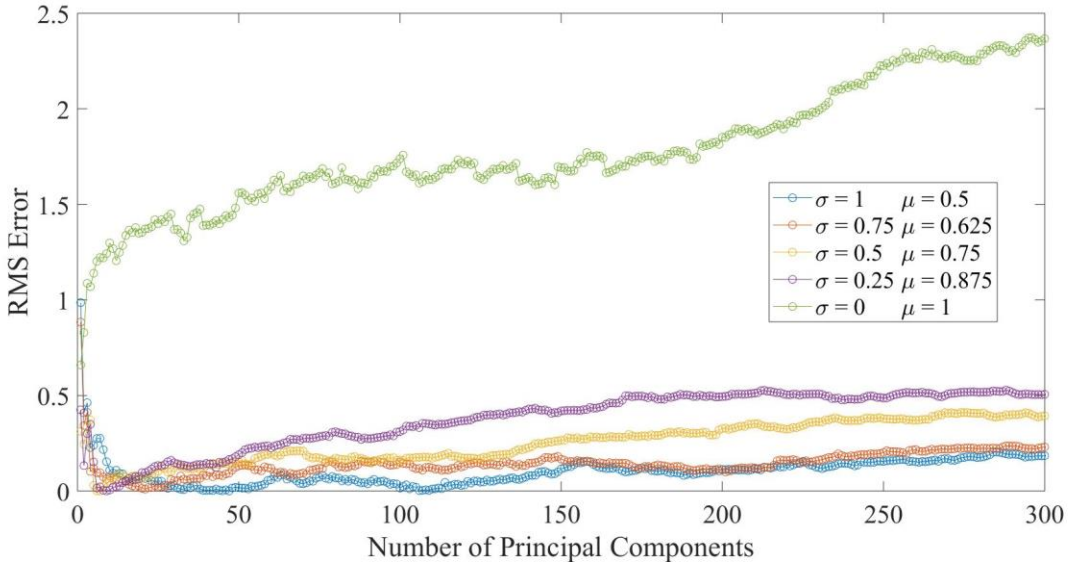


**Figure 5.26:** Pump 172 error with gains applied to training set

An important result of this analysis is that a gain applied to the training data appears to reduce the RMS error across all pumps. Gains of 15-20% amplitude result in the lowest RMS regression error.

### 5.5.3 Noise Optimization for Swash Angle Response using Experimental Data

A similar optimization was performed for only swashplate angle dynamics. The application of gain to the training dataset when using only swashplate response data had similar effects to the other signal combinations. Figure 5.27 shows how applying a gain larger than unity increases the performance of the prediction algorithm.

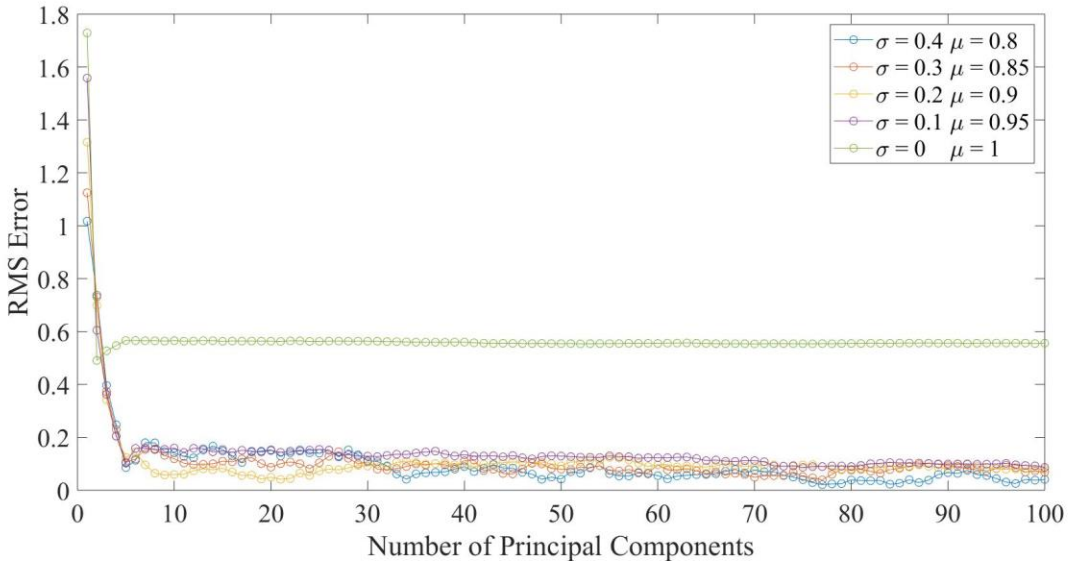


**Figure 5.27:** Noise optimization for swash angle

Evaluating the predictive capabilities of all pumps with the optimized gain applied to the training dataset gives the algorithm error shown in Figure 5.28.

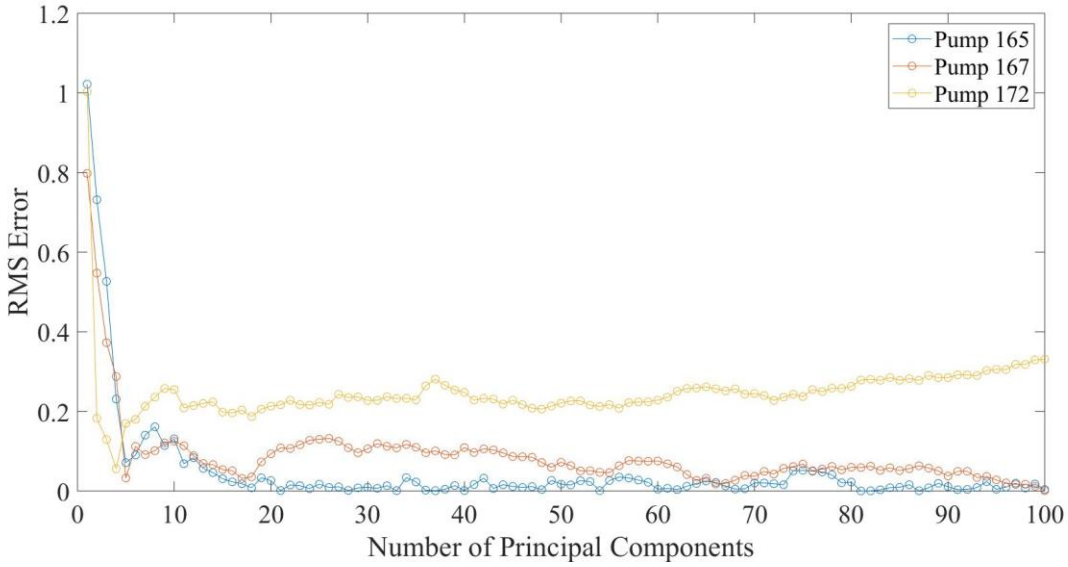


**Figure 5.28:** All pumps prediction error using only swashplate dynamics

## 5.6 Small Step Data Investigation

This section investigates the performance of the regression algorithm using small step data at different operating points for the full signal content (using pump pressure, control piston pressure, and swash angle). As outlined in Section 3.3 the best resolution (most pole movement) occurs at high pressure. Appendix C shows increasing pump pressure dynamic data as a result of a staircase increase in load pressure. The data were segmented into three steps. Each step occurs at the same load flow, however, the pressure range that the step occurs increases. The performance of the leakage estimation algorithm is compared for each step and for each pump. Using the optimized noise values obtained in the previous sections, Figure 5.29 - Figure **5.31** provide the RMS error that results when the algorithm attempts to predict the leakage factor of each pump.

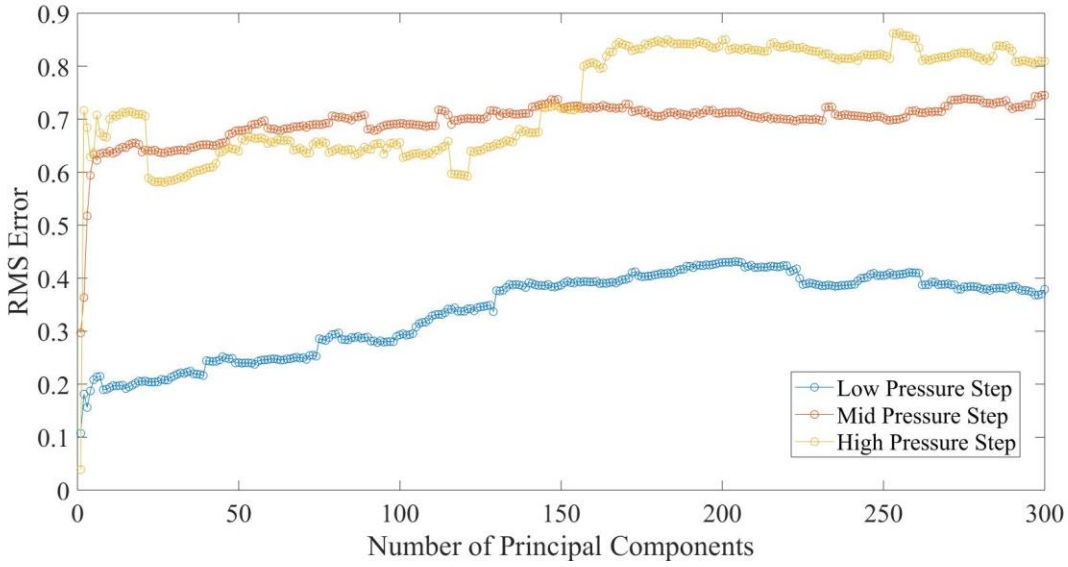


**Figure 5.29:** Pump 165 leakage prediction error at different load pressures

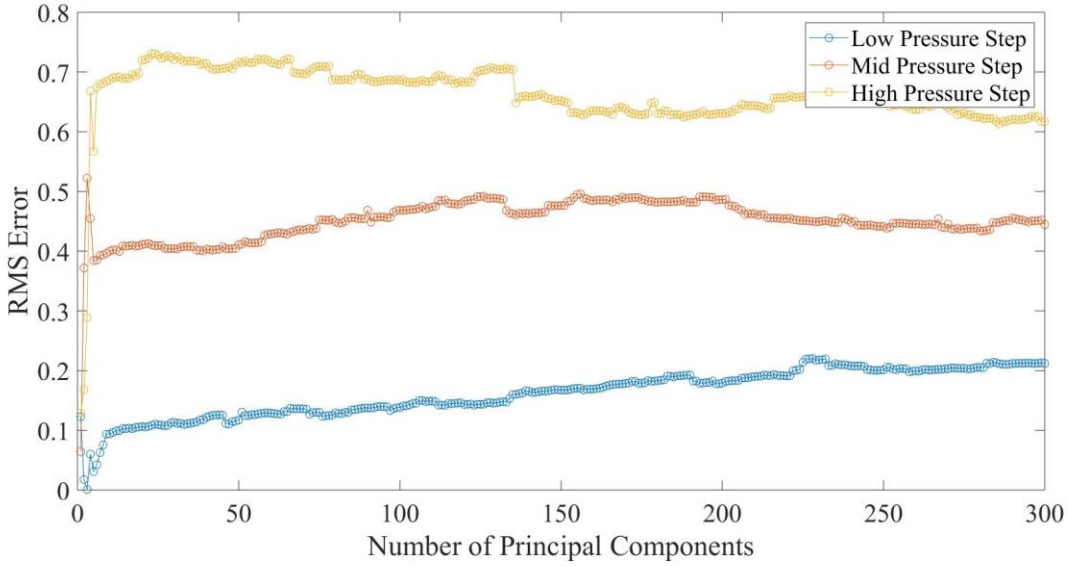


**Figure 5.30:** Pump 167 leakage prediction error at different load pressures

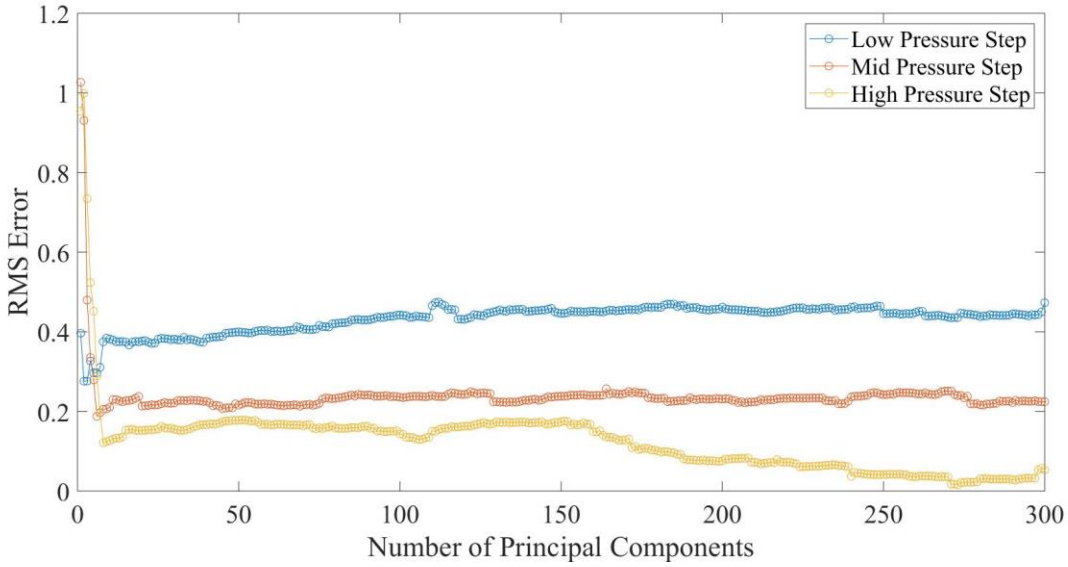


**Figure 5.31:** Pump 172 leakage prediction error at different load pressures

Figure 5.29 - Figure **5.31** show conflicting results. It appears that for Pumps 165 and 167, the lower pressure step gives the best error, while for pump 172 the opposite is true. This may suggest that for pumps with low wear, it may be better to obtain response data at high pressures, whereas pumps of high wear should be tested at low pressure. Further investigation is warranted.

# Chapter 6 Conclusions and Recommendations

The conclusions section summarizes the objectives and goals of each chapter and follows with a brief section on recommendations for future work.

## 6.1 Conclusions

The main objective of this research was to investigate the feasibility, design, and optimization of a condition monitoring device that detects pump condition through dynamic data. Pump condition in this research is strictly defined as a measure of case drain leakage flow.

Chapter 1 outlines the need for further development of PCLS axial piston pump condition monitoring device through a summary of past research efforts as well as outlining current technologies. Chapter 2 details the results of a sensitivity analysis, used for guidance, as well as final model validation plot results for pump sensor outputs. The validation results closely matched experimentally obtained data. Chapter 3 investigates the best operating point to test the pump to give the most dramatic changes when the pump leakage increases as it wears. This was determined to be at high pressure.

Chapter 4 presents a feasibility study, simulation based, that applies a machine learning algorithm, PCA, to extract feature data from a training set and shows how a regression can predict the pump leakage given only dynamic information. It was determined that the best results are from a combination of pump pressure, control piston pressure, and swashplate angle. An investigation is performed to determine how many training samples give the best prediction capabilities. Up to 1000 data samples are optimal; more than that does not help performance. In the anticipation of sensor error given experimental data, an investigation into how to apply PCA with noisy data is outlined. The leakage prediction algorithm performs optimally, in simulation, with the addition of noise in the form of a bias, gain, and random noise if the prediction dataset is expected to be noisy.

The following chapter, Chapter 5, assesses the prediction algorithm designed in Chapter 4 and its effectiveness at predicting leakage given experimental response information. A filtering

frequency 10% lower than the pump piston frequency gives the best prediction performance. The noise addition in Chapter 4 was applied to the leakage prediction algorithm when using raw experimental pump data. The amount of noise added to the training dataset was optimized, and confirmed to decrease the prediction error.

## 6.2 Recommendations

This research presents a framework for the design of a condition monitoring device that predicts pump condition through dynamic information. There is much work still to be done before the device sees practical implementation. In this research, a high speed valve was relied on to give a unit step input in load pressure. This is a costly valve and gives inaccurate results since it does not come to the same position when used with different pumps (see Appendix C). This valve was used because model validation was difficult with a slow acting valve. An improvement on the circuit would be to use a high speed valve for switching and manufacture drilled, fixed orifices to produce the load pressure. This would eliminate any variations in the lumped orifice parameter constants.

Different excitations should be investigated. The only excitation investigated was a step input. Furthermore, it may be valuable to investigate, instead of a step increase in load pressure, a step decrease. It is still unknown whether the resolution of leakage is better with an increasing or decreasing load pressure.

In sampling the simulation and experimental data, a constant sampling rate was used. An investigation into increasing the number of samples is necessary as well as the captured portion of dynamic response. A study should be performed to see how well the prediction algorithm performs with higher sampling frequency and only using the dynamic portion of the response data. This effectively eliminates the steady state components.

Finally, some investigation into the differences in margin from low to high pressure would be valuable. This is believed to have caused a lot of error in the predictive performance of the algorithm since it is one of the largest differences between the experimental and simulation studies.

# References


Atkinson, R. H. (1979). *The effects of solid contamination in hydraulic fluids on axial piston pumps*. Doctoral dissertation, Aston University, Birmingham, UK.

Barraclough, T., Henning, P., Velasquez, A., Saikia, J., & Michael, P. (2018). Detection of abnormal wear particles in hydraulic fluids via electromagnetic sensor and particle imaging technologies. *Spectro Scientific*. Retrieved June 10, 2019, from https://www.spectrosci.com/resource-center/lubrication-analysis/literature/whitepapers/white-paper-abnormal-wear-particles/

Battat, B., & Babcock, W. (2006). The effects of contamination on hydraulic fluids and systems. *Machinery and Lubrication.* Retrieved July 15, 2019, from https://www.machinerylubrication.com/Read/957/hydraulic-fluids-contamination

Bitner, D. V. (1986). *Analytical and experimental analysis of a load sensing pump*. Master's thesis, Mechanical Engineering, University of Saskatchewan, Sasksatoon, SK, Canada.

Ding, X. J., & Mei, T. X. (2009). Condition monitoring of rail vehicle suspensions based on changes in system dynamic interactions. *Vehicle System Dynamics*, 47:9, 1167-1181, doi: 10.1080/00423110802553087

Eaton Corporation. (2002). *Pump Failure Analysis*. Document No. V-PUOV-TS001-E.

Fey, C., Totten, G. E., & Sun, Y. H. (2001). Analysis of common failure modes of axial piston pumps. G. Totten, D. Wills, & D. Feldmann (Eds.), *STP1339-EB Hydraulic Failure Analysis: Fluids, Components, and System Effects* (299-317). https://doi.org/10.152]0/STP38283S

Gholizadeh, H. (2013). *Modeling and experimental evaluation of the effective bulk modulus for a mixture of hydraulic oil and air*. Doctoral thesis, Mechanical Engineering, University of Saskatchewan, Sasksatoon, SK, Canada.

Guyon, I. & Elisseeff, A. (2003). An introduction to variable and feature selection. *Journal of Machine Learning Research 3,* 1157-1182.

Hamed, M. (2016). *Characterization of the dynamics of an automotive suspension system for on-line condition monitoring.* (Publication No. 10297901) Doctoral dissertation, University of Huddersfield, UK.

Hindman, J., Burton, R., & Schoenau, G. (2002). Condition monitoring of fluid power systems: A survey. *SAE Transactions*, 111(2), 69-75.

Kavanagh, G. (1987). *The dynamic modelling of an axial piston hydraulic pump*. Master's thesis, Mechanical Engineering, University of Saskatchewan, Saskatoon, Saskatchewan. HARVEST- University of Saskatchewan's Research Archive.

Kohavi, R. (1995). A study of cross-validation and bootstrap for accuracy estimation and model selection. *Proceedings of the 14th International Joint Conference on Artificial Intelligence*, Volume 2, 1137-1143.

Latas, W., & Stojek, J. (2011). Dynamic model of axial piston swash-plate pump for diagnostics of wear in elements. *Archive of Mechanical Engineering*, *58*(2), 135.

Manring, N. D. (2005). *Hydraulic Control Systems*. Wiley, New Jersey, USA.

Manring, N. D., & Mehta, V. S. (2011). Physical limitations for the bandwidth frequency of a pressure controlled, axial-piston pump. *Journal of Dynamic Systems, Measurement, and Control*, *6*, 61005.

Mba, D., & Rao, R. B. K. N. (2006). Development of acoustic emission technology for condition monitoring and diagnosis of rotating machines: Bearings, pumps, gearboxes, engines, and rotating structures. *The Shock and Vibration Digest*, 38(1), 3-16.

Merritt, H. E. (1967). *Hydraulic Control Systems*. Wiley. New York, USA.

Neale, M. (1995). Condition monitoring. *The Tribology Handbook*, (2nd ed., D11.1-D11.4). Butterworth-Heinemann, Oxford, UK.

Schoenau, G. J., Burton, R. T., & Kavanagh, G. P. (1990). Dynamic analysis of a variable displacement pump. *Journal of Dynamic Systems, Measurement, and Control*. 112(1): 122–132. https://doi.org/10.1115/1.2894129

Schuhler, G., Jourani, A., Bouvier, S., & Perrochat, J. M. (2017). Multi technical analysis of wear mechanisms in axial piston pumps. *Journal of Physics: Conference Series*, *843*. doi: 10.1088/1742-6596/843/1/012077

Shinn, T., Carpenter, R., & Fales, R. C. (2015). State estimation techniques for axial piston pump health monitoring. Proceedings of the ASME/BATH 2015 Symposium on Fluid Power and Motion Control, Chicago, Illinois, USA. https://doi.org/10.1115/FPMC2015-9621.

Smith, E. D., Szidarovszky, F., Karnavas, W. J., & Bahill, A. T. (2008). Sensitivity analysis, a powerful system validation technique. *Open Cybernetics and Systemics Journal*, *2*, 39. doi:10.2174/1874110X00802010039

Wagner, Z. D. (2014). *Modeling, simulation, and stability of a hydraulic load-sensing pump system with investigation of a hard nonlinearity in the pump displacement control system*. Master's thesis, Mechanical Engineering, University of Missouri-Columbia, Missouri, USA.

Watton, J. (2007). Why implement condition monitoring. *Modelling, Monitoring and Diagnostic Techniques for Fluid Power Systems,* (pp. 1-5). Springer-Verlag London.

Wiens, T., & Fernandes, J. (2019). Application of data reduction techniques to dynamic condition monitoring of an axial piston pump. Proceedings of the ASME/BATH 2019 Symposium on Fluid Power and Motion Control, Long Boat Key, Florida, USA. https://doi.org/10.1115/FPMC2019-1685

Woch, M., Zieja, M., Tomaszewska, J., & Janicki, M. (2019). Statistical analysis of aviation accidents and incidents caused by failure of hydraulic systems. *MATEC Web of Conferences.* 291(2). 01005. doi:10.1051/matecconf/201929101005

Wolfe, G. (2018, March 19). Vibration points to piston pump failure. Retrieved June 5, 2018, from *Efficient Planning Magazine*. https://www.efficientplantmag.com/2018/03/vibration-points-piston-pump-failure/

Wu, D., (2003). *Modeling and experimental evaluation of a load-sensing and pressure compensated hydraulic system.* (Publication No. NQ90565) Doctoral thesis, Mechanical Engineering, University of Saskatchewan, Sasksatoon, SK, Canada.

Li, Z. (2005). *Condition monitoring of axial piston pump.* Master's thesis, Mechanical Engineering, University of Saskatchewan, Sasksatoon, SK, Canada.

# Appendix A Modelling Details

## A.1 Model Parameters

This section summarizes the parameters used to run the Simulink model as well as the solver type.

**Table A.1:** Base parameter set

| Parameter | Value | Description | Units |
|---|---|---|---|
| $c$ | 0.0375 | Control piston clearance | [mm] |
| $C_c$ | 0.61 | Contraction coefficient | |
| $C_d$ | 0.62 | Discharge coefficient | |
| $C_{cc}$ | 8.5 | Charging orifice correction constant | |
| $C_{dc}$ | 3.5 | Discharging orifice correction constant | |
| $cp_{guide}$ | 16.87 | Control piston guide diameter | [mm] |
| $d_{ls}$ | 4.5 | Load sense spool damping | $[\mathrm{Nm^{-1}s^{-1}}]$ |
| $F_{bias}$ | 100 | Bias spring preload | [N] |
| $f_{gain}$ | 0.0018 | Flow gain of pump | $[\mathrm{m^3s^{-1}rad^{-1}}]$ |
| $K_{ag}$ | 1000 | Swashplate assembly damping term | $[\mathrm{Nm^{-1}s^{-1}}]$ |
| $k_{bias}$ | 12470 | Bias spring constant | $[\mathrm{Nm^{-1}}]$ |
| $k_{ls}$ | 47306 | Load sense spring constant | $[\mathrm{Nm^{-1}}]$ |
| $L$ | 55 | Moment arm of bias and control pistons | [mm] |
| $LP_{max}$ | 33.9 | Maximum control piston leakage path length | [mm] |
| $LP_{min}$ | 12.7 | Minimum control piston leakage path length | [mm] |
| $m_{bias}$ | 72 | Mass of bias piston | [g] |
| $m_{cp}$ | 51.3 | Mass of control piston | [g] |
| $m_{ls}$ | 9.22 | Mass of load sense spool | [g] |
| $m_p$ | 34.6 | Mass of single pumping piston | [g] |
| $N$ | 9 | Number of pumping pistons | |

| | | | |
|---|---|---|---|
| $O_s$ | 1.1 | Measured offset of load sense spool from end | [mm] |
| $O_l$ | 0.12 | Measured overlap of load sense spool | [mm] |
| $r$ | 28 | Piston pitch radius | [mm] |
| $r_{cpo}$ | 0.53 | Radius of control piston damping orifice | [mm] |
| $r_{ls}$ | 3.5 | Radius of load sense spool | [mm] |
| $r_{pls}$ | 2.1 | Radius of charging/discharging orifice | [mm] |
| $r_{pso}$ | 1.9 | Radius of charging orifice | [mm] |
| $T_{celc}$ | 50 | Temperature | [°C] |
| $VB_{load}$ | 0.09 | Load volume | [L] |
| $VB_{pump}$ | 1.1 | Pump volume | [L] |
| $V_{cp}$ | 2 | Nominal control piston volume | $[mm^3]$ |
| $V_d$ | 18 | Pump theoretical displacement | [cc] |
| $Y_{max}$ | 18 | Maximum control piston travel | [mm] |
| $\alpha$ | 1.204 | Jet angle for flow forces | [rad] |
| $\beta_{cp}$ | 1.75 | Control piston volume bulk modulus | [GPa] |
| $\beta_l$ | 1.4 | Load volume bulk modulus | [GPa] |
| $\beta_{ps}$ | 1 | Pump volume bulk modulus | [GPa] |
| $\gamma$ | 0.0582 | Pressure carryover angle | [rad] |
| $\mu_k$ | 0.3897 | Kinematic viscosity of hydraulic fluid | $[m^2s^{-1}]$ |
| $\omega$ | 1740 | Pump rotational speed | [rpm] |
| $\rho$ | 882 | Density of hydraulic fluid | $[Kgm^{-3}]$ |

Solver: ode23tb (stiff/TR-BDF2)

## A.2 Orifice Correction Constants

Flow in the charging and discharging galleries of the compensator was initially assumed turbulent. Upon closer inspection of the experimental data, the swashplate rotational velocity was significantly higher than modelled. To investigate the charging and discharging flow within

the compensator, it was decided to approximate the control piston velocity with swashplate angular velocity and derive an estimate of the actual flow within the control piston. The experimental data used in this analysis are the pump data collected during a step increase in load pressure. The input to the system is a decrease in the simulated load orifice area. As this area decreases, the load pressure spikes. When the load pressure spikes, the immediate effect happens first at the load sense spool. The load pressure will cause the load sense spool to displace in the negative $x_{ls}$ direction (refer to Section 2.4) causing the discharging orifice path to become active. With no input pressure to the control piston, it is forced by the bias spring and bias piston to a position of higher flow. As the control piston moves to a higher flow position, the pump flow will increase. The increase in pump flow is transient event. As a result of a momentary increase in flow, the pressure within the pump volume increases to a new steady state pump discharge pressure. The pump pressure spikes and causes the load sense spool to move in the positive $x_{ls}$ direction resulting in the charging orifice path to become active. When this path activates, flow will supply the control piston volume and pump pressure will cause the control piston to reach its original position. In summary, during this transient event, the charging and discharging paths of the compensator are active. These events manifest as the rise and fall of the swashplate dynamics as depicted in Figure 6.1. Using the swashplates angular velocity by differentiating the position measurement, and calculating the approximate flow using the control piston area, Figure 6.2 shows the discharging and charging flow through the compensator.

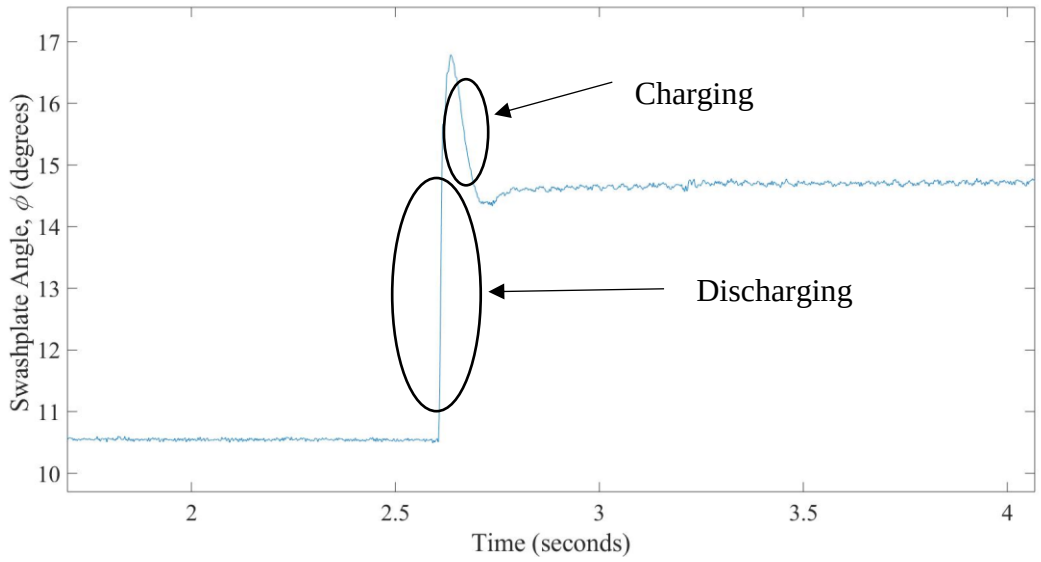


**Figure 6.1**: Experimental swashplate dynamic response

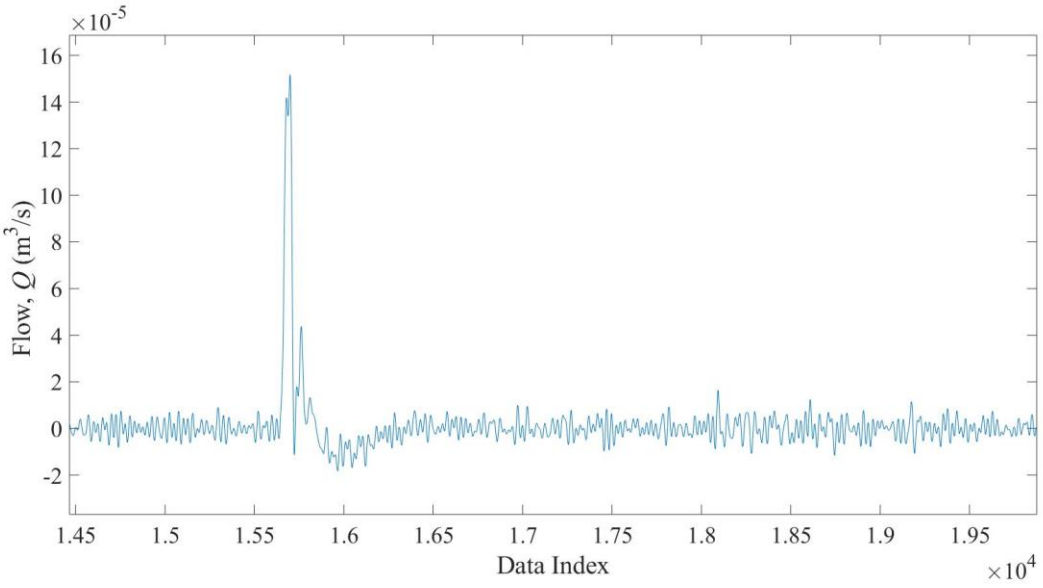


**Figure 6.2:** Estimated flow within the control piston

The first very large peak represents the maximum discharging flow, and the smaller, noisy peak represents the maximum charging flow occurring during a dynamic response. The experimental flow from this analyses is significantly higher than the flow using the detailed compensator model. The control piston pressures were very similar. It is believed that the flow

may be in the laminar regime and could be higher than the turbulent orifice approximation would predict. The compensator galleries are small and long and this may be a reason to approximate the flow with a short tube orifice model. For simplicity, correction factors were applied to the area gradients for the cumulative charging and discharging orifices. The correction factors are simply gains and were also used in tuning the model validation. The correction factors have a notable effect on the total time of the response. In addition, by incorporating a gain to the resultant charging or discharging flow, the area gradient is preserved, an important property especially within small spool movements.

## A.3 Model Validation Procedure

The procedure to validate the dynamic model utilizes the sensitivity results presented in Section 2.5. As the results show, some parameters have little effect on the dynamic or steady state results. Parameters with large influence were selected. Each parameter was varied through a Monte Carlo approach and an RMS error was calculated between the response variations and experimental data. The parameter was then determined for which value resulted in the lowest RMS error. Some parameters were highly sensitive and a two-dimensional Monte Carlo method was used with variations in both parameters. These parameters were the pump and load volume as well as the three bulk moduli. This iterative process derived the set of base parameters given in Table A.1.

## A.4 Details of Modelling for Linearization Procedure

The parameter set for linearization is the same as developed for model validation, however, one parameter adjustment was necessary. Discussed in Section 2.4 is the piecewise model that determines the orifice area for charging and discharging flow in the compensator. For linearization, the charging and discharging area cannot be a function of both positive and negative travel. The dynamic model has incorporated leakage out of the control piston. For linearization, this leakage was increased until the load sense spool operates in the positive spool direction. The charging and discharging area in the positive load sense spool regime is a complex function, see Section 2.4. This area was linearized for small spool movements.

# Appendix B Wear Testing

## B.1 Pump Wear Test Procedure

The section summarizes the procedure used to purposely wear three pumps. In order to assess the effectiveness of the predictive algorithm designed in Chapter 4, worn pumps are required. Since no pumps were available, it was decided to perform wear tests and produce three worn pumps. The general objectives of the wear testing procedure are:

- Wear 3 pumps to various noticeable volumetric efficiency levels, determined by changes in case drain leakage flow
- To avoid catastrophic failure, pumps need to be operational for dynamic and steady state tests
- Obtain three realistically worn pumps

Acquired for the purpose of this research were three Parker P1 Load Sensing Pressure Compensated Axial Piston Pumps in new condition. There exists some research on accelerated wear testing of Hydraulic Components. Atkinson (1979) at Oklahoma State University performed extensive accelerated wear tests on fixed displacement axial piston pumps to study the effects of particle contamination on pump wear. He presents valuable pump performance plots that show the decrease in volumetric efficiency of a pump over operating time subject to varying degrees of contamination. The contamination used for the tests was Air Cleaner Fine Test Dust. These data acted as a rough guide in determining how long and at what contamination concentration would result in a certain volumetric efficiency. Predicting flow based off of this literature has the potential for error since there are many differences, specifically in equipment. The pumps used in this research are PCLS axial piston pumps and the pumps used by Atkinson were fixed displacement. As previously mentioned, this literature acts as a starting point. The pump circuit configuration as illustrated in Figure B.1 was used for the wear tests.

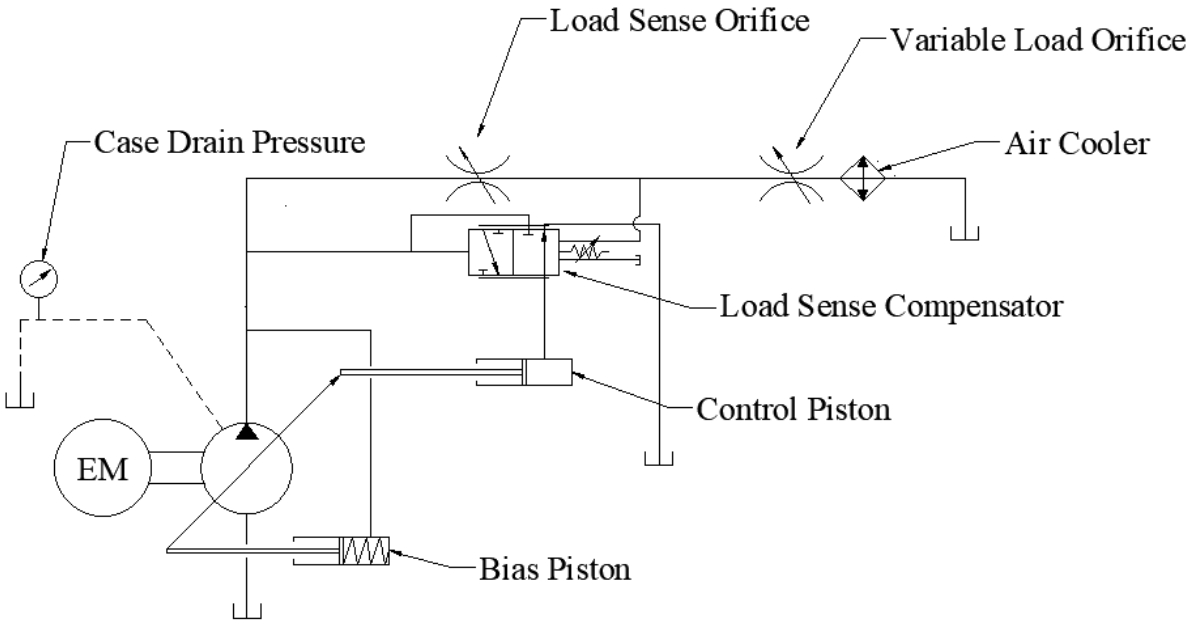


**Figure B.1**: Test stand for forced wear experiments

The hydraulic schematic of the accelerated wear testing circuit appears in Figure B.1. After the first pump wear test for pump 165, the circuit was adapted to include the pressure transducer in Figure B.1, measuring case drain pressure. The intent was to predict case drain leakage by case estimating the orifice constant for the leakage line. The PCLS pump was installed to be driven, through a flexible coupling by an electric motor, EM 1. Before any pump tests were performed, a shaft alignment procedure was performed to ensure good shaft alignment. Fey et al. (2001) describe the importance of proper shaft alignment by explaining that it can cause premature wearing of bearings and may result in significant vibration. The circuit was assembled with clean components. The flow control and simulated load pressure valve were only used to demand random variations in pump flow and pressure. These valves were disposable. Atkinson (1979) suggests that the reservoir should be tapered to ensure all contamination is drawn in by the pump inlet line. Unfortunately, a tapered reservoir was unavailable. Although prone to damage caused by abrasives, rubber hoses were used to connect all circuit components. These hoses were disposed of after their use; they were deemed unsafe due to potential internal structure compromise from abrasive exposure.

The wear test procedure was iterative. The first pump wear experiment was designed around the results from Atkinson (1979), volumetric flow as a function of time exposed to contaminant.

## Experimental Steps for First Pump

- Clean pump was installed onto electrically driven pump stand
- System was brought to operating temperature using high load pressure
- Initial contamination level was 9 g ACFTD to 23 l of hydraulic oil (Nuto 68)
- Contamination was thoroughly mixed with small sample of oil using blender
- During operation, contaminant was introduced into the reservoir slowly
- System timer was started
- Random variations in load and pump pressure were made (but not recorded)
- Upon reaching 60 min, the stand was promptly shut down
- Pump removed for thorough disassembly and inspection

## Constants

Temperature was attempted to be held constant (air cooler) at a target 50 ºC in order to accurately predict case drain flow through constant fluid viscosity.

## Refinement

The worn pump was cleaned and assembled and installed on the fully instrumented setup. The pump performance was measured and documented. Since the fully instrumented setup contains case drain flow measuring potential, a linear relationship was derived from the case drain pressure and case drain flow. This relationship was used for wearing of the remaining two pumps. The same procedure was followed as the first pump, however, using the linear relationship between case drain pressure and flow, the pumps were run to a target condition. This condition represented the case drain flow as determined by case drain pressure.

The wear testing produced three worn pumps that were then used for assessing the leakage predicting potential of the designed algorithm. Performance testing was done on the

three pumps on a fully instrumented test stand.  These tests are described in the following sections.

# Appendix C Performance Evaluation

## C.1 Steady State Performance Testing After Wear

The worn pumps were installed on the fully instrumented setup, Figure C.1, and were subject to various performance tests. The first test is a constant flow, increasing pressure, steady state performance test and its characteristics are outlined below.

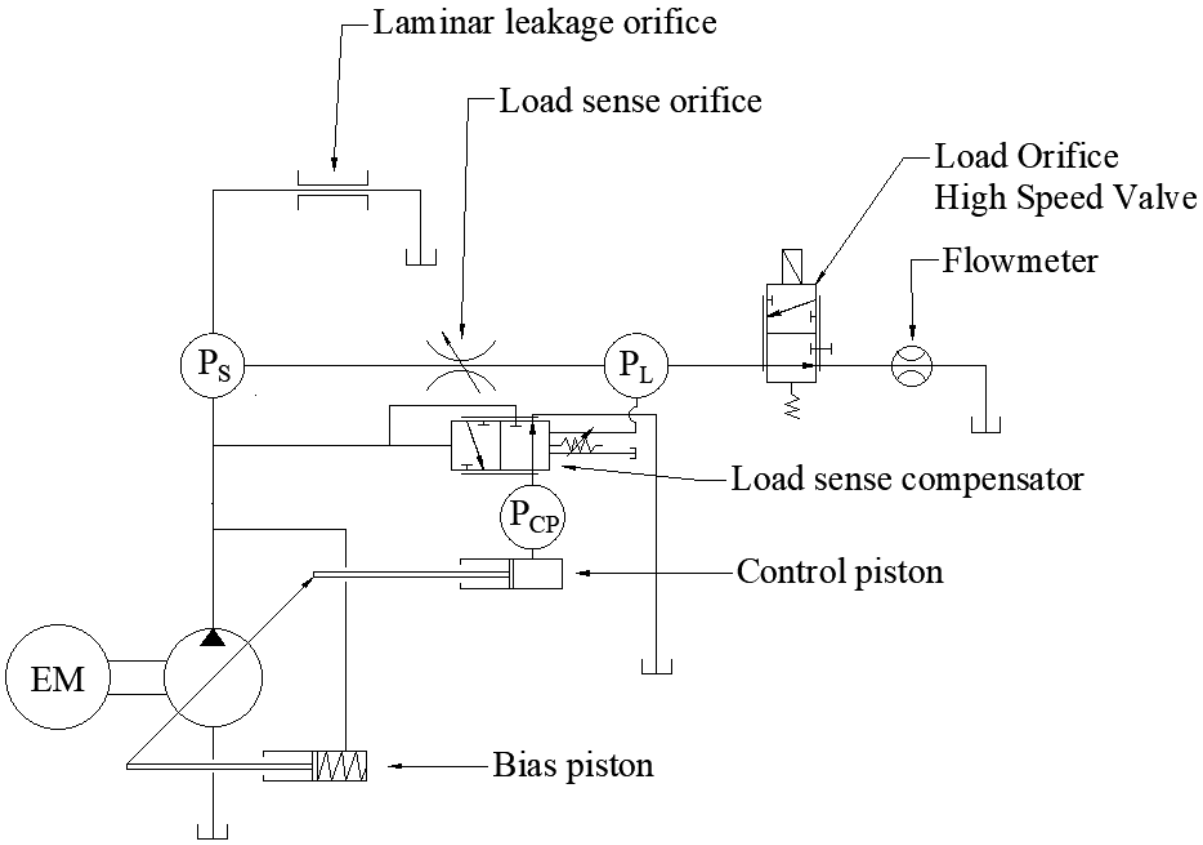


**Figure C.1:** Test stand circuit for data acquisition

**Objectives**

- Capture large amount of sensor information of pumps operating at steady state
- Determine trends in data

**Purpose**

- Derive leakage parameters for model validation
- Characterize pump leakage
- Investigate relationship with temperature
- Assess repeatability

**Constants**

- Temperature was attempted to be held constant (air and water cooler) at a target 50 degrees Celcius
- Flow control orifice was fixed (locked with set screw for all tests)

**Experiment logic**

- 10 second samples enough to average all pressure and temperature data
- 10 seconds enough time to log flowmeter pulses so that enough pulses occur to calculate the rotational frequency
- 1000 – 2800 [psi] is a typical operating range
- Required air cooler and water cooler to reduce temperature fluctuations
- Load pressure did not need to be precise since plotting anyways

**Experiment 1 procedure**

- Pumps were cleaned using non corrosive solvent and reassembled with clean, compatible hydraulic oil from the system reservoir
- Case drain was filled prior to start-up
- Pump was turned by hand to prime system and prevent fluid shock to flowmeters
- Load valve was fully open prior to start up to prevent high pressure upon start up
- Once operational, system was checked for leaks
- System was operated at a random wide range of flow and pressure to bleed any air from the pump and system and to allow air to dissipate in reservoir
- System temperature was increased to operating temperature by increasing load pressure

- Once system operating temperature was achieved, the load pressure was set to 1000 [psi] and a 10 s data capture was logged
- The load pressure was then increased incrementally by 200 [psi] 10 times to a final pressure of 2800 [psi] for the last logged data capture
- Once the last log was attained, the pump was set to a no load condition where it could cool down to start of test temperature
- It was noted that the temperature did increase with pressure as expected

The following are plots of the pumps case drain leakage as pump pressure increases including temperature for the three load sensing axial piston pumps and for the specified operating conditions. For these steady state leakage tests, the pumps were tested at a constant load flow. This was approximately half of the total pump flow. Figure C.2 - Figure C**.4** plot the pump leakage as a function of pressure and temperature.

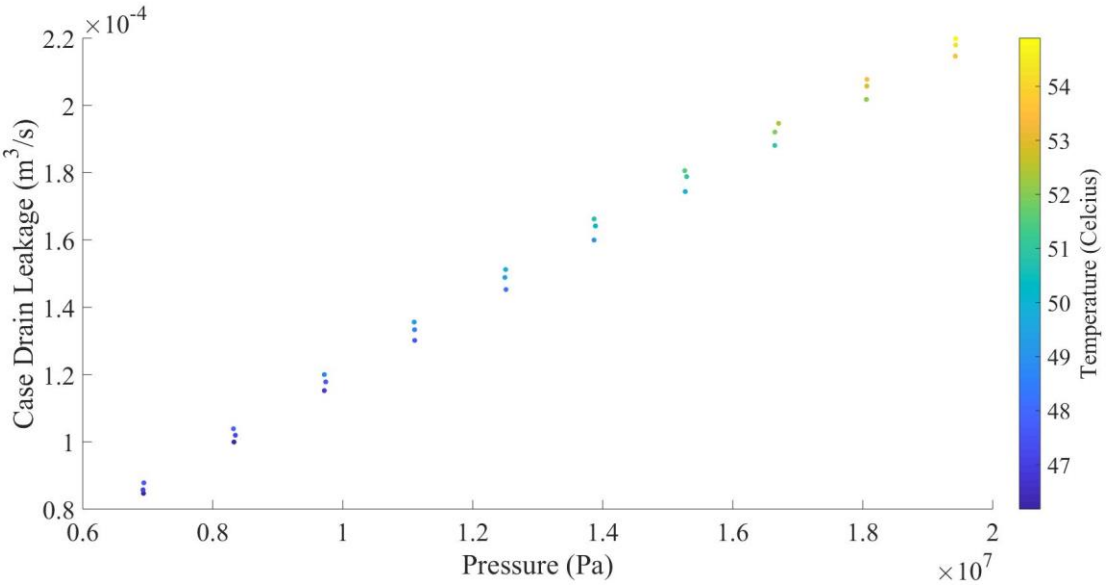


**Figure C.2:** Pump 165 leakage flow relationship to increasing pump pressure

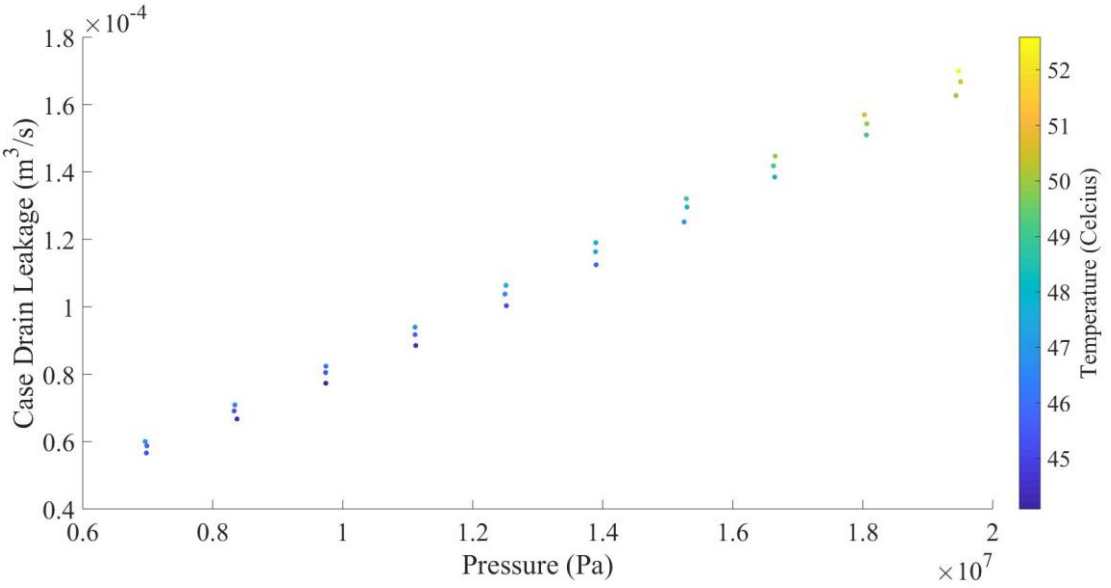


**Figure C.3:** Pump 167, leakage flow relationship to increasing pump pressure

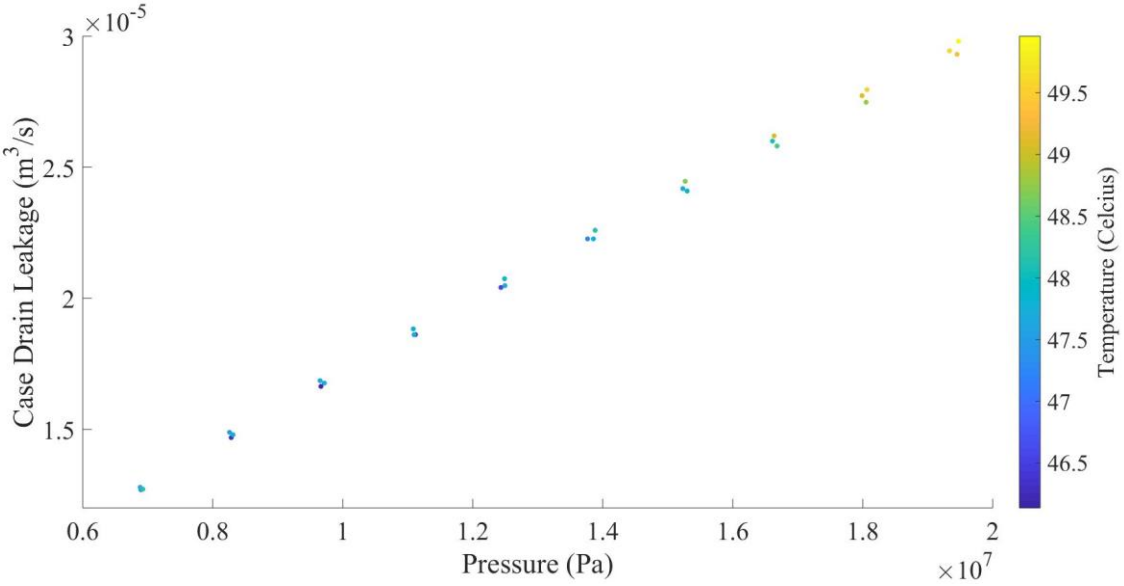


**Figure C.4:** Pump 172, leakage flow relationship to increasing pump pressure

Figure C.2 - Figure C**.4** show linear behavior. That is, the pump leakage behaves fairly linear with changes in pressure, however, the case drain flow temperature varies upwards of 7 ºC. The case drain flow leakage temperature is measured at the outlet of the case drain. Attempting to update the accuracy of these plots by correcting for viscosity changes only destroys this linear relationship. Because the case drain fluid temperature is measured at the outlet, it is inaccurate to relate this to the fluids temperature before and through the laminar

orifice. This a complex relationship that is outside the scope of this research. The main purpose of these plots is to investigate any interesting features across the pumps and do derive an expression to represent the leakage with respect to the pumps pressure.

In performing a regression to find the slope and intercept to model the leakage of each pump, it was observed that the last few data points diverge as temperature increases. Nonetheless, a linear regression was performed and the leakage parameter $R_{slope}$ , and $y_{int}$ were determined and presented in Table C.1.

**Table C.1:** Experimentally derived leakage parameters

| **Serial** | $\boldsymbol{R_{slope}}$ $[m^3 s^{-1}\ Pa^{-1}]$ | $\boldsymbol{y_{int}}$ $[m^3 s^{-1}]$ | **Classification** |
|---|---|---|---|
| **Pump 165** | $1.06e^{-11}$ | $1.47e^{-5}$ | End of life |
| **Pump 167** | $8.75e^{-12}$ | $-4.58e^{-6}$ | Mid life |
| **Pump 172** | $1.33e^{-12}$ | $3.78e^{-6}$ | Slight wear |
| **Median of range** | $5.97e^{-12}$ | $5.06e^{-6}$ | |

Table C.1 organizes the regression weights for the pressure, leakage plots. Initially it was decided to use an average of the y intercept. Practically, the y intercept is the pump leakage with no pressure. Ideally, this would be zero, however, there exists some intercept with the linear fit. This is more likely due to measurement error and fitting optimization then to there actually existing pump leakage at no pump pressure. It was decided to take a median of the intercept value and use this as a constant for all pumps. The slopes of the plots represent a laminar leakage conductance denoted $R_{slope}$. This is an input to the nonlinear dynamic model outlined in Chapter 2 as well as the parameter attempted to be predicted in this research.

## C.2 Dynamic Testing on Worn Pumps

Chapter 3 outlines the optimal operating point to perform the testing, however, this gives no information about step size as it is a local analysis.

From the design analysis in Chapter 3 it was determined that the best operating point that gives the best resolution to a small (linear) step in load pressure is high flow and high pressure. It is still unknown what step size gives the best resolution of leakage, that is, what size step in load pressure results in the largest dynamic change for varying leakage. It was decided to conduct two types of dynamic tests with the worn pumps. The first was large step dynamic testing. This involves exciting the pump with a large step change in simulated load pressure and capturing the dynamic response as the pump compensates. The second was small, incremental steps in load pressure.

As discussed in Chapter 3, there are two operating conditions that must be selected, flow and pressure. As initial experimentation was conducted, in order to give a large step in load pressure, the pump flow could not be set too high or else the pump swashplate would reach its end stop. The best compromise was the maximum possible flow without saturation. This was roughly half the total theoretical pump flow and was determined iteratively during pump testing.

## C.3 Large Step Load Pressure Dynamic Testing on Worn pumps

**Objectives**

- Capture dynamic response with large step input to load pressure
- Capture dynamic response with small incremental increases in load pressure

**Purpose**

- Using Large step data, determine PCA effectiveness
- Using small step data, determine effectiveness of PCA at range of operating points

**Constants**

- Temperature was attempted to be held constant (air and water cooler) at a target 50 ºC

- Flow control orifice was fixed (locked with set screw for all tests)

**Experiment logic**

- 10s samples enough to average all pressure and temperature data
- 10s  enough time to log flowmeter pulses so that enough pulses occur to calculate the rotational frequency
- 1000 – 2800 [psi] is a typical operating range
- Required air cooler and water cooler to reduce temperature fluctuations
- Trial and error procedure to determine flow setting so that dynamic response of all sensor did not saturate (swashplate does not reach end of travel)

**Experiment procedure**

- Pumps were cleaned using non corrosive solvent and reassembled with clean, compatible hydraulic oil from the system reservoir
- Case drain was filled prior to start-up
- Pump was turned by hand to prime system and prevent fluid shock to flowmeters
- Load valve was fully open prior to start up to prevent high pressure upon start up
- Once operational, system was checked for leaks
- System was operated at a random wide range of flow and pressure to bleed any air from the pump and system and to allow air to dissipate in reservoir
- System temperature was increased to operating temperature by increasing load pressure
- Step input generator was programmed to give a large scale alternating step and small scale incremental steps
- The step input to the high speed valve occurs as a predetermined voltage waveform and is the same each time
- Recordings were taken for three trials of one full cycle of the small steps and 60s of alternating large step input

The pressure response and swashplate angle experimental data is shown for each pump in Figure C.5 - Figure C**.10**.

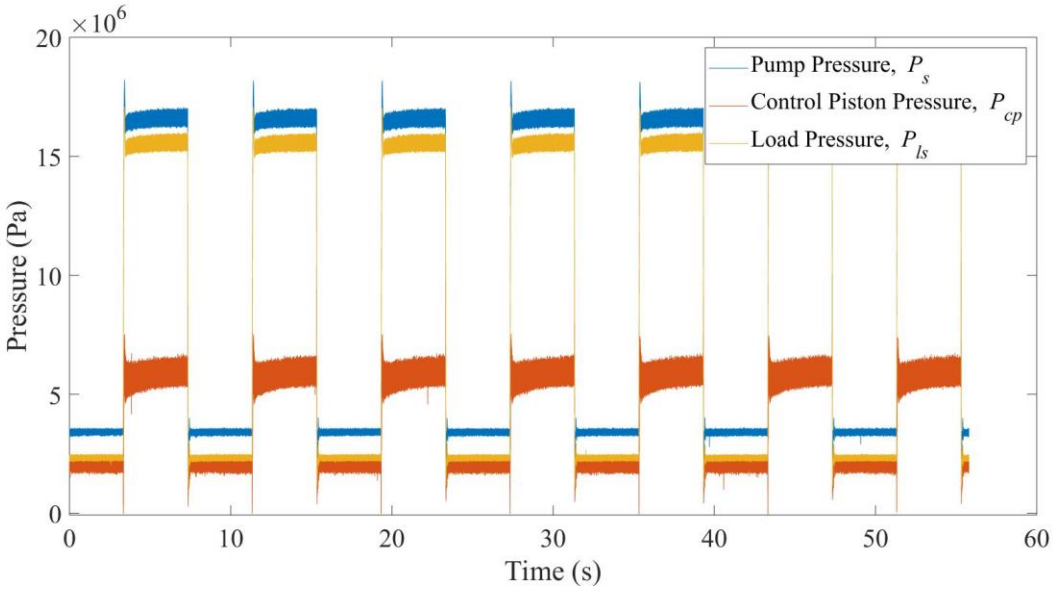


**Figure C.5:** Pump 165 large step pressure response data

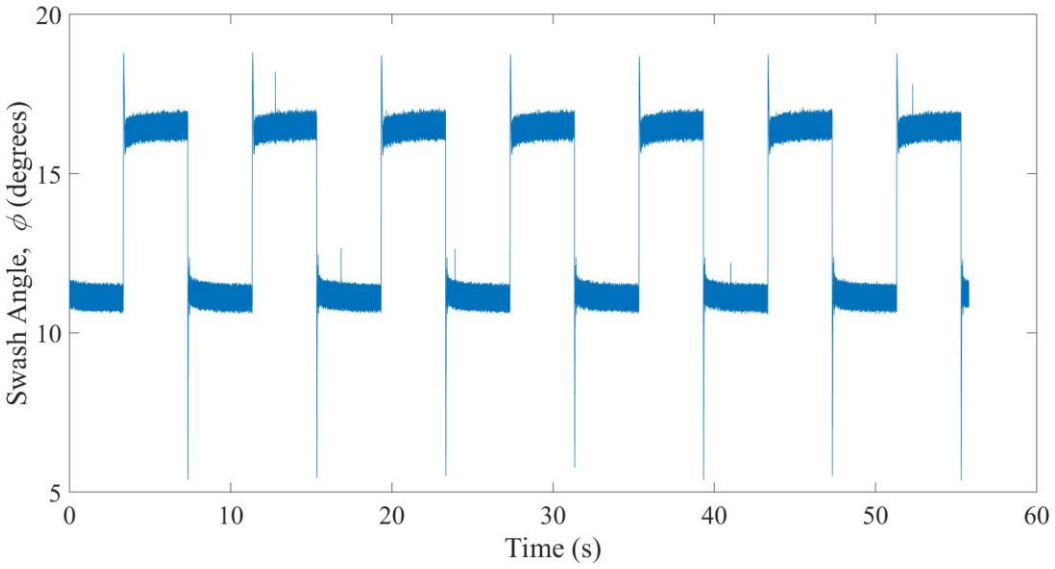


**Figure C.6:** Pump 165 large step swash angle response data

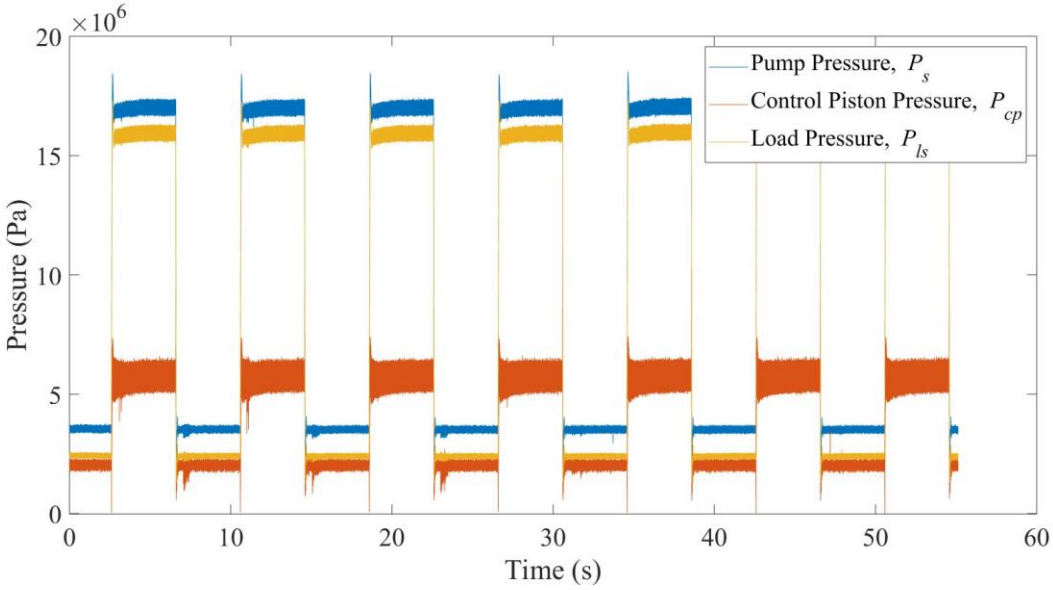


**Figure C.7:** Pump 167 large step pressure response data

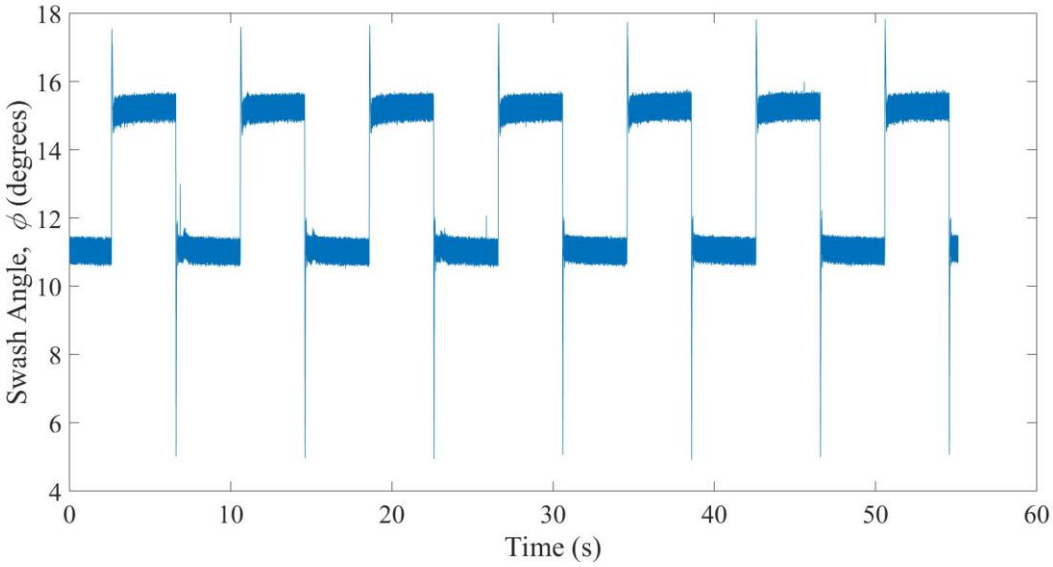


**Figure C.8:** Pump 167 large step swash angle response data

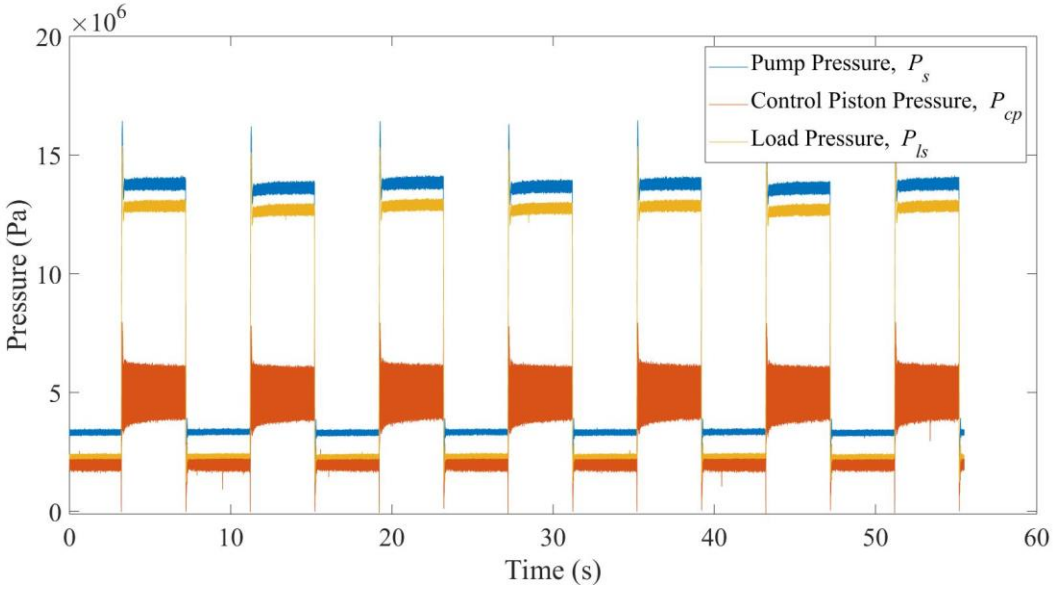


**Figure C.9:** Pump 172 large step pressure response data

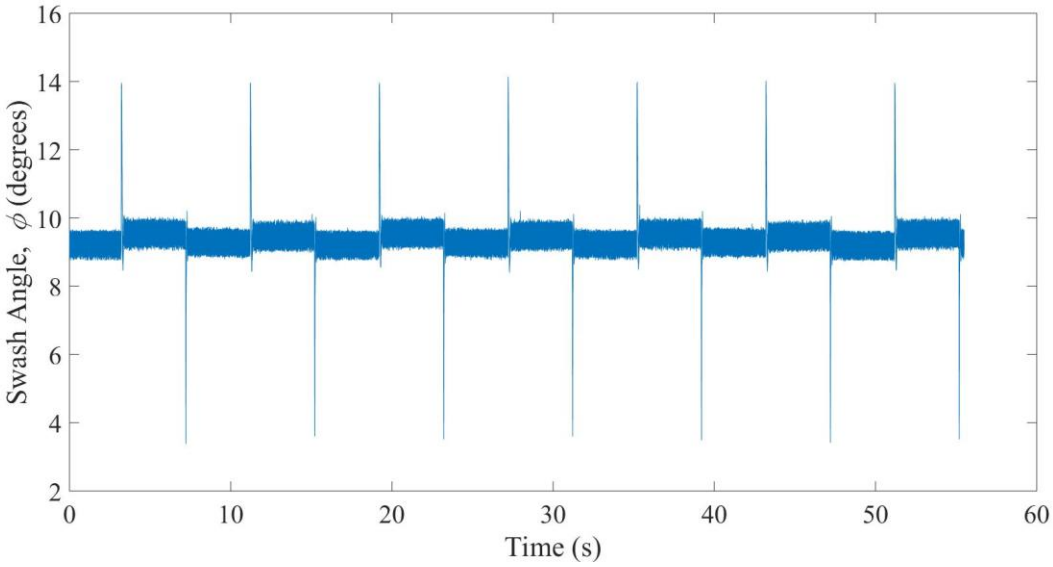


**Figure C.10:** Pump 172 large step swash angle response data

## C.4 Small Step Load pressure Dynamic Testing on Worn pumps

This test was similar to the large step testing, however, in this experiment a series of small steps in load pressure were used to excite the pump. The procedure follows that of large

step testing.  Figure C.11 - Figure C**.16** are plots of the small step excitation experimental response data.

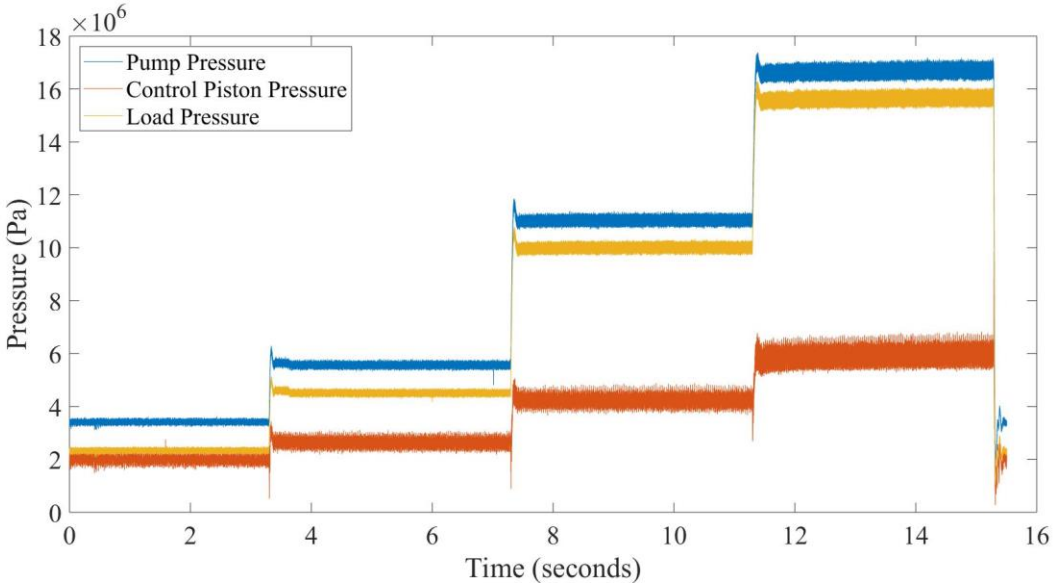


**Figure C.11:** Pump 165 small step pressure response data

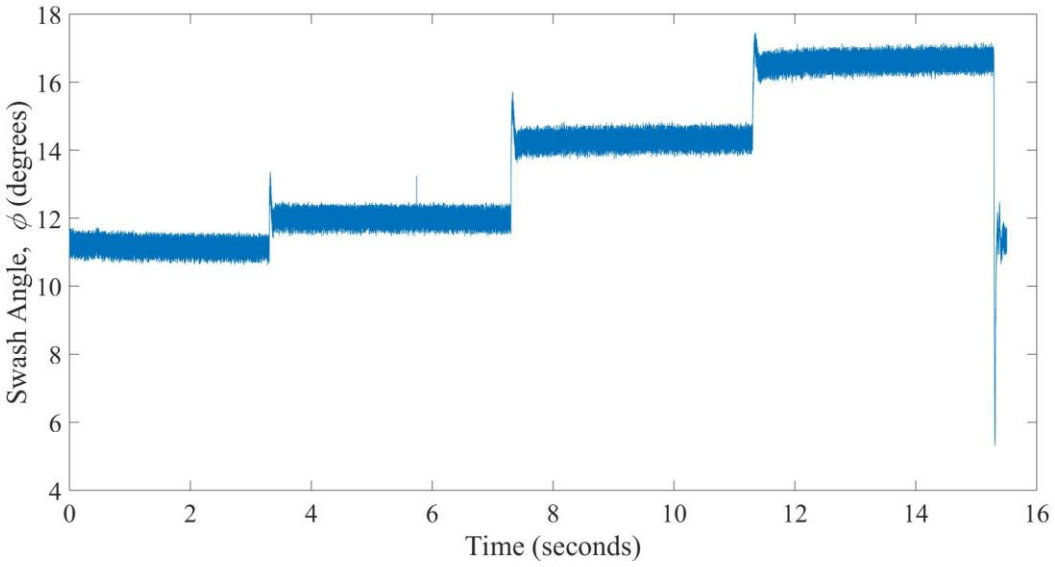


**Figure C.12:** Pump 165 small step swash angle response data

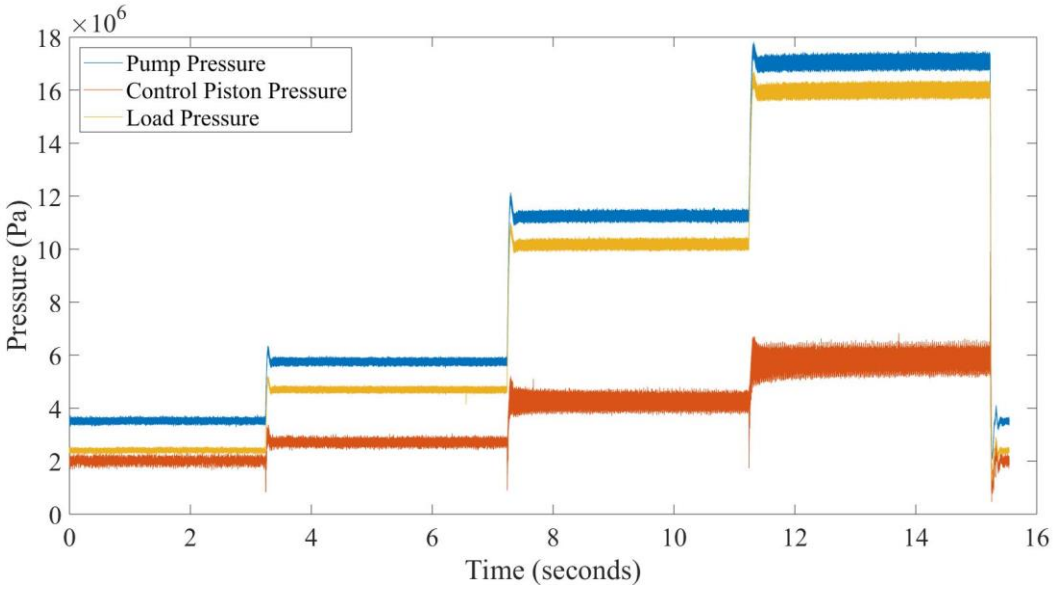


**Figure C.13:** Pump 167 small step pressure response data

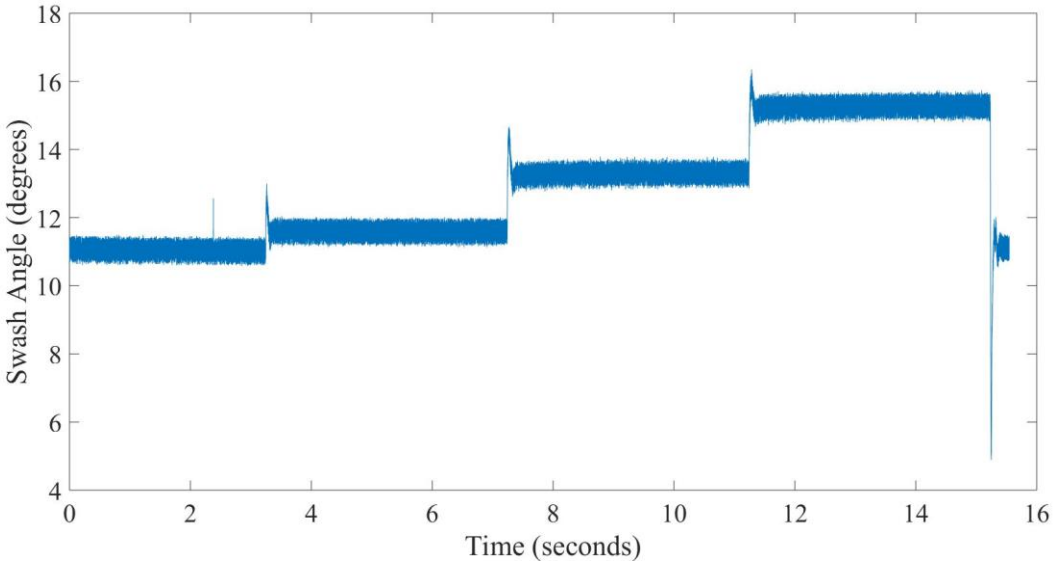


**Figure C.14:** Pump 167 small step swash angle response data

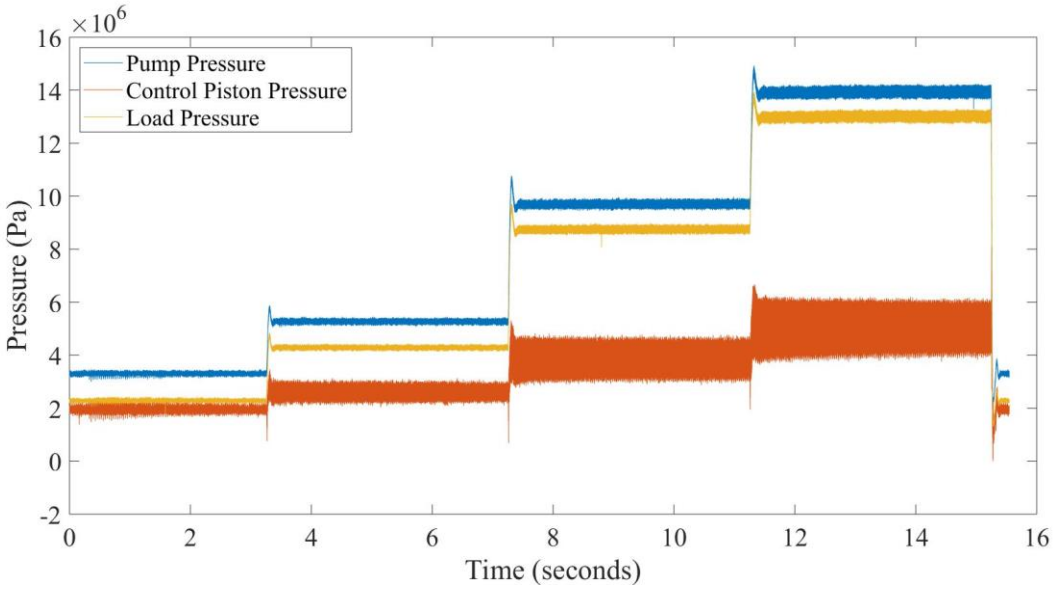


**Figure C.15:** Pump 172 small step pressure response data

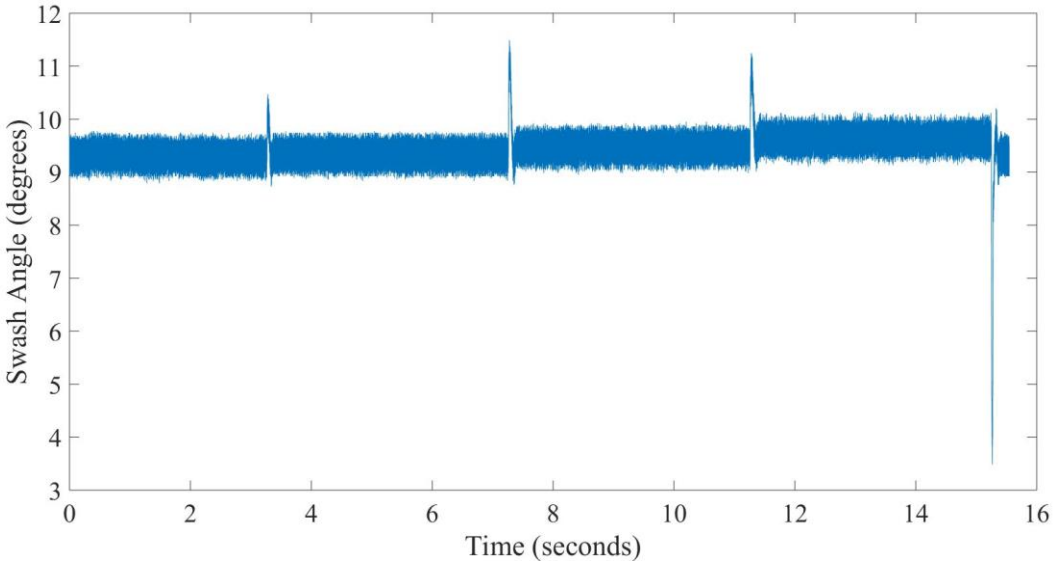


**Figure C.16:** Pump 172 small step swash angle response data

## C.5 Analysis of Steady State Differences in Pump Discharge Pressure

The experimental results show noticeable differences in steady state pressure, control piston pressure, and swashplate angle. The swashplate angle differences are expected since the pumps have different leakage characteristic because of the wear testing. This is also true for differences in control piston pressure since, for a different swashplate angle, the control piston will require different steady state pressures due to the bias spring forces changing. The load sense orifice, responsible for setting the target flow was fixed mechanically, however the orifice that controls the simulated load pressure is variable. The load orifice area is a result of the translation of a high speed valve. Since the valve was given the same voltage, it would be expected that it comes to the same position for each experiment thus resulting in the same load orifice area and load pressure for each test. To facilitate a thorough investigation into why the pump discharge pressures are different, Table C.2 summarizes important flow and pressure data.

**Table C.2:** Summary of flow and margin data for all pumps

| **Pump** | **Condition** | **Load flow, $Q_l$, ($m^3/s$)** | **Margin, $P_m$, (MPa)** |
|---|---|---|---|
| Pump 165 | Before step | 2.95E-04 | 1.09 |
| | After step | 2.96E-04 | 1.07 |
| Pump 167 | Before step | 2.98E-04 | 1.12 |
| | After step | 3.00E-04 | 1.11 |
| Pump 172 | Before step | 2.82E-04 | 1.03 |
| | After step | 2.71E-04 | 9.67 |

Upon closer inspection, the measured margin pressure is slightly different for each pump. This is reasonable, however, it appears that the *difference* in margin pressure before and after the step is significantly more for pump 172, the pump with the least amount of wear. The margin pressure for Pumps 165 and 167 decreases slightly after the step in load pressure. This phenomenon was also noticed by Wagner (2014). The margin pressure is a result of the margin spring preload and spring constant which is not expected to change during such short operating.

It may be concluded that the difference in margin at high and low pressure could be a result of two changes. The first is the discharge coefficient of the orifices. This could change

based on flow type. The other is some change in load sense spool valve characteristics. This could include differences in flow forces as a result of change in spool overlap due to wear.

Further investigation is outside the scope of this research but this phenomenon has been realized and taken into consideration in performing PCA to predict pump leakage.

## C.6 Determination of Orifice Constants for PCA Training Data

The orifice constants $K_{load}$ and $K_{ls}$ are inputs to the dynamic model. $K_{load}$ acts to set the target load pressure and the pump pressure will maintain margin pressure above the load pressure. $K_{ls}$ sets the pump flow. Section Appendix A describes a large difference in both orifice constants due to a change in margin pressure. This sections describes how the orifice constants are selected to generally represent the response of all three pumps and how they are used to generate the training data for the experimental evaluation of PCA.

Table C.3 summarizes the load orifice constants determined from the experimental pressure and flow data and using the turbulent orifice equation.

**Table C.3:** Estimated orifice constants from experimental data

| | $K_{load}$ **before step** | $K_{load}$ **after step** |
|---|---|---|
| **Pump 165** | 4.055E-06 | 1.571E-06 |
| **Pump 167** | 4.027E-06 | 1.572E-06 |
| **Pump 172** | 3.823E-06 | 1.624E-06 |
| **Median of range** | 3.939E-06 | 1.598E-06 |

The median of the range of $K_{load}$ values calculated from the experimental data was used to create the training dataset. $K_{ls}$ was determined by assuming constant values for the margin pressure and target flow, even though experimental data shows that these were off to some degree. This was decided because in practice measuring flow and margin may be tedious and the addition of noise to the training dataset may account for slight variations in experimental and simulated data.

**Table C.4:** Parameter used to determine the load sense orifice constant

| | |
|---|---|
| **Margin, $P_m$** | 1 MPa |
| **Target Load Flow, $Q_{load}$** | 2.90 E-4 $m^3/s$ |
| $K_{ls}$ | 6.09 E-06 |

Figure C.17 - Figure C**.22** illustrate the new model 'fit' using the orifice constants and margin pressure from Table C.3 and Table C.4.

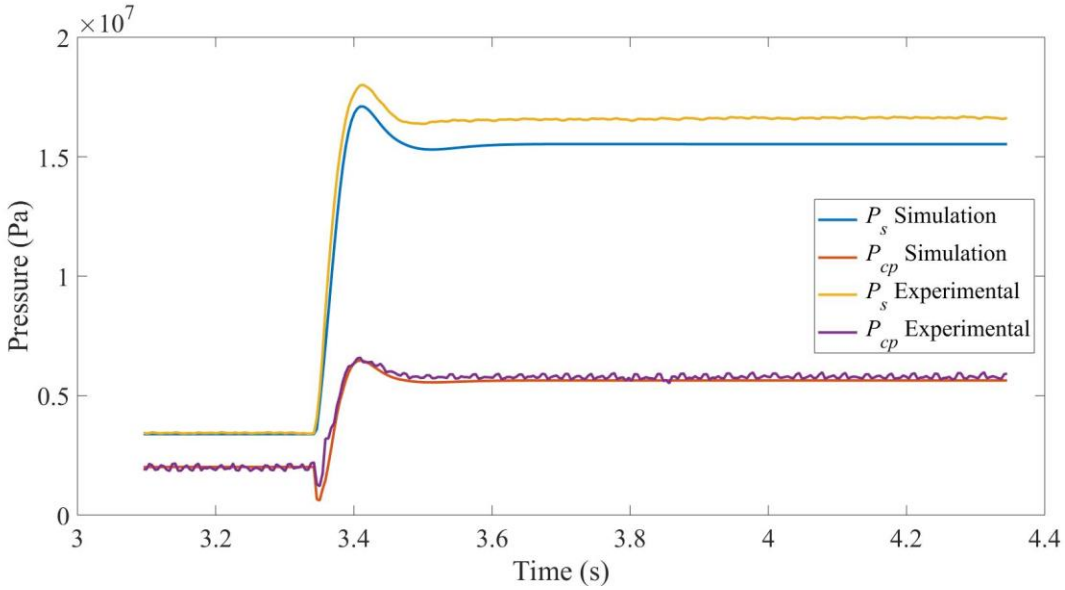


**Figure C.17:** Model fit for pump 165 pressure dynamics using median of orifice constant range

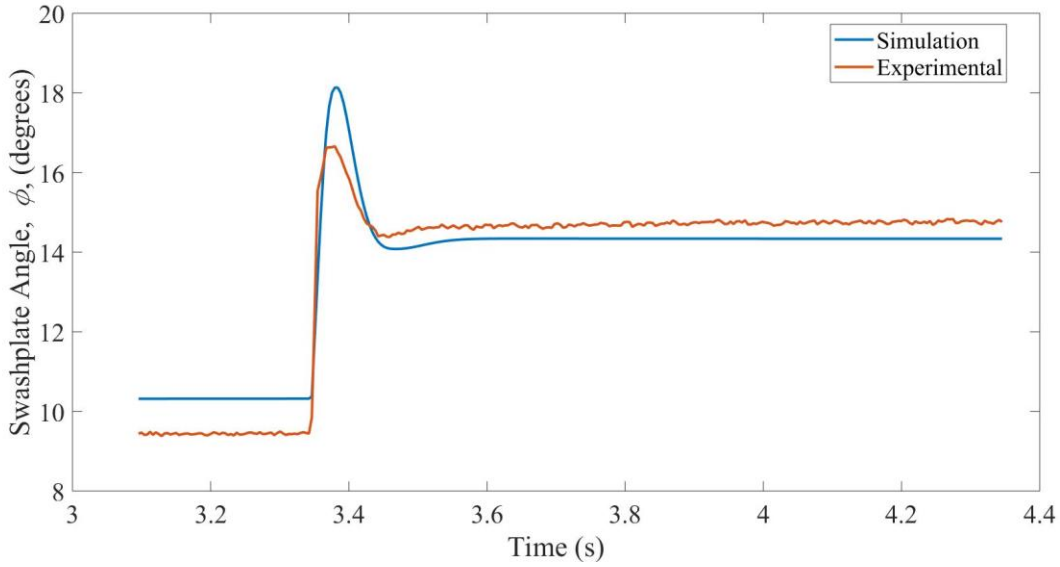


**Figure C.18:** Model fit for pump 165 swashplate dynamics using median of orifice constant range

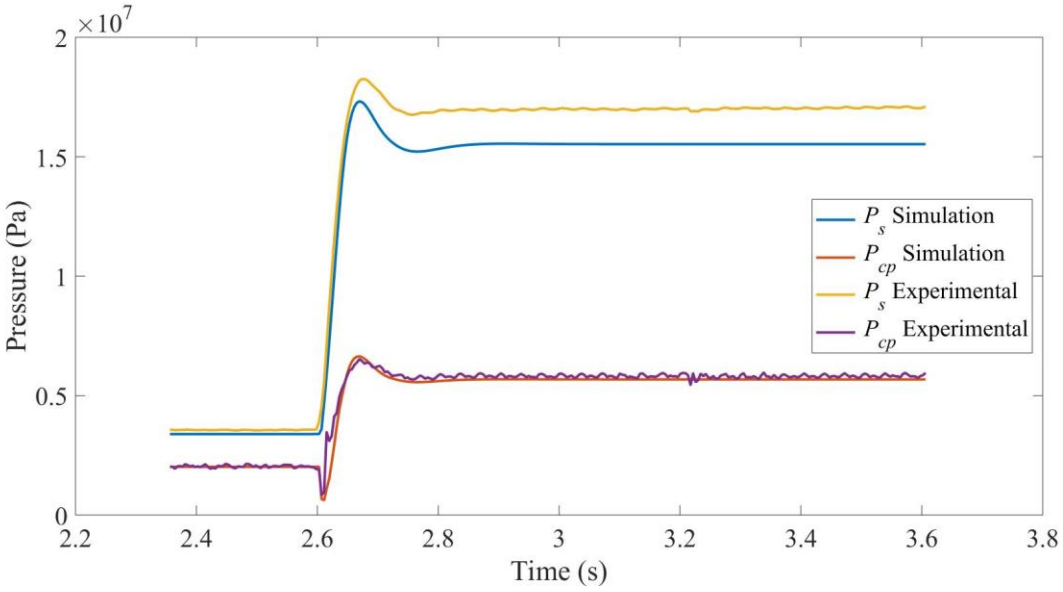


**Figure C.19:** Model fit for pump 167 pressure dynamics using median of orifice constant range

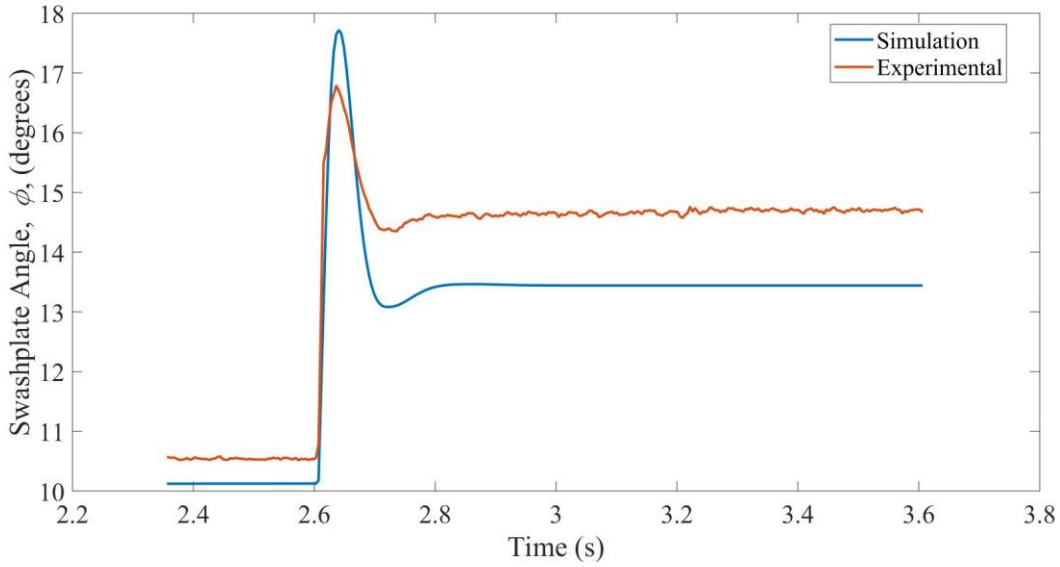


**Figure C.20:** Model fit for pump 167 swashplate dynamics using median of orifice constant range

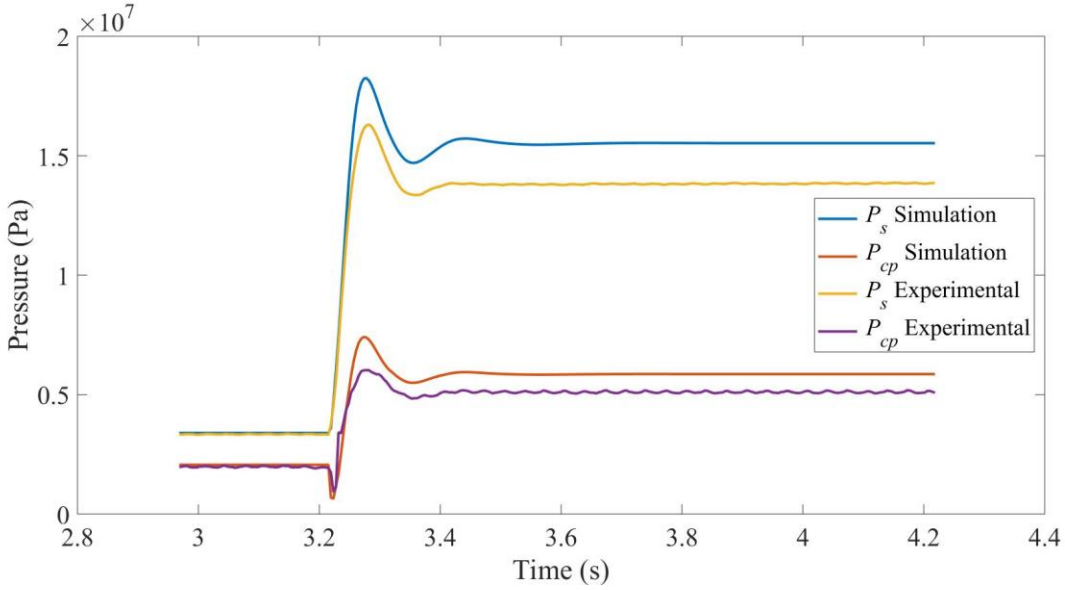


**Figure C.21:** Model fit for pump 172 pressure dynamics using median of orifice constant range

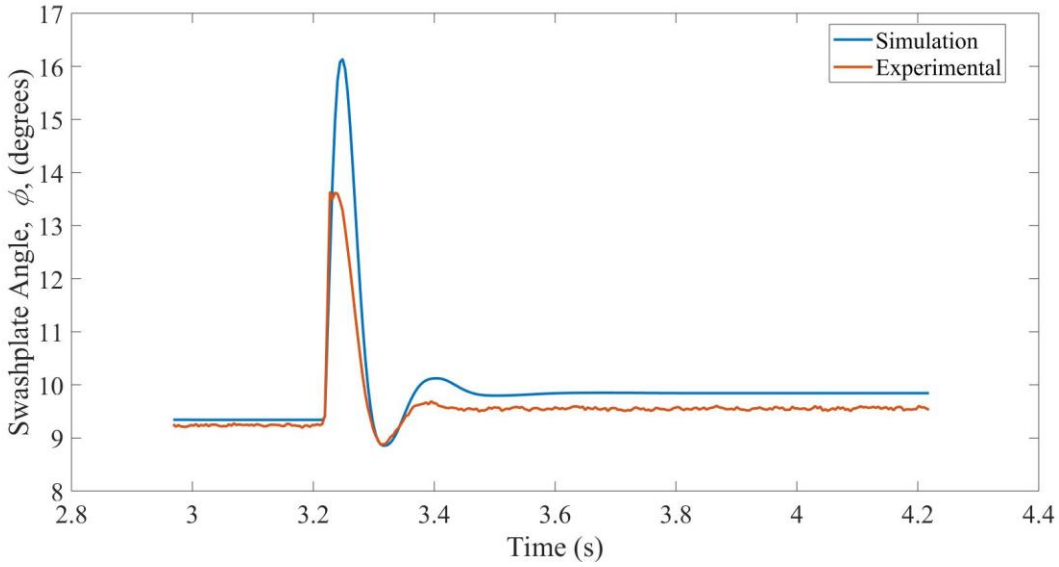


**Figure C.22:** Model fit for pump 172 swashplate dynamics using median of orifice constant range

As expected there is more discrepancy between the model and experimental dynamic when using the median of the range for the orifice constants.

# Appendix D Linearized Equations

## D.1 Linearized Equations

Linearized equations are provided in this section. The state is labeled and the column headings correspond to the derivative of that state.

| X1 | 1 | 2 | 3 | 4 | 5 | 6 | 7 |
|---|---|---|---|---|---|---|---|
| | 0 | 1 | 0 | 0 | 0 | 0 | 0 |

| X2 | 1 | 2 | 3 | 4 | 5 | 6 |
|---|---|---|---|---|---|---|
| | $-\frac{k_{ls}}{m_{ls}} + \frac{2K_{chrg}C_d^2C_{cc}\cos(\alpha)(x_3 - x_7)}{C_c m_{ls}}$ | $-\frac{d_{ls}}{m_{ls}}$ | $\frac{2K_{chrg}C_d^2\,x_1C_{cc}\cos(\alpha}{C_c m_{ls}}$ | 0 | 0 | $-\frac{A_{ls}}{m_{ls}}$ |

| X2 | 7 |
|---|---|
| | $\frac{A_{ls}}{m_{ls}} - \frac{2C_{cc}K_{chrg}C_d^2\,x_1\cos(\alpha)}{C_c m_{ls}}$ |

| X3 | 1 | 2 | 3 |
|---|---|---|---|
| | $\frac{\sqrt{2}K_{chrg}C_d\beta_{ps}C_{cc}\sqrt{\frac{(x_7 - x_3)}{\rho}}}{V_{cp} + A_{cp}x_4}$ | 0 | $-(\beta_{pcp}(\frac{C_{cp}}{LP_{max} - LP_{slope}x_4} + \frac{\sqrt{2}K_{chrg}C_{cc}C_d x_1}{\left(2\rho\sqrt{\frac{x_7 - x_3}{\rho}}\right)(V_{cp} + A_{cp}x_4)})$ |

| X3 | 4 |
|---|---|
| | $$-\frac{A_{cp}\beta_{pcp}C_{cp}(P_{tank}-x_3)}{LP_{max}+LP_{slope}x_4}-A_{cp}x_5+\frac{\sqrt{2}C_{cc}K_{chrg}C_dx_1\sqrt{\frac{x_7-x_3}{\rho}}}{\left(V_{cp}+A_{cp}x_4\right)^2}+\frac{C_{cp}LP_{slope}\beta_{pcp}(P_{tank}-x_3)}{(V_{cp}+A_{cp}x_4)(LP_{max}+LP_{slope}x_4)^2}$$ |

| X3 | 5 | 6 | 7 |
|---|---|---|---|
| | $\frac{-A_{cp}\beta_{pcp}}{V_{vcp}+A_{cp}x_4}$ | 0 | $\frac{\sqrt{2}C_{cc}K_{chrg}C_dx_1\beta_{pcp}}{2\rho(V_{cp}+A_{cp}x_4)\sqrt{\frac{x_7-x_3}{\rho}}}$ |

| X4 | 1 | 2 | 3 | 4 | 5 | 6 | 7 |
|---|---|---|---|---|---|---|---|
| | 0 | 0 | 0 | 0 | 1 | 0 | 0 |

| X5 | 1 | 2 | 3 | 4 |
|---|---|---|---|---|
| | 0 | 0 | $\frac{A_{cp}}{m_{bias}+m_{cp}}$ | $-\frac{k_1}{m_{cp}+m_{bias}}+\frac{C_1}{((Y_{max}-x_4)^2+L^2)(m_{cp}+m_{bias})}$ |

| X5 | 5 | 6 | 7 |
|---|---|---|---|
| | $-\frac{K_{ag}}{m_{cp}+m_{bias}}$ | 0 | $-(\frac{A_{bias}-\frac{C_2}{L}}{m_{cp}+m_{bias}})$ |

| X6 | 1 | 2 | 3 | 4 | 5 | 6 |
|---|---|---|---|---|---|---|

| | | | | | | |
|---|---|---|---|---|---|---|
| | 0 | 0 | 0 | 0 | 0 | $-\frac{\beta_{pls}}{VB_{load}}\left(\frac{\sqrt{2}K_{ls}}{2\rho\sqrt{\frac{x_7-x_6}{\rho}}}+\frac{\sqrt{2}K_{load}}{2\rho\sqrt{\frac{x_6-P_{tank}}{\rho}}}\right)$ |

| **X6** | **7** |
|---|---|
| | $\frac{\sqrt{2}K_{ls}\beta_{pls}}{2\rho VB_{load}\sqrt{\frac{x_7-x_6}{\rho}}}$ |

| **X7** | **1** | **2** | **3** |
|---|---|---|---|
| | $\frac{-\sqrt{2}K_{chrg}C_d\beta_{ps}C_{cc}}{VB_{pump}}\sqrt{\frac{x_7-x_3}{\rho}}$ | 0 | $-(\frac{C_{cp}}{LP_{max}-LP_{slope}x_4}-\left(\frac{\sqrt{2}K_{chrg}C_dC_{cc}x_1}{2\rho\sqrt{\frac{x_7-x_3}{\rho}}}\right))\frac{\beta_{ps}}{VB_{pump}}$ |

| **X7** | **4** |
|---|---|
| | $-\frac{\beta_{ps}}{VB_{pump}}\left(\frac{f_{gain}}{L(\frac{(Y_{max}-x_4)^2}{L^2}+1)}-\frac{C_{cp}LP_{slope}(P_{tank}-x_3)}{(LP_{max}+LP_{slope}x_4)^2}\right)$ |

| **X7** | **5** | **6** | **7** |
|---|---|---|---|
| | 0 | $\frac{\sqrt{2}K_{ls}\beta_{ps}}{2VB_{pump}\rho\sqrt{\frac{x_7-x_6}{\rho}}}$ | $-\frac{\beta_{ps}}{VB_{pump}}\left(R_{slope}+\frac{\sqrt{2}K_{ls}}{2\rho\sqrt{\frac{x_7-x_6}{\rho}}}+\frac{\sqrt{2}C_{cc}K_{chrg}C_dx_1}{2\rho\sqrt{\frac{x_7-x_3}{\rho}}}\right)$ |

# Appendix E Two-Dimensional PCA example

This Appendix section provides a simple illustration of PCA for a two-dimensional example. This is not an original example as it closely follows the example given by Wiens and Fernandes (2019). The example outlines the effectiveness of PCA in reducing dimensions and extracting features. To begin, consider a two dimensional dataset that is correlated to a parameter, $y$. The parameter $y$ is created as a random normal distribution of 1000 numbers. Two variables, $X_1$ and $X_2$, are vectors that are functions of the parameter $y$. Plotting the data shows certain correlation between $X_1$ and $X_2$ in Figure E.1.

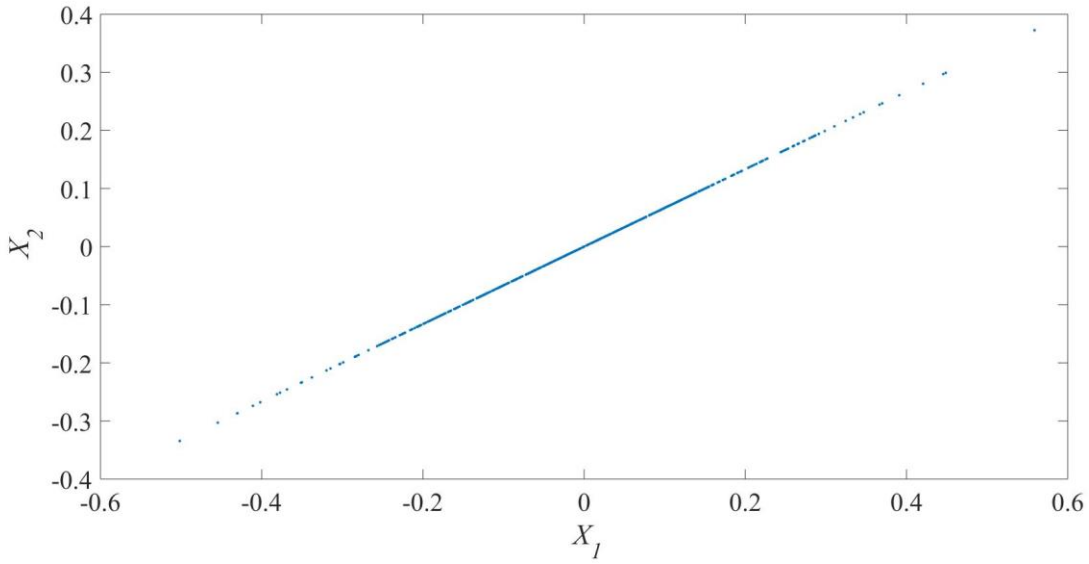


**Figure E.1:** Clean data with no noise and clear correlation between $X_1$ and $X_2$

The correlation between $X_1$ and $X_2$ is obvious since a single value of $X_1$ corresponds to a single value of $X_2$. A vertical line in this same plot would indicate no correlation since a single value of $X_1$ would be any value of $X_2$. Adding noise to the dataset reduces the correlation. The dataset is formulated as:

$$X_1 = 3y + \epsilon\,, \qquad \text{D.1}$$

and

$$X_2 = 2y + \epsilon\ . \qquad \text{D.2}$$

The noise, $\epsilon$ is drawn from a normal distribution with a variance of 0.01. Figure E.2 illustrates the dataset.

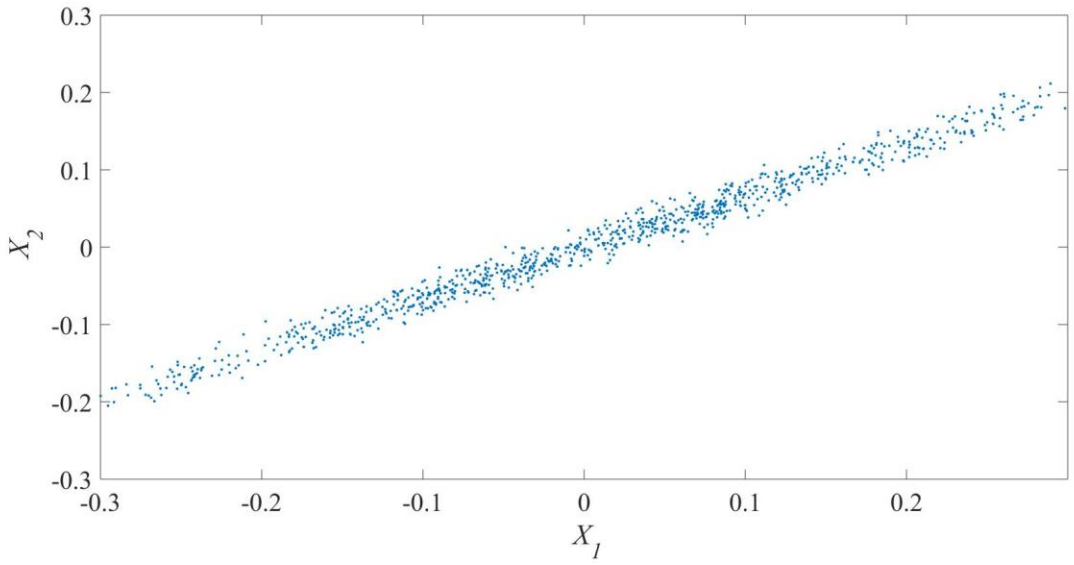


**Figure E.2:** Generated dataset for illustration of PCA

By adding random noise to the parameters $X_1$ and $X_2$, their correlation is reduced.

Performing PCA on this two-dimensional dataset begins by determining the covariance matrix. In this case it is

$$\sigma = \begin{bmatrix} 0.0236 & 0.0158 \\ 0.0156 & 0.0105 \end{bmatrix}.$$

The resulting eigenvalues and eigenvectors of the covariance matrix are

$$\boldsymbol{U_1} = \begin{bmatrix} -0.8321 \\ -0.5547 \end{bmatrix} \lambda 1 = 0.0341;$$

$$\boldsymbol{U_2} = \begin{bmatrix} 0.5547 \\ -0.8321 \end{bmatrix} \lambda 2 = 1.735e^{-18}.$$

The eigenvectors indicate the direction of highest variance, and in the case of a square matrix, are orthogonal. The eigenvalues represent how strong the variance is in the corresponding direction. In this example it is clear that $\boldsymbol{U_1}$ is the direction of highest variance of

the original dataset and is significantly stronger than the next orthogonal direction since the eigenvalue is many orders of magnitude larger.

The next step in PCA is to transform the original dataset onto new axes. The dataset in Figure E.2 can visually be rotated so that the largest variance direction becomes the new x dimension. Mathematically, the transformation is:

$$X_{pc1} = \boldsymbol{XU_1}\,,. \qquad \text{D.3}$$

for the first principal component and

$$X_{pc2} = \boldsymbol{XU_2}\,, \qquad \text{D.3}$$

for the second.

The new dataset can be plotted and is shown in Figure E.3.

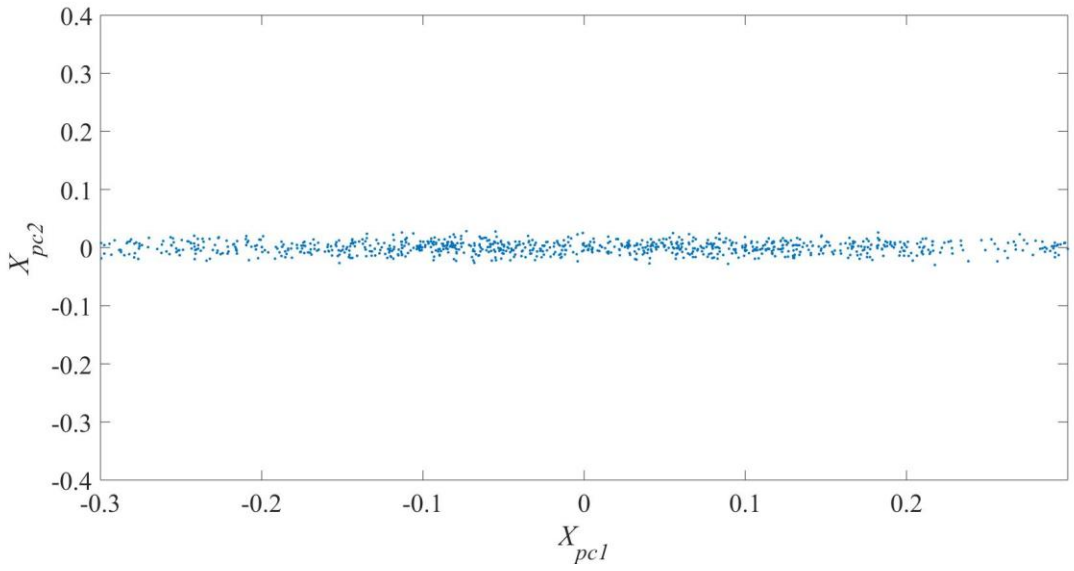


**Figure E.3:** Transformed dataset onto new axes called principal components

Observing Figure E**.3**, the data along dimension $X_{pc1}$ have very large variance and along $X_{pc2}$ there is significantly less variance. The variance along $X_{pc2}$ represents the normally

distributed noise added to the data. By removing this dimension, the dataset can be reduced to a single dimension.

Figure E.4 emphasizes the correlation of the strong principal component, as determined by the strongest eigenvalue, with $y$.

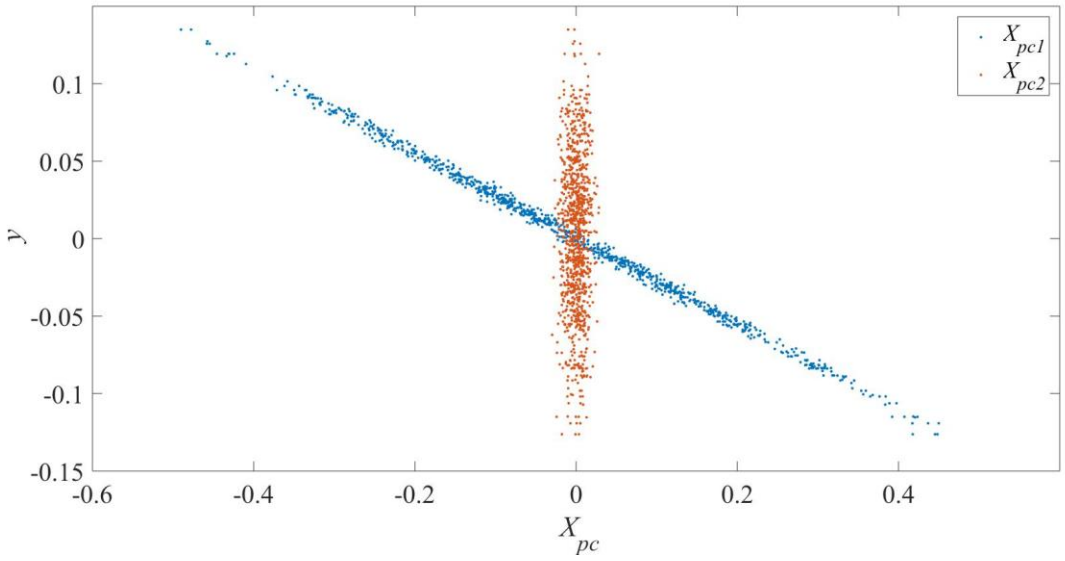


**Figure E.4:** Correlation of $X_{pc1}$ and $X_{pc2}$ with the parameter $y$.

As expected, $X_{pc2}$, the weaker principal component, shows essentially no correlation with $y$.

A simple regression can be performed, given some new $X_1$ and $X_2$ data, to predict the parameter $y$. This regression would be done using two dimensions. By using principal components analysis and removing the unimportant dimension, a regression can be done using one dimensional data to predict $y$. This may not seem useful in this two dimensional example, but, consider the data reduction potential when managing datasets with hundreds of dimensions, as is the case in this research.

# Appendix F Instrumentation for Experiments

## F.1 Instrumentation

- Pressure transducers – PX419-5.0KG5V
- Flowmeters
    - Flomec EGM015A001-821 – Case drain flow
    - Flomec EGM020S001-821 – Load flow
- DAQ – USB – 1408FS-Plus
- Flow control valve specs
- Parker High Speed Valve – D1FPE50MA9NB0036
- Electric motor for wear tests spec
    - G.E.C Machines Limited Alpak, 1735 RPM, 20hp
- Electric motor for performance test specs
    - Crompton Parkinson – 1740 RPM, 75hp
- Swash angle specs
    - A16271L
- Thermocouple specs
    - T1 thermocouple
- Coolers
    - Hayden, Inc.  LT208A
- Nuto 68 hydraulic oil